A MATHEMATICAL MODEL OF HELICAL OSCILLATING
HEAT PIPE

NARIN SIRIWAN

A dissertation submitted in partial fulfillment of the requirements for

the degree of Doctor of Philosophy in Mechanical Engineering

at Mahasarakham University

August 2016

Mahasarakham University

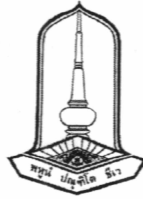# A MATHEMATICAL MODEL OF HELICAL OSCILLATING
HEAT PIPE

NARIN SIRIWAN

A dissertation submitted in partial fulfillment of the requirements for

the degree of Doctor of Philosophy in Mechanical Engineering

at Mahasarakham University

August 2016

Mahasarakham University

The examining committee has unanimously approved this dissertation, submitted by Mr. Narin Siriwan, as a partial fulfillment of the requirements for the degree for Doctor of Philosophy in Mechanical Engineering at Mahasarakham University.

Examining Committee

.... Chairman

(Assoc. Prof. Bopit Bubphachot, Ph.D.)   (Faculty graduate committee)

.... Committee

(Prof. Sampan Rittidech, Ph.D.)   (Advisor)

.... Committee

(Asst. Prof. Teerapat Chompookham, Ph.D.)   (Co-advisor)

.... Committee

(Prof. Yulong Ding, Ph.D.)   (Co-advisor)

.... Committee

(Asst. Prof. Kiattisin Kanjanavanichkul, Ph.D.) (Faculty graduate committee)

.... Committee

(Asst. Prof. Thanya Parametthanuwat, Ph.D.)   (External expert)

Mahasarakham University has granted approval to accept this dissertation as a partial fulfillment of the requirements for the degree of Doctor of Philosophy in Mechanical Engineering

....

(Assoc. Prof. Anongrit Kangrang, Ph.D.)   (Prof. Pradit Terdtoon, Ph.D.)

Dean of the Faculty of Engineering   Dean of Graduate School

Mahasarakham University   August 31, 2016

ACKNOWLEDGEMENT

The dissertation would not have been accomplished without help from several people. First of all, I would like to thank Professor Dr. Sampan Rittidech, the chairperson of my advisory committee, for inspiration, knowledge, experience, research perspective and valuable suggestions that allowed this study to be completed. I would also like to thank my advisory committee, Assistant Professor Dr. Teerapat Chompookham and Professor Dr. Yulong Ding and also Assistant Professor Dr. Thanya Parametthanuwat, my external examiner for many helpful suggestions.

I am very thankful to all the students of the Heat Pipe and Thermal Tools Design Research Unit (HTDR), Mahasarakham University, Thailand, both my friends and colleagues, for all their help.

I would also like to thank to all the students in the Yulong Laboratory, School of Chemical Engineering, University of Birmingham.

I was very fortunate to have many friends, both within and outside the Faculty of Engineering, during my doctoral life. I thank them all for being very supportive. I also owe thanks and many other people in a long list that might take several pages for support in many ways. Finally, I would like to express my deepest gratefulness to Mr. Sutut, Mrs. Yupawan, Mr. Weera, Mr. Bua and Mrs. Buapan Siriwan, for valuable love, care, help, willpower and support in my whole life.

Narin Siriwan

TITLE	A Mathematical Model of Helical Oscillating Heat Pipe
AUTHOR	Narin Siriwan
DEGREE	Doctor of Philosophy (Mechanical Engineering)
ADVISOR	Prof. Sampan Rittidech, Ph.D.
	Asst. Prof. Teerapat Chompookham, Ph.D.
	Prof. Yulong Ding, Ph.D.
UNIVERSITY	Mahasarakham University **YEAR** 2016

ABSTRACT

This thesis studied heat transfer with a numerical model and experimental evaluation of a helical oscillating heat pipe (HOHP). Firstly, I created a numeric model of the HOHP to predict the time required to reach the steady state temperature, the heat transfer of the HOHP and the heat transfer of the HOHP heat exchanger under transient conditions. Secondly, I measured the temperature at the pipe wall and evaluated the heat transfer rate and compared them with the numeric model. Thirdly, I applied results from the numeric model and experiments to select the parameters to obtain the best heat transfer rates for constructed the HOHP heat exchanger.

The model allowed determination of the temperature profiles at the pipe wall, heat transfer profiles of the HOHP itself and heat transfer profiles of the HOHP heat exchanger. The governing equation for the pipe wall is the conduction equation, and the governing equations for the vapor core are the continuity, the momentum and the energy equations. All of the governing equations were solved numerically using finite difference methods. The time required to reach the steady state temperature of the pipe wall, the heat transfer of the HOHP and the heat transfer of the HOHP heat exchanger were determined in this part. The results show that a temperature for the evaporator section of 60ºC had a time to the steady state temperature and steady state heat transfer that was less than the temperatures for the evaporator section of 70 and 80ºC. A temperature of 80ºC for the evaporator section had the highest heat transfer of the HOHP and the HOHP heat exchanger.

The second part measured the temperature profiles of the pipe wall and the heat transfer profiles of the HOHP. The HOHP was constructed from copper tubes and the

working fluids were water, ethanol and R11; the temperatures of the evaporator section were 60, 70 and 80ºC; the inner diameters of the pipe were 1.6, 1.8 and 2.0 mm; the thickness was 0.5 mm; the total lengths of the pipe at the evaporator and the condenser sections were 850 mm; length of the adiabatic section was 50 mm; the temperature of the water in the condenser section was 20ºC; the mass flow rate of the water at the inlet of the evaporator and the condenser sections was 0.25 kg/min; the filling ratio was 80% with respect to the total volume of the HOHP; inclination angle was 90 degrees from the horizontal; the evaporator and the condenser sections had five coils; the diameter of the coil was 50 mm; and pitch was 10 mm. The time required to reach the steady state temperature of the pipe wall and the heat transfer of the HOHP were measured in this part and the results from the experimental evaluation of the HOHP were compared with the model from the first part. The results show that R11 working fluid had the highest heat transfer for the HOHP, the temperature for the evaporator section of 80ºC had the highest heat transfer for the HOHP and 2.0 mm inner diameter had the highest heat transfer for the HOHP. The results from the experimental evaluation and those from the model were in good agreement.

The third part shows the heat transfer of the HOHP heat exchanger from the experimental evaluation. The HOHP heat exchanger was constructed from copper tubes and the parameters in the experiment were the same as the HOHP experiment and the selected working fluid, temperature, inner diameter of pipe and total lengths of pipe at the evaporator and the condenser sections were those provided the best heat transfer from the scope of the experiment. The mass flow rate of the water at the evaporator and the condenser sections was 1.5 kg/min and the HOHP heat exchanger used a counter flow arrangement. The time required to reach the steady state heat transfer for the HOHP heat exchanger was determined in this part and found to be in good agreement with predictions from the model and experiments.

Key words: Helical oscillating heat pipe; Mathematical model; Heat transfer; Heat exchanger

Mahasarakham University

CONTENTS

List of Tables

Mahasarakham University

List of Figures

Page

Page

List of Abbreviations

Abbreviations		Unit
A	Area in heat transfer	m^2
a	Radial of the HOHP	m
C_p	Specific heat	J/kg °C
D	Diameter of pipe	m
h	Convective heat transfer coefficient	J/kg
L	Length of pipe	m
$\dot{m}$	Mass flow rate	kg/s
N	Number of tube	
Q	Heat transfer of the HOHP	W
r	Radial	m
T	Temperature	°C
t	Time	s
w	Velocity	m/s
z	Overall resistance	°C/W

Greek symbols

ε	Effective of heat exchanger	
ρ	Density	kg/m^3
κ	Torsion	m
τ	Curvature	m

Subscribe

a	Adiabatic section
c	Condenser section
cond	Condenser section

e	Evaporator section
evap	Evaporator section
i	Position in analysis
in	Inlet
out	Outlet
r	Radial direction
s	Circumferential direction
v	Vapor phase
w	Pipe wall
θ	Angle direction

CHAPTER 1

INTRODUCTION

1.1 Background

A heat pipe has a high heat transfer. In 1972, the idea of the heat pipe was presented by R.S. Gaugler; however, in 1960, G.M. Grover had invented the heat pipe. Since then, there has been development of the heat transfer properties of the heat pipe and the heat pipe is widely known in the present. First, heat pipes are used in space technology, satellites and nuclear power plants and in the present the heat pipe can be used to reduce the heat in electronic devices, such as computers, or used to save energy and for heat exchange in industry. A heat pipe has three section: the evaporator, the adiabatic and the condenser sections. The heat pipe uses the principles of heat transfer from the state change of the working fluid within the pipe, which does not require external energy. The heat pipe has the principle of the boiling of the working fluid, when the working fluid within the evaporator section receives heat it will evaporate and reduce the heat at the condenser section. The working fluid will form condensation and the heat from the condensation will be lost to the environment, then the working fluid will be liquid and flow to the evaporator section by gravity [1]. In the present, the heat pipe is appropriate for use but the effectiveness of them needs increasing, so the heat pipe has changed schematically quickly. The helical oscillating heat pipe (HOHP) is a heat pipe of another type, for use to solve the problems from above.

The HOHP is complex, and needs to be analyzed by a mathematical model. The mathematical model uses math to describe the system by assumptions, or set of boundary conditions in the analysis. To predict the behavior of the heat transfer of the heat pipe, commonly mathematical methods are used to solve the problems. The analysis for the solution will use numerical methods to solve the engineering problem by using a computer program for the calculation. Using a computer programing in the calculation will give the similar value as with the true value, mostly. The finite difference method is a numerical method used to solve the differential equations and it is common for the analysis to solve engineering and science problems, due to it being

able to simulate the structure or the workpiece complexity. In using the finite difference method, we will use a computer for the calculation to provide a fast calculation. However, at present, the HOHP does not have the background information to analyze it in depth. Which means no researchers have created a mathematical model to predict the performance of the HOHP.

Therefore, this research aims to develop a mathematical model of a helical oscillating heat pipe and the application of the finite difference method to solve the governing equations for the transient condition by using a computer program for the calculation.

1.2 Objectives of study

1.2.1 To create a mathematical model for the prediction of the heat transfer of a HOHP.

1.2.2 To compare the results from the mathematical model and an experiments.

1.2.3 To design and create a heat exchanger.

1.2.4 To compare the performance of the heat exchanger from the model with the experiments.

1.3 Scope of study

1.3.1 Scope of mathematical model

1.3.1.1 Apply the numerical method for the mathematical model of the HOHP.

1.3.1.2 Apply the computer program to solve the mathematical model of the HOHP.

1.3.1.3 Analyze the HOHP in 1-D.

1.3.2 Scope of experimental evaluation

1.3.2.1   Independent parameters

1) Working fluids were water, ethanol and R11.

2) Temperatures of the evaporator section were 60, 70 and 80ºC.

3) HOHP was made from copper pipe with the inner diameters of 1.6, 1.8 and 2.0 mm and thickness was 0.5 mm.

1.3.2.2   Dependent parameters

1) Temperature of the HOHP.

2) Heat transfer of the HOHP.

1.3.2.3   Control parameters

1) Total length of the pipe at the evaporator section was 850 mm.

2) Total length of the pipe at the condenser section was 850 mm.

3) Length of the adiabatic section was 50 mm.

4) Temperature of the water in the condenser section was 20ºC.

5) Mass flow rate of the water at the inlet of the evaporator and the condenser sections was 0.25 kg/min.

6) Filling ratio was 80% with respect to the total volume of the HOHP.

7) Inclination angle was 90º from the horizontal.

8) Number of coils in the evaporator and the condenser sections was 5.

9) Diameter of coil was 50 mm.

10) Pitch was 10 mm.

1.3.3 Scope of heat exchanger

To prove that the HOHP heat exchanger can exchange a heat of 1000 W and that it has the conditions as follows:

1) Working fluid that provides the best heat transfer from the scope of the experiment in topic 1.3.2.

2) Temperature that provides the best heat transfer from the scope of the experiment in topic 1.3.2.

3) HOHP made from copper pipe that provides the best heat transfer from the scope of the experiment in topic 1.3.2.

4) Temperature of water in the condenser section was 20ºC.

5) Mass flow rate of the water at the evaporator and the condenser sections was 0.25 kg/min.

6) Total length of the pipe at the evaporator section that provides the best heat transfer from the scope of the experiment in topic 1.3.2.

7) Total length of the pipe at the condenser section that provides the best heat transfer from the scope of the experiment in topic 1.3.2.

8) Adiabatic section was 50 mm.

9) Inclination angle was 90 degrees from the horizontal.

10) Heat exchanger has counter flow arrangement.

1.4 Benefits of this study

1.4.1 Mathematical model for the prediction the heat transfer of the HOHP.

1.4.2 Comparison of the results from the mathematical model and the experiments.

1.4.3 Design and creation of the heat exchanger.

1.4.4 Comparison of the performance of the heat exchanger from the model with the experiments.

CHAPTER 2

THEORY AND LITERATURE REVIEWS

For the study of a mathematical model of a HOHP, the numerical method needs to know the basic information about the HOHP, which can be describe as follows:

1. Theory of oscillating heat pipe (OHP)
2. Theory of HOHP
3. Theory of mathematical model of HOHP
4. Numerical method
5. Theory of HOHP heat exchanger
6. Literature reviews

2.1 Theory of oscillating heat pipe (OHP)

An OHP is heat transfer equipment that does not use external energy. The OHP consists of three sections: the evaporator section (L_e), the adiabatic section (L_a) and the condenser section (L_c). The OHP can be operated by adding a working fluid to the capillary tube, for which, when the working fluid is in the saturated liquid state boiling occurs, and it is condensed into steam by the latent heat of vaporization and moves to the condenser section. The condenser section has a lower temperature, the steam condenses and moves to the other end of the pipe. Therefore, the working fluid steam can transfer the heat from one end of the pipe to the other end of the pipe, if the temperatures of the evaporator and the condenser sections are different. OHPs can be classified into four types: closed-end oscillating heat pipe (CEOHP), closed-loop oscillating heat pipe (CLOHP), closed-loop oscillating heat pipe with check valve (CLOHP/CV) and helical oscillating heat pipe (HOHP) [2], which are shown in figure 2.1.
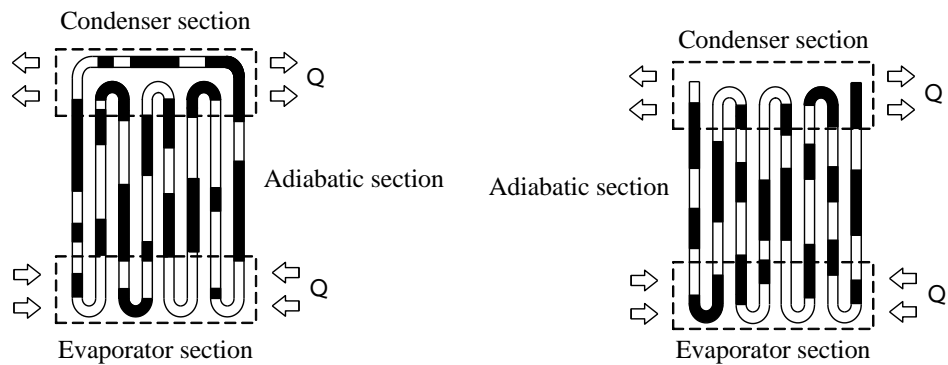
Condenser section

Adiabatic section

Q

Evaporator section

Q

(a) Closed-end oscillating heat pipe

(CEOHP)

Condenser section

Adiabatic section

Q

Evaporator section

Q

(b) Closed-loop oscillating heat pipe

(CLOHP)

Condenser section

Adiabatic section

Q

Evaporator section

Q

(c) Closed-loop oscillating heat pipe

with check valve (CLOHP/CV)

Pitch

Condenser Section

Adiabatic Section

Evaporator Section

Diameter of coil
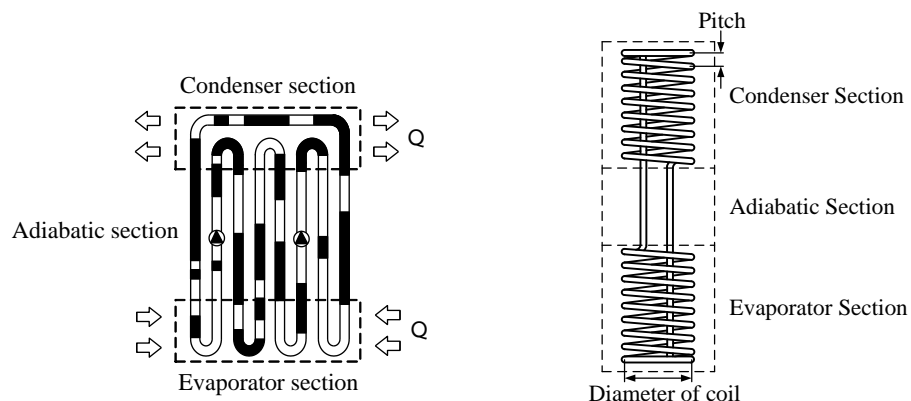
(d) Helical oscillating heat pipe

(HOHP) [25]

Figure 2.1 Oscillating heat pipes (OHP) [2]

The heat transfer characteristic of the OHP is the relationship of the actual heat transfer (Q), the overall heat transfer (Z) and the difference between the temperature of the heat source and the heat sink (ΔT). Which can be calculated by equation (2.1) [2].

$$Q = \frac{\Delta T}{Z} \tag{2.1}$$

The heat transfer of the OHP, also has the parameter control of the thermal resistance, which can be calculated by equation (2.2) [2].

$$Z = \frac{(T_{evap} - T_{cond})}{Q} \qquad (2.2)$$

The calculation of the heat transfer of the OHP can be done by measuring the temperature of the cooling substance at the inlet and outlet of the condenser section, which can be calculated by equation (2.3) [2].

$$Q = \dot{m} c_p (T_{out} - T_{in}) \qquad (2.3)$$

2.2 Theory of HOHP

The HOHP is a small pipe that has a high heat transfer coefficient. HOHPs are widely used in industry, such as in heat recovery systems, air conditioning and the food industry. The HOHP increases the heat transfer area more than the loop heat pipe, and it can be installed in a small area. The HOHP design has the evaporator and the condenser sections as pipes bent into a coil spring, and the adiabatic section is a straight pipe. A schematic of a HOHP is shown in figure 2.2. In which the length of the evaporator section is L_e, the length of the adiabatic section is L_a, the length of the condenser section is L_c, the radial of the coil is r_a, the radial of the pipe is a and the pitch is p_s [3].
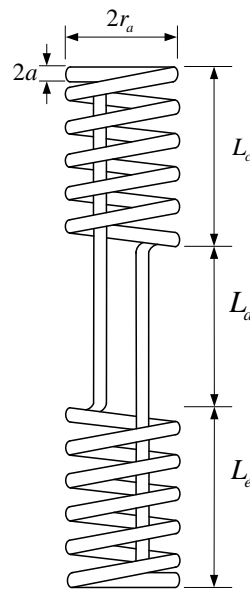
Figure 2.2 Schematic of HOHP [3]

2.2.1 Geometry of HOHP

The geometry of the HOHP is shown in figure 2.3(a); the pitch p_s is increased by the number of coils in the equation $2\pi p_s$ and it has important equations that consist of those for the curvature (κ) and the torsion (τ). These can be seen in equation (2.4) and equation (2.5).

$$\kappa = \frac{r_a^2}{(r_a^2 + p_s^2)} \tag{2.4}$$

$$\tau = \frac{p_s^2}{(r_a^2 + p_s^2)} \tag{2.5}$$

(a) Geometry of HOHP   (b) Coordinate system of HOHP
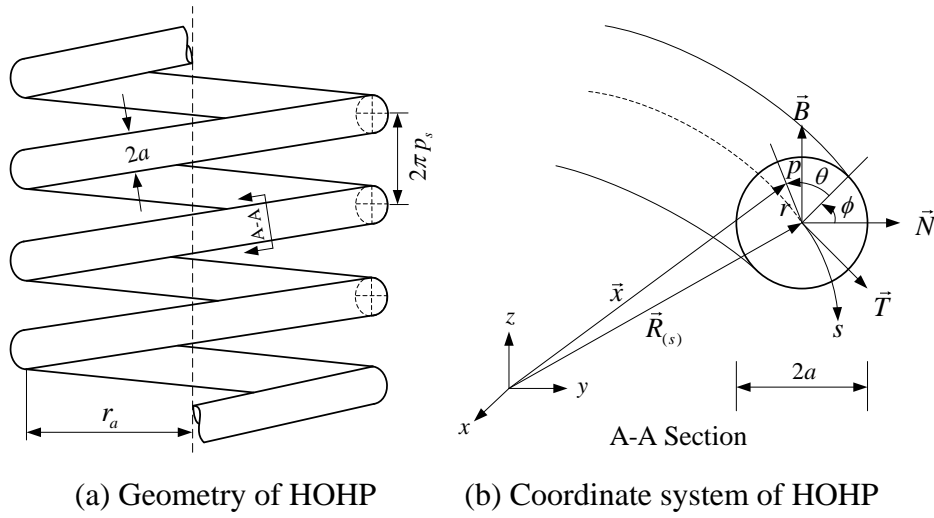
Figure 2.3 Geometry and coordinate system of HOHP [4]

2.2.2 Coordinate system of HOHP

The coordinate system of the HOHP can be considered as a master Cartesian coordinate system (x, y, z). The coordinate system of the HOHP can be seen in figure 2.3(b), where s is the curvature direction, r is the radial direction and θ is the angle direction. The vector in the coordinate system of the HOHP is $\vec{R}_{(s)}$, which can be calculate in equation (2.6).

$$\vec{R}_{(s)} = a\cos(s)\vec{i} + a\sin(s)\vec{j} + b(s)\vec{k} \tag{2.6}$$

where $\vec{i}$, $\vec{j}$ and $\vec{k}$ are the unit vectors and s is the vector in the curvature of the HOHP. The position x of the HOHP can be written in vector $\vec{X}$ as can be calculate in equation (2.7).

$$\vec{X} = \vec{R}_{(s)} - r\sin(\theta - \tau s)\vec{N}_{(s)} + r\cos(\theta - \tau s)\vec{B}_{(s)} \tag{2.7}$$

The metric in the coordinate system of the HOHP can be shown in equation (2.8).

$$d\vec{x} \cdot d\vec{x} = (1 + \kappa r \sin(\theta - \tau s))^2 ds^2 + dr^2 + r^2 d\theta^2 \qquad (2.8)$$

when ds, dr and $d\theta$ are the variation in the rate in the axial, radial and angle directions, respectively. The unit matrix h_s can be calculated from equation (2.9).

$$h_s = 1 + \kappa r \sin(\theta - \tau s) \qquad (2.9)$$

2.3 Theory of mathematical model of HOHP

When studying the details of the HOHP, it is very complex because the HOHP has more parameters in the analysis, in which the analysis of the HOHP will include the pipe wall and the vapor core of the HOHP. The pipe wall of the HOHP has the governing equation as the conduction equation. The vapor core in the HOHP has the governing equation as the continuity, the mass and the energy equations. These can be describe as follows:

2.3.1 Conduction equation

The conduction equation at the pipe wall of the HOHP can be shown from the control volume in the coordinate system as in figure 2.4. The conduction rate along the HOHP is q_s.
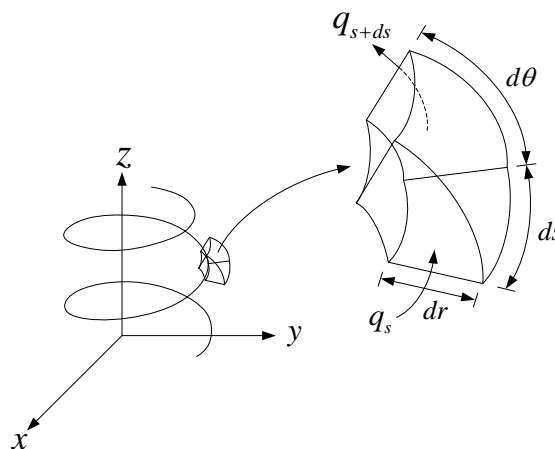
Figure 2.4 Control volume on coordinate system of HOHP

From the control volume in figure 2.4, the energy conservation is:

$$\dot{E}_{in} + \dot{E}_g - \dot{E}_{out} = \dot{E}_{st} \qquad (2.10)$$

where $\dot{E}_{in}$ is the energy inflow, $\dot{E}_{out}$ is the energy outflow, $\dot{E}_g$ is the energy generation and $\dot{E}_{st}$ is the energy storage.

2.3.2 Conservation of mass equation

Consider the fluid particle as shown in figure 2.5, the lengths of each side of the fluid particle are dr, $d\theta$ and ds according to the coordinates x, y and z of the particle and the fluid will be have the mass flux though the flow as can be seen in figure 2.5.
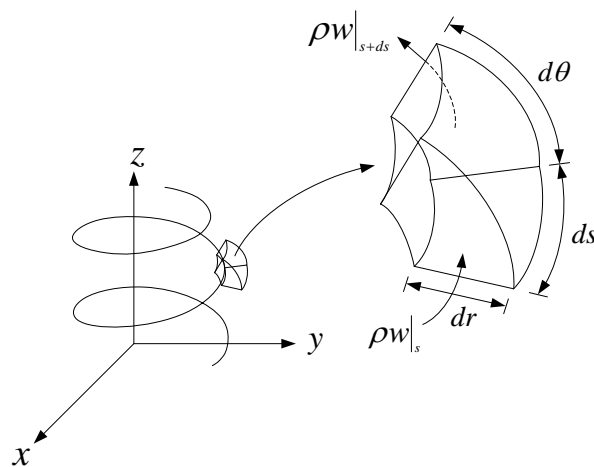
Figure 2.5 Mass flux though small area of fluid

The control volumes are the volume of the fluid particle and the conservation of mass equations, as shown in equation (2.11).

$$\frac{\partial}{\partial t} \int_{cv} \rho \, d\forall + \int_{cs} \rho \vec{V} \cdot d\vec{A} = 0 \qquad (2.11)$$

where ρ is the density of mass, $\forall$ is the volume of mass, $\vec{V}$ is the velocity vector in the flow and $\vec{A}$ is the vector of the cross section area of the small area.

2.3.3 Conservation of momentum equation

When considering the fluid particle as shown in figure 2.6, the control volumes are dr, $d\theta$ and ds, as can be shown by the following:

$$\vec{F} = \vec{F}_S + \vec{F}_B = \frac{\partial}{\partial t} \int_{cv} \vec{V} \rho d\forall + \int_{cs} \vec{V} \rho \vec{V} \cdot d\vec{A} \qquad (2.12)$$

where $\vec{F}_S$ is the surface tension force on the control volume and $\vec{F}_B$ is the weight of the control volume.
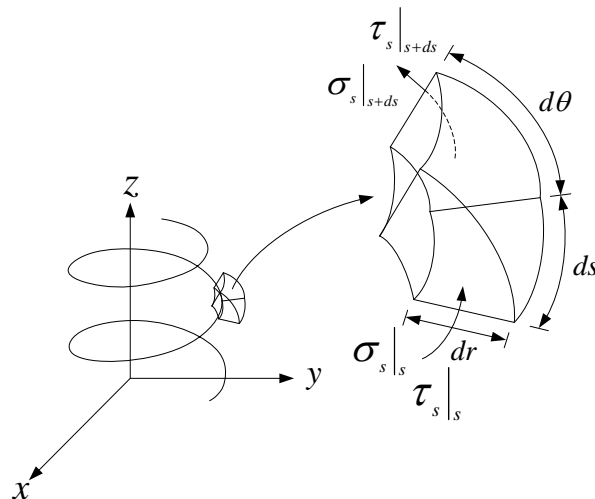
Figure 2.6 Stress on surface of control volume

2.3.4 Conservation of energy equation

When considering the fluid particle, as shown in figure 2.7, the control volumes of the fluid particle are dr, $d\theta$ and ds. The differential equation of the energy can be created by the first thermodynamic law, therefore the energy equation can be calculated from equation (2.13).

$$\rho \frac{D}{Dt}\left(e+\frac{V^2}{2}\right)ds = \left[\rho\bar{Q} - \frac{\partial q_s}{\partial s}\right]ds + \rho\vec{f}\cdot\vec{V}ds \qquad (2.13)$$

where e is the internal energy, $\dfrac{V^2}{2}$ is the kinetic energy of the mass, $\vec{V}$ is the velocity of the flow, $\bar{Q}$ is the heat flux occurring within the mass, $\vec{f}$ is the force from the weight of the mass and q_s is the heat flux in the s direction.
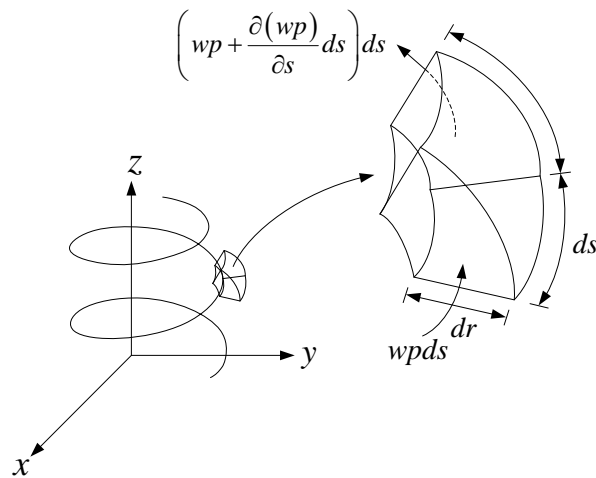
Figure 2.7 Work on control volume

2.3.5 Heat transfer calculation of HOHP from model

The calculation of the heat transfer for the HOHP from the model can be defined as the overall heat transfer from the evaporator section to the condenser section, or due to the heat transfer between the pipe wall and the working fluid. The heat transfer from the state change of the working fluid can be calculated from equation (2.14) and the heat transfer at the surface can be calculated from equation (2.15) [2].

$$Q_v = \dot{m}_v h_{fg,i} \qquad (2.14)$$

$$Q_{out} = \int_{i=1}^{n} \pi D h_c (T_{v,i} - T_{w,i})dx \qquad (2.15)$$

where Q_v is the heat transfer of the working fluid, $\dot{m}_v$ is the mass flow rate of the working fluid, h_{fg} is the latent heat of the vaporization of the working fluid, Q_{out} is the heat transfer at the outlet of the condenser section, D is the diameter of the pipe, h is the convective heat transfer coefficient, T_v is the temperature of the working fluid in the pipe and T_w is the temperature of the heat pipe wall.

2.3.6 Heat transfer calculation of HOHP from experiment

The calculation of the heat transfer for the HOHP from the experiment can be done by the calorimeter method, which uses the measurement of the inlet and outlet temperatures of the water at the condenser section of the HOHP, when the values were calculated for the heat transfer using equation (2.16) and equation (2.17).

$$Q = \dot{m}c_p(T_{out} - T_{in}) \tag{2.16}$$

where Q is   the heat transfer of the HOHP (W).

          $\dot{m}$ is   the mass flow rate (kg/s).

          c_p is   the specific heat (J/kg ^{o}C).

          T_{in} is   the inlet temperature at the condenser section (^{o}C).

          T_{out} is the outlet temperature at the condenser section (^{o}C).

2.4 Numerical method

The numerical method [5] used in the analysis of the mathematical model of the HOHP is the Crank-Nicolson method, which can be used to solve the heat equation as well and has high accuracy and few errors. The Crank-Nicolson method performs the calculation by estimating the term of the first time derivative of the variation with the time for the middle during of the period of the calculation as time n and n+1, which can be calculated from equation (2.17).

$$\frac{\partial T}{\partial t} = \frac{T_i^{n+1} - T_i^n}{\Delta t} \tag{2.17}$$

The first time derivative has variation with distance and can be calculated from equation (2.18).

$$\frac{\partial T}{\partial x} = \frac{1}{2}\left(\frac{T_{i+1}^{n+1} - T_{i-1}^{n+1}}{2\Delta x} + \frac{T_{i+1}^n - T_{i-1}^n}{2\Delta x} \right) \tag{2.18}$$

The second time derivative has variation with distance and can be calculated from equation (2.19).

$$\frac{\partial^2 T}{\partial x^2} = \frac{1}{2}\left(\frac{T_{i+1}^{n+1} - 2T_i^{n+1} + T_{i-1}^{n+1}}{\Delta x^2} + \frac{T_{i+1}^n - 2T_i^n + T_{i-1}^n}{\Delta x^2} \right) \tag{2.19}$$

The terms that do not vary with time and distance can be calculated from equation (2.20).

$$T = \frac{1}{2}\left(T_i^{n+1} - T_i^n \right) \tag{2.20}$$

2.5 Theory of HOHP heat exchanger

A heat exchanger is the application of several combined heat pipes for heat exchange from two types of fluid. The application of the heat pipe for heat exchange is called a heat pipe heat exchanger. The heat pipe heat exchanger is a closed system for the heat exchange from the hot fluid and the cool fluid, air or gas. Heat exchangers are designed to be used in hot systems and cold systems, such as the processes of electricity produced from gas or steam, refrigeration, cooling and in the food and chemical industries, etc. The heat exchanger has the principles of heat transfer from three processes that are heat conduction, heat convection and heat radiation. The design of a heat exchanger needs to consider the operating conditions above, as well as the money

invested, the performance, the size and the economic evaluation. We also must consider the materials used for the assembly, the corrosion resistance to chemicals and the physical properties of the heat, too [1].

For the analysis of the heat exchanger we must know the flow of the heat exchanger, the calculation of the number of tubes of the heat exchanger, the placement of the pipe in the heat exchanger, the overall heat transfer coefficient of the heat exchanger and the analysis and the calculation of the heat exchanger. Each of which are described as in the following:

2.5.1 Flow of heat exchanger

There are many types of heat exchanger and the heat pipe heat exchanger is a closed system, which has the hot fluid and the cool fluid within the heat exchanger for the heat exchange. The heat pipe heat exchanger can be classification by the two flow arrangements: the parallel flow and the counter flow [1]. In this study, we choose the counter flow due to it having the higher heat transfer and the efficiency in the exchange is better than the parallel flow. The counter flow is shown in figure 2.8.
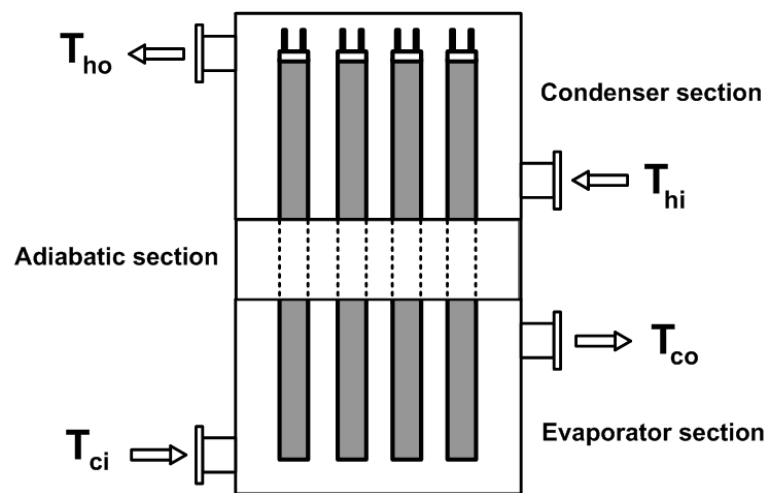
Figure 2.8 Counter flow in heat exchanger [1]

2.5.2 Calculation for number of tubes in heat exchanger

The calculation of the number of tubes in the heat exchanger can be determined from equation (2.21).

$$N = \frac{Q}{Q_{Theory}} \tag{2.21}$$

where N is the number of tubes in the heat exchanger.

   Q is the actual heat transfer (W).

   Q_{Theory} is the heat transfer from the model (W).

2.5.3 Tube alignment in heat exchanger

The alignment of the tubes in the heat exchanger is very important in the heat exchange of the heat exchanger, in which the best alignment can help to give a higher heat transfer. The alignment of the tubes can be arranged in two ways, which are staggered or in-line [1]. In this study, we choose the staggered alignment because it has a higher heat transfer than the in-line alignment. The staggered alignment is shown in figure 2.9.
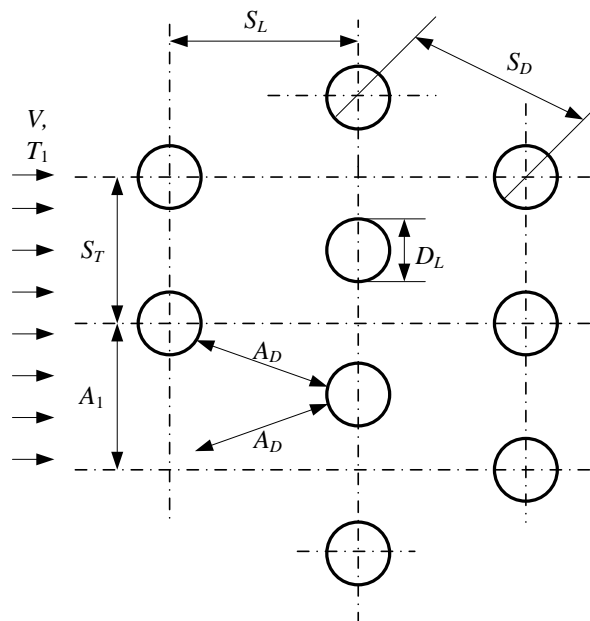
Figure 2.9 Staggered alignment [6]

Figure 2.9 shows the staggered alignment, which has the parameters in the analysis of the heat transfer of the heat exchanger as follows [6]:

S_T is the transverse pitch.

S_L is the longitudinal pitch.

S_D is the diagonal pitch.

where S_D can be calculated from equation (2.22).

$$S_D = \left[S_L^2 + \left(\frac{S_T}{2} \right)^2 \right]^{\frac{1}{2}} \tag{2.22}$$

The A_l group of tubes can be calculated from equation (2.23).

$$A_1 = S_T L \tag{2.23}$$

The A_D group of tubes can be calculated from equation (2.24).

$$A_D = (S_D - D_o)L \tag{2.24}$$

The staggered alignment has the maximum velocity at the horizontal plane (A_1) or the diagonal (A_D), in which V_{max} will occurred at A_D when $2(S_D - D_o) < (S_T - D_o)$ or $SD < \dfrac{S_T + D_o}{2}$ and V_{max} can be calculated from equation (2.25).

$$V_{max} = \left[\frac{S_T}{2(S_D - D_o)} \right] V \tag{2.25}$$

However, on the other hand, if V_{max} occurred at A_1 then V_{max} can be calculated from equation (2.26).

$$V_{\max} = \left[\frac{S_T}{S_T - D_o} \right] V \tag{2.26}$$

$V_{\max}$ is very important for the fluid flow, when it flows through a group of tubes. The Reynolds number can be calculated from $V_{\max}$ in equation (2.27).

$$\text{Re}_D = \frac{\rho V_{\max} D_o}{\mu} \tag{2.27}$$

The heat transfer coefficient can be calculated from equation (2.28).

$$h = \frac{Nu_D K}{D_o} \tag{2.28}$$

The Nusselt number, obtained when using air to flow though the group of 10 tubes that has $NL \geq 10$ and can be calculated from equation (2.29).

$$Nu_D = C_1 \text{Re}_{D,\max}^m, 2000 < \text{Re}_{D,\max}^m < 40000, \text{Pr} = 0.7 \tag{2.29}$$

C_1 and m can be seen from table 2.1.

When using air to flow through a group of tubes that is less than 10 tubes $NL < 10$, the Nusselt number can be calculated from equation (2.30).

$$Nu_D = C_1 C_2 \text{Re}_{D,\max}^m \tag{2.30}$$

C_2 and m can be seen from table 2.2.

When using other fluids to flow through the group of 10 tubes $NL \geq 10$, the Nusselt number can be calculated from equation (2.31).

$$Nu_D = 1.13 C_1 \, \mathrm{Re}_{D,\mathrm{max}}^m \, \mathrm{Pr}^{1/3}, 2000 < \mathrm{Re}_{D,\mathrm{max}}^m < 40000, \mathrm{Pr} \geq 0.7 \qquad (2.31)$$

When using other fluids to flow through a group of tubes that is less than 10 tubes $NL < 10$, the Nusselt number can be calculated from equation (2.32).

$$Nu_D = 1.13 C_1 C_2 \, \mathrm{Re}_{D,\mathrm{max}}^m \, \mathrm{Pr}^{1/3} \qquad (2.32)$$

2.5.4 Overall heat transfer coefficient of heat exchanger

In the analysis of the heat exchanger, we used the overall heat transfer (U) as the value that indicates the heat transfer from fluid to fluid. The heat transfer between the two fluids has the temperature difference of ΔT, which can be calculated from equation (2.33) [6].

$$Q = UA\Delta T \qquad (2.33)$$

where U is the overall heat transfer coefficient for the heat exchanger, which can be calculated from equation (2.34).

$$U = \frac{1}{(1/h_e)} + \frac{1}{(1/h_c)} \qquad (2.34)$$

Table 2.1 Edit value C_1 when $NL \geq 10$ [6].

S_L/D	S_T/D							
	1.25		1.5		2.0		3.0	
	C_1	m	C_1	m	C_1	m	C_1	m
In-line								
1.25	0.348	0.592	0.275	0.608	0.100	0.704	0.0633	0.752
1.50	0.367	0.586	0.250	0.620	0.101	0.702	0.0678	0.744
2.00	0.418	0.570	0.299	0.602	0.229	0.632	0.198	0.648
3.00	0.290	0.601	0.357	0.584	0.374	0.581	0.286	0.608
Staggered								
0.600	-	-	-	-	-	-	0.213	0.636
0.900	-	-	-	-	0.446	0.571	0.401	0.581
1.000	-	-	0.497	0.558	-	-	-	-
1.125	-	-	-	-	-	-	-	-
1.250	0.518	0.556	0.505	0.554	0.519	0.556	0.522	0.562
1.500	0.451	0.568	0.460	0.562	0.452	0.568	0.488	0.568
2.000	0.404	0.572	0.416	0.568	0.482	0.556	0.499	0.570
3.000	0.310	0.592	0.356	0.580	0.440	0.562	0.428	0.574

Table 2.2 Edit value C_2 when $NL < 10$ [6]

NL	1	2	3	4	5	6	7	8	9
In-line	0.64	0.80	0.87	0.90	0.92	0.94	0.96	0.98	0.99
Staggered	0.68	0.75	0.83	0.89	0.92	0.95	0.97	0.98	0.99

2.5.5 Analysis and calculation of heat exchanger

The basis of the analysis and calculation of the heat exchanger is the calculation of the area in the heat exchange, and after that we can defined the shapes and the sizes of the heat exchanger depending on the usage. The location is an important factor in determining the appropriate position, the size and the area. The analysis requires various information, such as the flow rate of the fluid, the temperatures of the inlet and outlet fluids, the capability of the heat transfer, the quantity of heat in the

transfer and the property of the fluid, etc. The analysis and calculation of the heat exchanger has two methods, which are the log mean temperature difference method (LMTD) and the number of transfer unit method (NTU). In this study, will show the analysis from the NTU method, which can be described as follows:

The analysis by the NTU method has advantages over the LMTD, as we must know the size, type of the heat exchanger, the inlet and outlet temperatures and the flow rate. The NTU method can be calculated from equation (2.35) [6].

$$Q = \varepsilon Q_{max} \tag{2.35}$$

where Q is the actual heat transfer (W).

Q_{max} is the maximum heat transfer (W).

ε is the effectiveness of the heat exchanger.

The actual heat transfer can be calculated from equation (2.36).

$$Q = C_c \left(T_{c,o} - T_{c,i} \right) \tag{2.36}$$

where C_c is the $\dot{m}c_p$ of the cooling fluid.

$T_{c,i}$ is the inlet temperature of the cooling fluid ($°C$).

$T_{c,o}$ is the outlet temperature of the cooling fluid ($°C$).

The maximum heat transfer can be calculated from equation (2.37).

$$Q_{max} = C_{min} \left(T_{h,i} - T_{c,i} \right) \tag{2.37}$$

where $T_{h,i}$ is the inlet temperature of the hot fluid ($°C$).

$T_{h,o}$ is the outlet temperature of the hot fluid ($°C$).

The C_{min} can be calculated from equation (2.38).

$$C_{min} = (\dot{m}c_p)_{min} \qquad (2.38)$$

The velocity (V) can be calculated from equation (2.39).

$$V = \frac{\dot{m}}{\rho A} \qquad (2.39)$$

when C_{min} is less than the $\dot{m}c_p$ between the hot fluid and the $\dot{m}c_p$ of the cool fluid, any value less, it is C_{min}, and likewise when the value is more, it is C_{max}. The value of ε is the ratio of C_{min}/C_{max} and will be analyzed by the NTU method from equation (2.40) [6].

$$NTU = \frac{UA}{C_{min}} \qquad (2.40)$$

The calculation of the effectiveness of the heat exchanger can be determined from equation (2.41) for the counter flow and when $N = NTU = UA/C_{min}$ and $C = C_{min}/C_{max}$ [6].

$$\varepsilon = \frac{1 - \exp\left[-NTU(1-C)\right]}{1 - C\exp\left[-NTU(1-C)\right]} \qquad (2.41)$$

2.6 Literature review

Sakulchangsatjatai [2] improved and extend the mathematical physical model of Shafii et al. (2001), which is used to predict the behavior of the liquid and vapor within a CEOHP and CLOHP at the top heat mode, by increasing the adiabatic section and number of meandering turns. The model of the liquid and vapor behavior was formulated using the following assumptions: the internal flow was a single-phase flow,

the pressure loss at the bend turn was neglected, the liquid was incompressible and the vapor followed the ideal gas law. The principles and theories of the internal friction flow, basic governing equations and finite difference scheme were applied to evaluate the heat transfer rate. The computer program used in this research was the MATLAB program. It was found that the heat transfer of the CEOHP and CLOHP were predicted using the model with the adiabatic section and number of turns and compared with the experimental data of Rittidech et al. (2000) and Charoensawan et al. (2000), respectively. It was concluded that for both types of OHP the calculation results were fairly good when compared with the experimental evaluation. When the number of turns increased, the heat flux was nearly constant due to the symmetry within the heat pipe, as the heat transfer rate is increased. The operations of the CEOHP and CLOHP from the prediction were similar. The CLOHP with ethanol exhibited the highest heat flux, while R123 and water had less heat flux. The heat flux was proportional to the inner diameter of the tube and inversely proportional to the evaporator length.

Pipatpaiboon et al. [3] presented a new type of oscillating heat pipe (OHPs) that was the HOHP. The research aimed to study the effect of the working temperature on the heat transfer characteristics of the HOHP. The HOHP in the research was made from copper tube with an inside diameter of 4 mm. The total length of the HOHP was 3.75 m and consisted of the evaporator and condenser of equal lengths of 1.75 m and the length of the adiabatic was 0.25 m. Water was used as the working fluid at a filling ratio of 50% by total volume. The evaporator section was heated with an electric heater and the condenser section was cooled using an air flow when the air velocity was controlled at 1 m/s. The controlled temperatures at the adiabatic section (working temperature) were 50, 60 and 70ºC respectively. The experimental inclination angles of 20, 40, 60, 80 and 90º from the horizontal axis were used. The results show that the working temperature increased the heat flux of the HOHP, and the maximum heat flux occurred at a working temperature of 70ºC and inclination angle of 60º and it was 3065.08 W/m^2. The HOHP works well at inclination angles between 60-90º

Germano [4] studied the effect of the torsion on a helical pipe. The Navier-Stokes equations for a steady incompressible viscous flow were explicitly written in this frame of reference. The result is that for curvatures and torsions of the same order and

for low Reynolds numbers, the curvature induces a flow with a first-order effect on the parameter $\varepsilon = \kappa a$, where κ is the curvature and a is the radius of the pipe.

Akbaridoust et al. [7] studied the laminar, steady state flow in helically coiled tubes at a constant wall temperature numerically and experimentally. In the experimental section, a heat exchanger was designed that was capable of providing a constant wall temperature for the coils with different curvatures and torsion ratios for the ease of assembly. In the numerical study, the three dimensional governing equations were solved by the finite difference method with a projection algorithm using the FORTRAN programming language. It was found that the heat transfer was observed for tubes with greater curvature ratios. The utilization of a base fluid in a helical tube with a greater curvature compared to the use of a nanofluid in straight tubes enhanced the heat transfer more effectively.

Boothaisong [8] studied a three-dimensional model to simulate the heat transfer rate on a heat pipe in a transient condition. This article presents the details of a calculation domain consisting of a wall, a wick and a vapor core. The governing equation was numerically simulated using the finite element method. The three dimensional model attempted to predict the transient temperature, the velocity and the heat transfer rate profiles. The values obtained from the model calculation were then compared with the results from the experiments. The experiment showed that the time required to attain a steady state was reasonably consistent with the model. The working fluid r134a was the quickest to reach the steady state and transferred the greatest amount of heat.

Jayakumar et al. [9] studied the CFD analysis of single-phase flows inside helically coiled tubes. It has been well established that the heat transfer in a helical coil is higher than that in a corresponding straight pipe. This study presented the variation of the local Nusselt number along the length and circumference at the wall of a helical pipe. CFD simulations are carried out for vertically oriented helical coils by varying the coil parameters, such as (i) pitch circle diameter, (ii) tube pitch and (iii) pipe diameter, and their influence on the heat transfer was studied. After establishing the influence of these parameters, correlations for the prediction of the Nusselt number were developed. A correlation to predict the local values of the Nusselt number as a function of the angular location of the point was also presented.

Mahasarakham University

Litster et al. [10] studied a 3D numerical analysis of the flow and mass transfer in helical pipes. The interpretation of the flow patterns and their impact on mass transfer is shown to require a non-orthogonal pseudo-stream function based visualization. The strong coupling between the torsion and curvature effects and the resulting secondary flow regimes are well characterized by a parameter combining both the Dean (Dn) and Germano numbers (Gn). For membrane separation applications, helical modules combining high curvature with low torsion would alleviate the concentration polarization and yield an appreciable flux improvement.

Nobari and Malvandi [11] studied the compressible viscous flow in a helical annulus numerically. A second order finite difference method based on the projection algorithm was used to solve the governing equations. Considering the hydrodynamically fully developed flow, the effects of different physical parameters, such as aspect ratio, torsion, curvature and Reynolds number, on the flow field were investigated in detail. The numerical results obtained indicated that a decrease in the aspect ratio and torsion number lead to an increase in the friction factor at a given Dean number.

Saffari and Moosavi [12] investigated the turbulent single-phase and two-phase (air–water) bubbly fluid flows in a vertical helical coil with analysis using computational fluid dynamics (CFD). The effects of the pipe diameter, coil diameter, coil pitch, Reynolds number and void fraction on the pressure loss, friction coefficient and flow characteristics were investigated. The three-dimensional governing equations of the continuity, momentum and energy were solved using the finite volume method. The SIMPLE algorithm was employed to solve the velocity and pressure fields. The results show that the friction coefficient increases with an increase in the curvature, pipe diameter and coil pitch and decreases with an increase in the coil diameter and void fraction. For void fractions up to 0.1, the numerical results indicate that the friction coefficient increases with an increase in the pipe diameter while keeping the coil pitch and diameter constant and decreases with an increase in the coil diameter. Finally, with an increase in the Reynolds number, the friction coefficient decreases while the void fraction increases.

Sakulchangsatjatai et al. [13] studied the heat transfer characteristics of a CEOHP and a CLOHP under normal operating conditions that were modeled using the explicit finite element method. The principles and theories of the internal friction flow,

basic governing equations and finite difference scheme were applied to evaluate the heat transfer rate. The predicted heat transfer rate, obtained from the model, was compared to the existing experimental data. The effects of the working fluid, evaporator length and inner diameter on the performance of a CEOHP and a CLOHP were also investigated.

Sriudom et al. [14] studied the effect of the evaporator temperature, pitch distance and working fluid on the internal flow pattern and the heat transfer characteristics of the helical oscillating heat pipe. A Pyrex tube with an inner diameter of 2.4 mm was used to study the flow pattern in the evaporator section. Water and R123 were used as working fluids. In the evaporator section, the water temperature was varied at 60, 75 and 90ºC. In the condenser section, the air had a temperature of 25ºC. From the results, it was found that there were four internal flow patterns (bubble flow, slug flow, annular flow and stratified wavy flow). The maximum heat fluxes were 2,132.6 and 1,773.4 W/m^2 for the working fluids of R123 and water, respectively.

CHAPTER 3

RESEARCH METHODOLOGY

This chapter sets out details of the research methodology of the HOHP mathematical model, it divided into three parts as follows:

1. Mathematical model and numerical solution.
2. Experimental evaluation.
3. HOHP application to a HOHP heat exchanger.

3.1 Mathematical model and numerical solution

3.1.1 Mathematical model

The mathematical model was established to check the accuracy of the program by comparing prediction with the experimental results using the following conditions:

1) Working fluids of water, ethanol and R11.
2) Temperatures at the evaporator section were 60, 70 and 80ºC.
3) Inner diameters were 1.6, 1.8 and 2.0 mm and thickness was 0.5 mm.
4) Total length of the pipe at the evaporator section was 850 mm.
5) Total length of the pipe at the condenser section was 850 mm.
6) Length of the adiabatic section was 50 mm.
7) Temperature of the water in the condenser section was 20ºC.
8) Inclination angle was 90º from the horizontal.
9) Number of coils in the evaporator and the condenser sections were 5.
10) Diameter of coil was 50 mm.
11) Pitch was 10 mm.

Assumptions used in model were as follows:

1) Initial temperature of the working fluid was 25ºC.
2) Gravity does not effect on the HOHP.
3) The analysis assumed that the HOHP can be stretched in a straight line.

4) The convective heat transfer coefficient at the evaporator and the condenser sections were constant.

5) The working fluid in the HOHP was an idea gas.

6) The pressure in the HOHP was constant.

7) The temperatures of the evaporator and the condenser sections were constant.

8) The mass flow rate of the working fluid in the HOHP was constant.

From the assumptions above we can create the model for the analysis of the HOHP, as can be seen in figure 3.1(b).

3.1.2 Numerical solution

The numerical solution uses the numerical method with the temperature of the pipe wall and the temperature of the fluid within the HOHP, which can be seen in figure 3.1. The finite difference method is used for the solution of the conduction equation of the pipe wall and the flow equation of the vapor in the HOHP. The finite difference method divides the area into numerous small grids that have precise values in the calculation. The numerical solution of the HOHP is:

3.1.2.1 Condition in calculation

At the end of pipe ($x = 0$ and $x = L_e + L_a + L_c$):

$$w_v = 0 \tag{3.1}$$

At the evaporator section:

$$\frac{\partial T}{\partial x} = T_e \tag{3.2}$$

At the adiabatic section:

$$\frac{\partial T}{\partial x} = T_{initial} \qquad (3.3)$$

At the condenser section:

$$\frac{\partial T}{\partial x} = T_c \qquad (3.4)$$
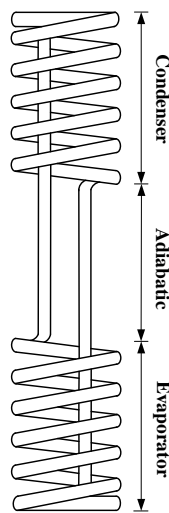
(a) The HOHP
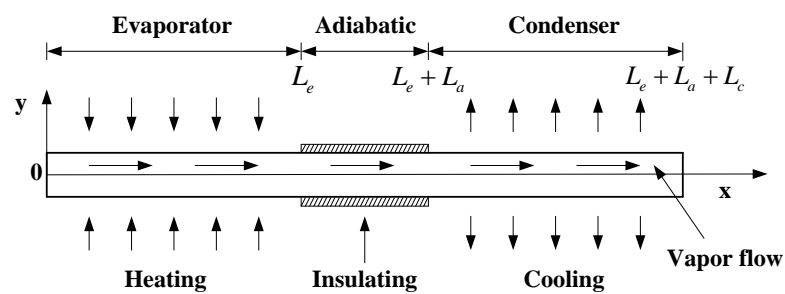
(b) Schematic of the HOHP used in the model

Figure 3.1 HOHP and schematic of HOHP used in analysis of model [21]

3.1.2.2 Solution of conduction equation

From the energy conservation in equation (2.10) in chapter 2, the energy inflow can be calculated from equation (3.5).

$$\dot{E}_{in} = q_s \tag{3.5}$$

where q_s is heat transfer rate in the s direction.

The energy outflow can be calculated from equation (3.6).

$$\dot{E}_{out} = -q_{s+ds} \tag{3.6}$$

when

$$q_{s+ds} = q_s + \frac{\partial q_s}{\partial s} ds \tag{3.7}$$

where q is heat transfer rate at $s+ds$ in the s direction.

Inside equation (2.10) has the energy term of the energy generation, which can be calculated from equation (3.8).

$$\dot{E}_g = \dot{q} \, ds \tag{3.8}$$

where $\dot{q}$ is the energy rate in the volume (W/m^3).

A variation will occur in the quantity of the heat energy stored in the material at the control volume. If it is assumed that the material does not experience a state change, therefore the term of the energy storage can be calculated from equation (3.9).

$$\dot{E}_{st} = \rho c_p \, \frac{\partial T}{\partial t} \, ds \tag{3.9}$$

where $\rho\, c_p\, \dfrac{\partial T}{\partial t}$ is the rate of the heat energy that is changed in an appropriate time per volume.

Substituting equations (3.5), (3.6), (3.8) and (3.9) into equation (2.10) in chapter 2, we obtain the energy conservation as:

$$q_s + \dot{q}ds - q_{s+ds} = \rho c_p \frac{\partial T}{\partial t}\, ds \tag{3.10}$$

Substituting equation (3.7) into equation (3.10), we obtain:

$$-\frac{\partial q_s}{\partial s}ds + \dot{q}ds = \rho c_p \frac{\partial T}{\partial t}\, ds \tag{3.11}$$

The conduction rate can be considered by Fourier's Law in equation (3.12).

$$q = -kA\, \Delta T \tag{3.12}$$

where q is the heat transfer rate, k is the thermal conductivity, A is the area for the heat transfer and ΔT is the difference in the temperature before and after the received heat, we obtain:

$$q_s = -k\frac{\partial T}{\partial s} \tag{3.13}$$

Substituting equation (3.13) into equation (3.11), we obtain:

$$-\frac{\partial}{\partial s}\left(-k\frac{\partial T}{\partial s}\right)ds + \dot{q}ds = \rho c_p \frac{\partial T}{\partial t}\, ds \tag{3.14}$$

Using ds to divide every term in equation (3.14) and rearranging the equation, we obtain the conduction equation of the HOHP in the 1-D transient as:

$$\rho_w c_{p,w} \frac{\partial T}{\partial t} = \frac{\partial}{\partial s}\left(k_w \frac{\partial T}{\partial s} \right) + \dot{q} \tag{3.15}$$

3.1.2.3 Solution of conservation of mass equation

From the conservation of mass equation in equation (2.11) in chapter 2, the first term is a variation in the rate of the mass in the control volume and when used with fluid particles can be obtain as:

$$\frac{\partial}{\partial t}\left(\rho ds \right) \tag{3.16}$$

The second term in equation (2.11) in chapter 2 is the variation in the rate of mass flow though the surface of the control volume, due to the density functions of distance and time, therefore the mass flow rate is:

In axial direction S $$\left(\rho w |_{s+ds} - \rho w |_s \right) = \left(\rho w + \frac{\partial(\rho w)}{\partial s} ds \right) \tag{3.17}$$

Substitution equation (3.16) and (3.17) into equation (2.11) in chapter 2, we obtain:

$$\frac{\partial}{\partial t}\left(\rho ds \right) + \left(\rho w + \frac{\partial \rho w}{\partial s} ds \right) = 0 \tag{3.18}$$

Dividing equation (3.18) by ds, we obtain the continuity equation of the HOHP [1]:

$$\frac{\partial rw}{\partial s} = 0 \tag{3.19}$$

3.1.2.4 Solution of conservation of momentum equation

From the conservation of momentum equation in equation (2.12) in chapter 2, when using ds to divide the momentum equation and taking the limit of volume ds into zero, to limit both equations, we obtain:

$$\lim_{ds \to 0} \frac{\vec{F}_S}{ds} + \lim_{ds \to 0} \frac{\vec{F}_B}{ds} = \lim_{ds \to 0} \frac{\frac{\partial}{\partial t} \int_{cv} \vec{V} \rho d\forall}{ds} + \lim_{ds \to 0} \frac{\int_{cs} \vec{V} \rho \vec{V} \cdot d\vec{A}}{ds} \tag{3.20}$$

For the two terms on the left hand side of equation (3.20), which are the force at the surface and the force per volume on the surface of the fluid particle, the details are shown in figure 2.6 in chapter 2, and can be written as the force at the surface and the force of the mass in the s direction as the following:

$$\vec{F}_S + \vec{F}_B = \left(\sigma_{ss}\big|_{s+ds} - \sigma_{ss}\big|_s \right) + \left(\tau_{ss}\big|_{s+ds} - \tau_{ss}\big|_s \right) \tag{3.21}$$

When using the force in the s direction and substituting in equation (3.21), we obtain:

$$\lim_{ds \to 0} \frac{\vec{F}_S}{ds} + \lim_{ds \to 0} \frac{\vec{F}_B}{ds} = \lim_{ds \to 0} \frac{\left(\sigma_{ss}\big|_{s+ds} - \sigma_{ss}\big|_s \right)}{ds} + \lim_{ds \to 0} \frac{\left(\tau_{ss}\big|_{s+dsr} - \tau_{ss}\big|_s \right)}{ds} \tag{3.22}$$

Equation (3.22) can be written as:

$$\lim_{ds \to 0} \frac{\vec{F}_S}{ds} + \lim_{ds \to 0} \frac{\vec{F}_B}{ds} = \frac{\partial \sigma_s}{\partial s} + \frac{\partial \tau_s}{\partial s} \tag{3.23}$$

For the first term on the right hand side in equation (3.20), its variation rate of the momentum within the control volume per unit of volume can be calculated from equation (3.24).

$$\lim_{ds \to 0} \frac{\dfrac{\partial}{\partial t} \displaystyle\int_{cv} \vec{V} \rho \, d\forall}{ds} = \lim_{ds \to 0} \frac{\partial}{\partial t}\left(\frac{\rho \vec{V} ds}{ds} \right) = \frac{\partial}{\partial t}\left(\rho \vec{V} \right) = \vec{V} \frac{\partial \rho}{\partial t} + \rho \frac{\partial \vec{V}}{\partial t} \qquad (3.24)$$

The second term on the right hand side in equation (3.20) is the variation of the flow of the momentum though the surface of the control volume per unit of volume, which can be calculated from equation (3.25).

$$\lim_{ds \to 0} \frac{\displaystyle\int_{cs} \vec{V} \rho \vec{V} \cdot d\vec{A}}{ds} = \lim_{ds \to 0} \frac{\left(\rho \vec{V} w \big|_{s+ds} - \rho \vec{V} w \big|_{s} \right)}{ds} \qquad (3.25)$$

Equation (3.25) can be written as:

$$\lim_{ds \to 0} \frac{\displaystyle\int_{cs} \vec{V} \rho \vec{V} \cdot d\vec{A}}{ds} = \lim_{ds \to 0} \frac{\left(\rho \vec{V} w \big|_{s+ds} - \rho \vec{V} w \big|_{s} \right)}{ds} = \frac{\partial}{\partial s}\left(\rho \vec{V} w \right) \qquad (3.26)$$

Re arranging equation (3.26), we obtain:

$$\lim_{ds \to 0} \frac{\displaystyle\int_{cs} \vec{V} \rho \vec{V} \cdot d\vec{A}}{ds} = \vec{V}\left[\frac{\partial}{\partial s}\left(\rho w \right) \right] + \rho \left[w \frac{\partial \vec{V}}{\partial s} \right] \qquad (3.27)$$

From the continuity equation in equation (3.19).

$$\frac{\partial}{\partial s}\left(\rho w \right) = 0$$

Therefore, equation (3.27) can be re written as:

$$\lim_{ds \to 0} \frac{\int_{cs} \vec{V} \rho \vec{V} \cdot d\vec{A}}{ds} = -\vec{V}\left[\frac{\partial \rho}{\partial t}\right] + \rho\left[w\frac{\partial \vec{V}}{\partial s}\right] \tag{3.28}$$

Substituting equations (3.23), (3.24) and (3.28) into equation (3.20), we obtain:

$$\rho\left(\frac{\partial w}{\partial t} + w\frac{\partial w}{\partial s}\right) = \frac{\partial \sigma_s}{\partial s} + \frac{\partial \tau_s}{\partial s} \tag{3.29}$$

The momentum conservation in equation (3.29) can be written as the momentum equation of the flow of the HOHP in the 1-D transient as [1]:

$$\frac{\partial w}{\partial t} + \frac{1}{h_s}\left(\frac{\partial w}{\partial s}\right) + \frac{\kappa \sin(\theta - \tau s)}{h_s}w + \frac{\kappa \cos(\theta - \tau s)}{h_s}w = -\frac{1}{h_s}\frac{\partial p}{\partial s} + \frac{1}{\mathrm{Re}}\left[\frac{1}{h_s}\frac{\partial}{\partial s}\left(\frac{1}{rh_s}\frac{\partial rw}{\partial s}\right)\right] \tag{3.30}$$

3.1.2.5 Solution of conservation of energy equation

From the conservation of energy equation in equation (2.13) in chapter 2, multiplying by the velocity of flow, it will become rate of work as:

$$\rho \vec{f} \cdot \vec{V} ds \tag{3.31}$$

From figure 2.7 in chapter 2, the rate of work occurring in the s direction can be calculated from equation (3.32).

$$\left[-\frac{\partial(wp)}{\partial s} + \frac{\partial(w\sigma_{ss})}{\partial s} + \frac{\partial(w\tau_{ss})}{\partial s}\right]ds + \rho \vec{f} \cdot \vec{v} ds \tag{3.32}$$

The heat flux occurring from the mass can be calculated from equation (3.33).

$$\rho \bar{Q}\, ds \tag{3.33}$$

The total heat flux from the heat transfer in the s direction can be calculated from equation (3.34).

$$\left[q_s - \left(q_s + \frac{\partial q_s}{\partial s} \right) \right] ds \tag{3.34}$$

Therefore, the total heat flux on the mass can be calculated from equation (3.35).

$$\left[\rho \bar{Q} - \frac{\partial q_s}{\partial s} \right] ds \tag{3.35}$$

From Fourier's Law, the heat flux q_s variation on the slope of the temperature can be seen in equation (3.36).

$$q_s = -k \frac{\partial T}{\partial s} \tag{3.36}$$

Substituting equation (3.35) into equation (3.36), we can calculate the total heat flux from equation (3.37).

$$\left[\rho \bar{Q} + \frac{\partial}{\partial s} \left(k \frac{\partial T}{\partial s} \right) \right] ds \tag{3.37}$$

Substituting equation (3.37) into the conservation of energy equation in equation (2.13) in chapter 2, we obtain the energy equation of the HOHP as:

$$\rho \frac{D}{Dt}\left(e+\frac{V^2}{2}\right)ds = \left[\rho\bar{Q}+\frac{\partial}{\partial s}\left(k\frac{\partial T}{\partial s}\right)\right]ds + \rho\vec{f}\cdot\vec{V}ds \qquad (3.38)$$

The equation (3.38) is in the form of absolute derivatives, which can be changed into simple derivatives for use with the conduction, the continuity and the momentum equations. The energy equation of the flow of the HOHP in the 1-D transient can be calculated from equation (3.39) [1].

$$\frac{\partial T}{\partial t}+\frac{w}{h_s}\frac{\partial T}{\partial s}=\frac{1}{\text{Re}\,\text{Pr}\,h_s r}\frac{\partial}{\partial s}\left(\frac{r}{h_s}\frac{\partial T}{\partial s}\right) \qquad (3.39)$$

3.1.2.6 Solution of heat transfer equation of HOHP

From the heat transfer equations in equations (2.14) and (2.15) in chapter 2, they can be changed to the finite difference method form, as is shown in equations (3.40) and (3.41).

$$Q_v^{new} = \dot{m}_v h_{fg,i} \qquad (3.40)$$

$$Q_{out}^{new} = \pi D h_c (T_{v,i}-T_{w,i}) \qquad (3.41)$$

3.1.2.7 Flow chart of program

The numerical procedure is illustrated in figure 3.2. The calculation procedure of the simulation program is as follows:

1) Input the lengths of the evaporator section (L_e), the adiabatic section (L_e) and the condenser section (L_c); the outer diameter (D_o) and inner diameter (D_i); the temperatures of the evaporator (T_e) and the condenser sections (T_c); and the working fluid within the HOHP.

2) Start calculation at the first point $i=1$.

3) Input the initial temperature of the pipe wall of the HOHP ($T_{w,ini}$), the thermal conductivity of the pipe wall (k_w), the density of the pipe wall (ρ_w), the specific heat ($C_{p,w}$) and the grid size in the s direction (Δs), and then calculate the temperature of the pipe wall in the conduction equation.

4) Input the initial velocity of the vapor in the HOHP (w_{ini}), the grid size in the s direction (Δs), the scale factor (h_s), the pressure (p), the Reynolds number (Re), the curvature ratio (κ), the inclination angle (θ) and the density of the working fluid (ρ), and then calculate the velocity of the vapor in the continuity and momentum equations.

5) Input the initial temperature of the vapor in the HOHP ($T_{v,ini}$), the velocity of the vapor (w), the grid size in the s direction (Δs), the scale factor (h_s), the Reynolds number (Re), the Prandtl number (Pr) and the radial of the HOHP (r), and then calculate the temperature of the vapor in the energy equation.

6) Receive the data of the temperature: the temperature of the pipe wall (T_w) and the temperature of the vapor (T_v) from the conduction and energy equations.

7) Input the inner diameter of the HOHP (D_i) and the convection heat transfer coefficient (h) and then calculate the heat transfer of the HOHP in the heat transfer equation.

8) Calculate the next point $i = i + 1$, and check the last point in the calculation as to whether this is equal to the maximum point or not.

9) If the last point is equal to the maximum point, stop the calculation, or if it is not equal to the maximum point, return to the first step.

When the calculation is finished, the working fluid should be changed from water into ethanol and R11.
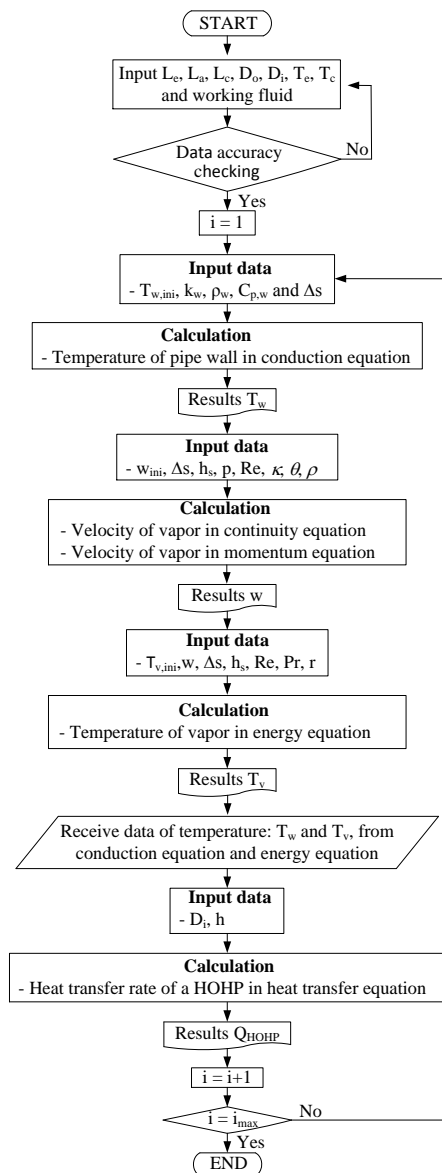
Figure 3.2 Flow chart for calculation of HOHP

3.2 Experimental evaluation

3.2.1 Variables in experiment

3.2.1.1 Dependent variables

1) Working fluids were water, ethanol and R11.

2) Temperatures of the evaporator section were 60, 70 and 80°C.

3) HOHP made from copper pipe with inner diameters of 1.6, 1.8 and 2.0 mm and thickness of 0.5 mm.

3.2.1.2 Dependent parameters

    1) Temperature of the HOHP.

    2) Heat transfer of the HOHP.

3.2.1.3 Control parameters

    1) Total length of the pipe at the evaporator section was 850 mm.

    2) Total length of the pipe at the condenser section was 850 mm.

    3) Length of the adiabatic section was 50 mm.

    4) Temperature of the water in the condenser section was 20ºC.

    5) Mass flow rate of the water at the evaporator and the condenser sections was 0.25 kg/min.

    6) Filling ratio was 80% with respect to the total volume of the HOHP.

    7) Inclination angle was 90º to the horizontal.

    8) Number of coils in the evaporator and the condenser sections were 5.

    9) Diameter of coil was 50 mm.

    10) Pitch was 10 mm.

3.2.2 HOHP in experimental evaluation

    3.2.2.1 The HOHP was made from copper pipe. The HOHP had three section: the evaporator, the adiabatic and the condenser sections, and is shown in figure 3.3.
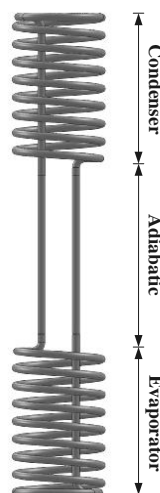
Figure 3.3 HOHP

3.2.3 Equipment and measurements used during experiment

3.2.3.1 Data logger

The data logger measured the temperature at any point and recorded the data. The data logger is a Yokogawa DX200 with ±0.1°C accuracy, 20 channel input and a -200°C to 1100°C measurement temperature range, as shown in figure 3.4.

Figure 3.4 Data logger

3.2.3.2 Thermocouples

The thermocouples used in the experimental were type K (OMEGA with ±0.1°C accuracy); the range of the operating temperature was between -100 and 1300°C, as shown in figure 3.5.

Figure 3.5 Thermocouples

3.2.3.3   Working fluid filling set

The working fluid filling set consisted of four valves: a burette or pipette was connected to valve A for filling the working fluid, valve B was connected to a vacuum pump, valve C was connected to the heat pipe or tube and valve D was connected to a pressure gauge for measuring the pressure in the tube, as shown in figure 3.6.
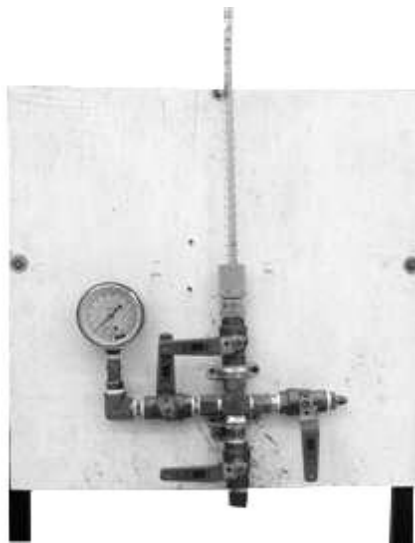
Figure 3.6 Working fluid filling set

3.2.3.4   Hot water bath

A hot water bath was used to control the temperature of the water and to heat it to set the temperature. This study used a TECHNE TE-10D with an operating range of -40 to 120°C and ±0.1°C accuracy, as shown in figure 3.7.
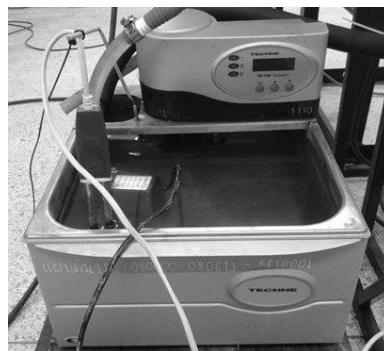
Figure 3.7 Hot bath

3.2.3.5   Cold water bath

The cold water bath was used to control the temperature and cool down the water to the set-up temperature. This study used an six liters EYELA CA -1111 with an operating temperature range of -20 to 30°C and ±2°C accuracy, as shown in figure 3.8.

Figure 3.8 Cool bath

3.2.3.6   Flow meter

The flow meter was used for measuring and controlling the flow rate of the water into the condenser and evaporator sections. This study used a PLATON PTF2 ASS-C with a flow rate of 0.2-1.5 liter/min. A floating rotameter was applied, as shown in figure 3.9.

Figure 3.9 Flow meter

3.2.3.7 Vacuum pump

A vacuum pump was used with the HOHP to create a vacuum before filling the working fluid shown in figure 3.10.
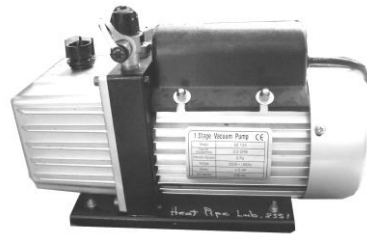
Figure 3.10 Vacuum pump

3.2.4 Experimental setup

The experimental setup of the HOHP is shown in figure 3.11, and a photograph of the experimental setup is shown in figure 3.12.
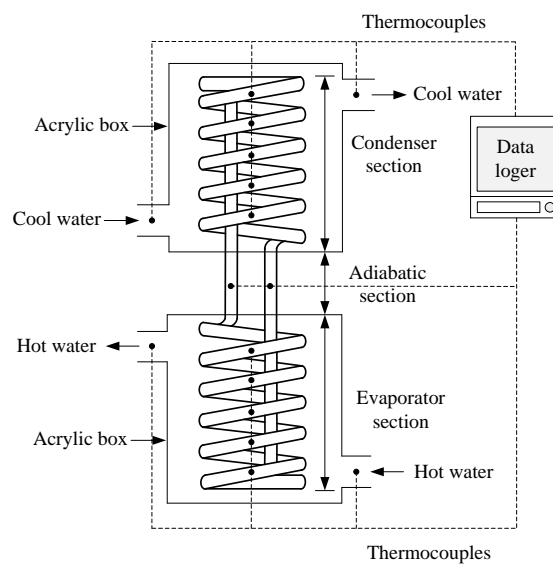
Figure 3.11 Schematic diagram of experimental setup of HOHP
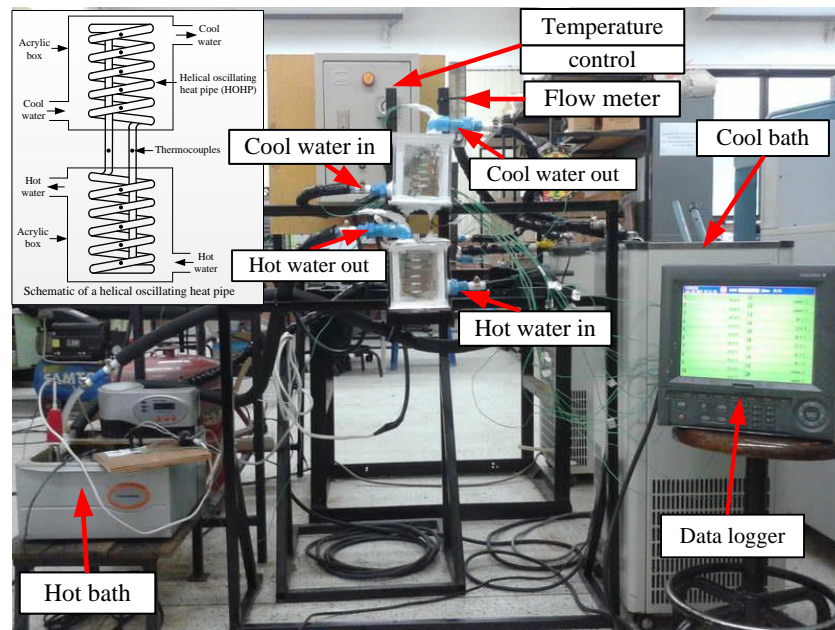
Figure 3.12 Experimental setup of HOHP

3.2.5 Experimental procedure

3.2.5.1   The HOHP was made from copper pipe with an inner diameter determined from the scope of the experiment.

3.2.5.2   Fill the working fluid into the HOHP using the working fluid filling set as shown in figure 3.6, for which the procedure is as follows:

1) Close valves A, B and C, then join the HOHP into the working fluid set.

2) Open the vacuum pump and open valves A, B, D, and C for suction of the air out of the HOHP. When the HOHP has a vacuum, which can be seen from the pressure gauge, close valves A, B and D.

3) Fill the working fluid into the glass tube, then open valve C for the working fluid to flow into the filling working fluid set, and then open valve B and the working fluid will be able to flow to the HOHP.

4) When the working fluid has flown into the HOHP, then close valve B and close the end of the pipe by welding it. We have the HOHP for the experiments.

3.2.5.3   Set up the HOHP with the experimental platform, which can be seen in figure 3.13.

3.2.5.4   Set the hot water bath for boiling the water to the temperature of 60ºC and open the pump that will pump the hot water to the evaporator section of the HOHP. At the condenser section, set the cold water bath for the cool water to the temperature of 20ºC and open the pump that will pump the cooling water to the condenser section of the HOHP.

3.2.5.5   Set the flow meter to 0.25 kg/min for the water at the inlets of the evaporator and the condenser sections.

3.2.5.6   Open the data logger to save the pipe wall temperature at the evaporator, the adiabatic and the condenser sections and the inlet and outlet temperatures of the condenser section.

3.2.5.7   Perform the experimental from the first step to the last step, for which the working fluids, the temperatures of the evaporator section and the inner diameters are as shown in the scope of the experiment.
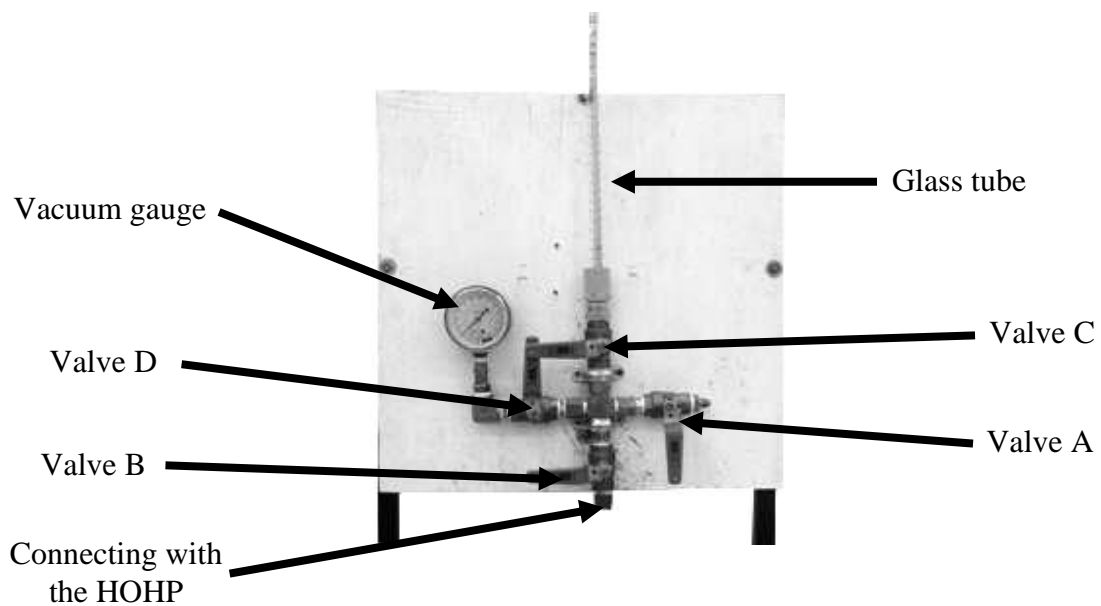
Figure 3.13 Filling working fluid procedure

3.2.6 Data analysis

The heat transfer of the HOHP can be calculated from equation (3.42).

$$Q = \dot{m} c_p (T_{out} - T_{in}) \qquad (3.42)$$

where Q is the heat transfer of the HOHP (W).

$\dot{m}$ is the mass flow rate of the cooling water (kg/s).

c_p is the specific heat of the cooling water (J/kg°C).

T_{in} is the inlet temperature of the cooling water at the condenser (°C).

T_{out} is the outlet temperature of the cooling water at the condenser

(°C).

3.3 HOHP application to a HOHP heat exchanger

In the application of the heat exchanger, we want the heat exchange from the heat exchanger to be 1000 W, which has the details as in the following:

3.3.1 Scope of HOHP heat exchanger

3.3.1.1   Working fluid that provided the best heat transfer from the scope of the experiment in topic 1.3.2 in chapter 1.

3.3.1.2   Temperature that provided the best heat transfer from the scope of the experiment in topic 1.3.2 in chapter 1.

3.3.1.3   HOHP made from copper pipe that provided the best heat transfer from the scope of the experiment in topic 1.3.2 in chapter 1.

3.3.1.4   Temperature of the water in the condenser section was 20°C.

3.3.1.5   Mass flow rates of the water at the evaporator and the condenser sections were 0.25 kg/min.

3.3.1.6   Total length of the pipe at the evaporator section that provided the best heat transfer from the scope of the experiment in topic 1.3.2 in chapter 1.

3.3.1.7   Total length of the pipe at the condenser section that provided the best heat transfer from the scope of the experiment in topic 1.3.2 in chapter 1.

3.3.1.8   Length of the adiabatic section was 50 mm.

3.3.1.9   Inclination angle was 90° from the horizontal.

3.3.1.10 Heat exchanger had counter flow arrangement.
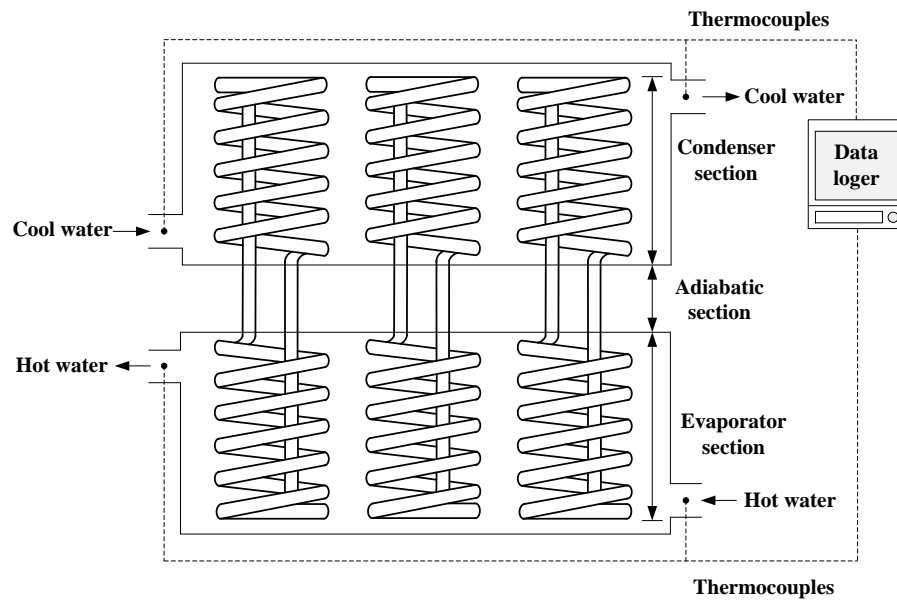
Figure 3.14 Schematic diagram of experimental setup of HOHP heat exchanger
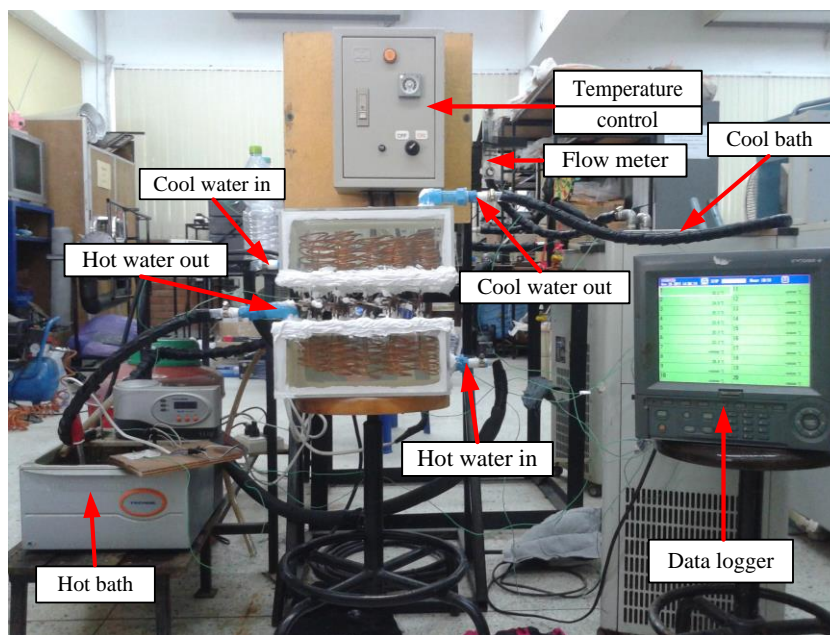
Figure 3.15 Experimental setup of HOHP heat exchanger

3.3.2 Experimental procedure of heat exchanger

3.3.2.1   Create the heat exchanger from the HOHP with the number of tubes as calculated by the model and with the inner diameter that performs the best heat transfer.

3.3.2.2   Filling of the working fluid that has best heat transfer into the HOHP, for which the procedure will be the same as with filling the working fluid of the HOHP.

3.3.2.3   Setup the heat exchanger with the experimental platform, which is shown in figure 3.14 and figure 3.15.

3.3.2.4   Open the hot water bath for the boiling water to the temperature has the highest heat transfer, and open the pump that pumps the hot water to the evaporator section of the heat exchanger. At the condenser section, open the cold water bath for cooling the water to the temperature of 20ºC, and open the pump that pumps the cooling water to the condenser section of the heat exchanger.

3.3.2.5   Set the flow meter to 0.25 kg/min for the water at the inlets of the evaporator and the condenser sections.

3.3.2.6   Open the data logger to save the temperatures at the inlet and outlet of the condenser section.

3.3.3 Data analysis of heat exchanger

The heat transfer of the heat exchanger can be calculated:

$$Q = \varepsilon Q_{max} \tag{3.43}$$

where Q is the actual heat transfer (W).

   Q_{max} is the maximum heat transfer (W).

   ε is the effectiveness of the heat exchanger.

CHAPTER 4

RESULTS AND DISCUSSION

This chapter describes the results and discussions about the temperature and the heat transfer of the HOHP when studying the mathematical model under the transient condition. It is divided into three parts as follows:

1. Results from mathematical model.
2. Results from experimental evaluation.
3. Comparison of results from model and experiment.

4.1 Results from mathematical model

4.1.1 Temperature at pipe wall of HOHP from model

Figure 4.1 shows the temperature profiles at the pipe wall of the HOHP at the evaporator, the adiabatic and the condenser sections from the numerical model with the outer wall temperatures at the evaporator section of 60, 70 and 80°C, and water as the working fluid. The transient temperature profiles were plotted as functions of time. It was found that the transient temperature profiles in the evaporator section increased from the initial temperature at the outer pipe wall (25°C) to the temperatures that were input at the evaporator section (60, 70 and 80°C). Since the material of the pipe wall was copper, thermal conduction was induced from the outer wall of the pipe to the inner wall of the pipe. In the adiabatic section, heat was induced by thermal conduction from the evaporator section. The temperature of the adiabatic section increased until it reached a steady state, at which it was close to the working temperatures (the average value of the temperatures between the evaporator and the condenser sections). However, the transient temperature profiles in the condenser section decreased because the initial temperature of the outer pipe wall (25°C) was more than the temperature of the condenser section (20°C). The times required to reach the steady state temperature at the end of the runs from the numerical model were about 1300, 1600 and 2000 s for the temperatures at the evaporator section of 60, 70 and 80°C, respectively. As seen from figure 4.1, the temperature at the evaporator section increased, and the time required to

reach the steady state temperature was increased because the temperature was dependent on the time.
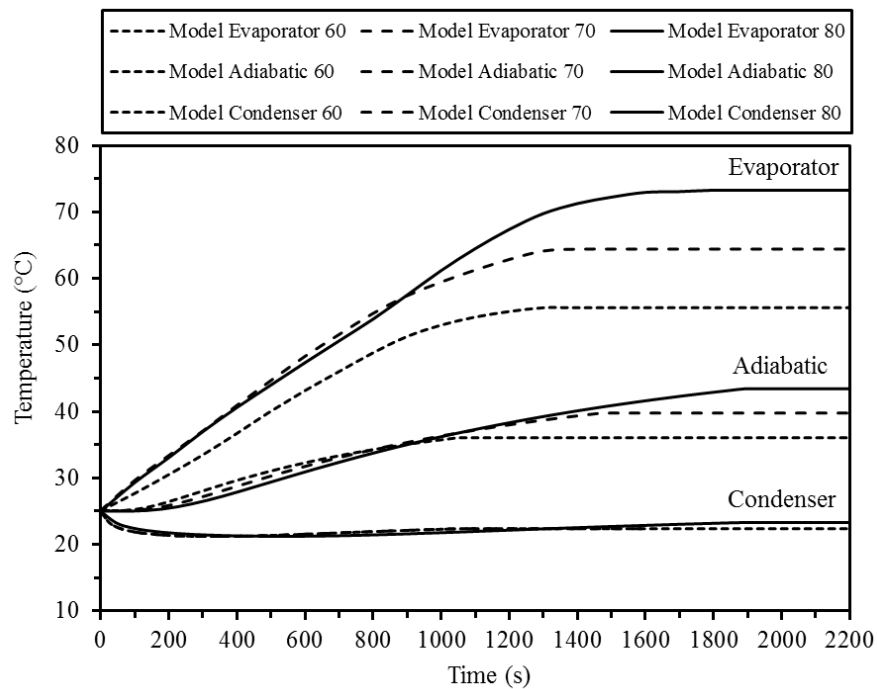
Figure 4.1 Temperature profiles at pipe wall of HOHP from model
at T_e = 60, 70 and 80°C with working fluid of water

Figure 4.2 shows the temperature profiles at the pipe wall of the HOHP at the evaporator, the adiabatic and the condenser sections from the numerical model with the outer wall temperatures at the evaporator section of 60, 70 and 80°C, and ethanol as the working fluid. The transient temperature profiles were plotted as functions of time. It was found that the transient temperature profiles in the evaporator section increased from the initial temperature at the outer pipe wall (25°C) to the temperatures that were input at the evaporator section (60, 70 and 80°C). Since the material of the pipe wall was copper, thermal conduction was then induced from the outer wall of the pipe to the inner wall of the pipe. In the adiabatic section, heat was induced by thermal conduction from the evaporator section. The temperature of the adiabatic section increased until it reached a steady state, in which it was close to the working temperatures (the average

value of the temperatures between the evaporator and the condenser sections). However, the transient temperature profiles in the condenser section decreased because the initial temperature of the outer pipe wall (25°C) was more than the temperature of the condenser section (20ºC). The times required to reach the steady state temperature at the end of the runs from the numerical model were about 1200, 1500 and 1900 s for the temperatures at the evaporator section of 60, 70 and 80ºC, respectively. As seen from figure 4.2, the temperature at the evaporator section increased, and the time required to reach the steady state temperature was increased because the temperature was dependent on the time.
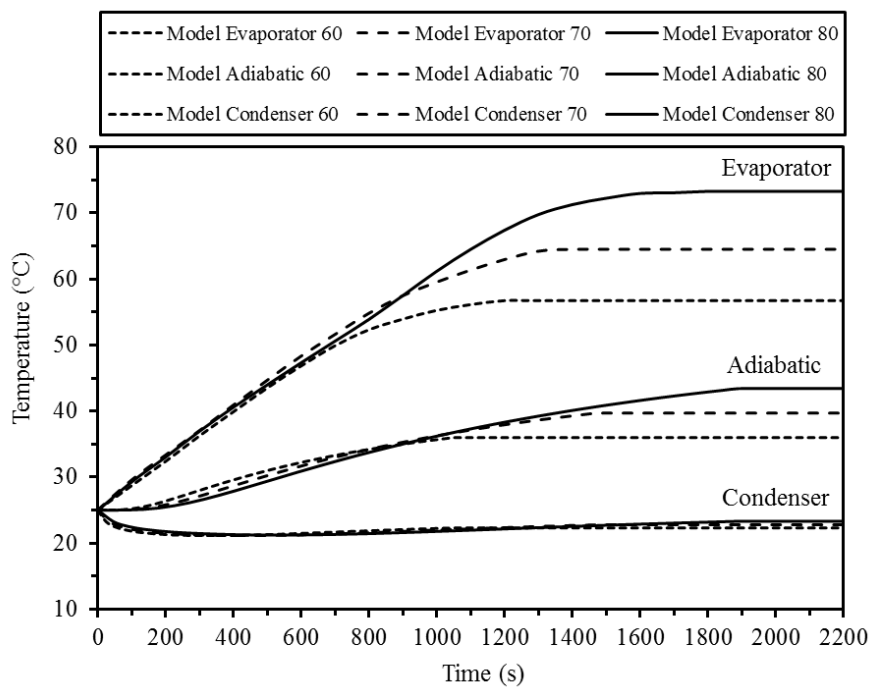
Figure 4.2 Temperature profiles at pipe wall of HOHP from model
at T_e = 60, 70 and 80ºC with working fluid of ethanol
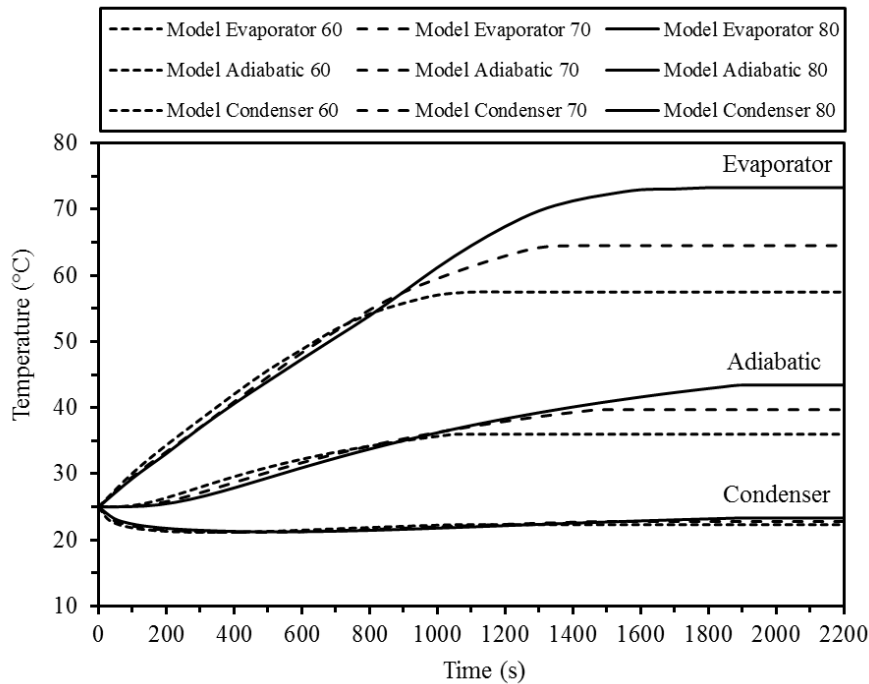
Figure 4.3 Temperature profiles at pipe wall of HOHP from model

at T_e = 60, 70 and 80ºC with working fluid of R11

Figure 4.3 shows the temperature profiles at the pipe wall of the HOHP at the evaporator, the adiabatic and the condenser sections from the numerical model with the outer wall temperatures at the evaporator section of 60, 70 and 80°C, and R11 as the working fluid. The transient temperature profiles were plotted as functions of time. It was found that the transient temperature profiles in the evaporator section increased from the initial temperature at the outer pipe wall (25°C) to the temperatures that were input at the evaporator section (60, 70 and 80°C). Since the material of the pipe wall was copper, thermal conduction was then induced from the outer wall of the pipe to the inner wall of the pipe. In the adiabatic section, heat was induced by thermal conduction from the evaporator section. The temperature of the adiabatic section increased until it reached a steady state, at which it was close to the working temperatures (the average value of the temperatures between the evaporator and the condenser sections). However, the transient temperature profiles in the condenser section decreased because the initial temperature of the outer pipe wall (25°C) was more than the temperature of the condenser section (20ºC). The times required to reach the steady state temperature at the

end of the runs from the numerical model were about 1100, 1400 and 1800 s for the temperatures at the evaporator section of 60, 70 and 80ºC, respectively. As seen from figure 4.3, the temperature at the evaporator section increased, and the time required to reach the steady state temperature was increased because the temperature was dependent on the time.

It can be concluded that the times required to reach the steady state temperature at the end of the runs from the numerical model of the HOHP with the working fluid of R11 required times that were less than the working fluids of ethanol and water.

4.1.2 Heat transfer of HOHP from model

Figure 4.4 shows the heat transfer profiles from the numerical model under the transient condition of the HOHP with the outer wall temperatures at the evaporator section of 60, 70 and 80°C, and water as the working fluid. It was found that the times to start-up for the heat transfer of the HOHP from the numerical model were about 700, 800 and 900 s for the temperatures at the evaporator section of 60, 70 and 80ºC, respectively. Moreover, this figure also shows the times required to reach the steady state heat transfer from the numerical model for the outer wall temperatures of 60, 70 and 80ºC, for which the times required to reach the steady heat transfer were about 2000, 2200 and 2400 s, respectively. The temperature at the evaporator section of 60ºC gave a time to reach the steady state heat transfer that was less than the temperatures at the evaporator section of 70 and 80 ºC. The temperature for the evaporator section of 80ºC had a higher heat transfer than the temperatures for the evaporator section of 70 and 60ºC. When the temperature of the evaporator section was 80ºC the heat transferred to the HOHP was more than the temperatures at the evaporator section of 70 and 60ºC. As can be seen from figure 4.4, the time required to reach the steady state heat transfer and the heat transfer of the HOHP depend on the outer wall temperatures at the evaporator section of the HOHP.

Figure 4.4 Heat transfer of HOHP from model at T_e = 60, 70 and 80°C

with working fluid of water

Figure 4.5 Heat transfer of HOHP from model at T_e = 60, 70 and 80°C

with working fluid of ethanol

Figure 4.5 shows the heat transfer profiles from the numerical model under the transient condition of the HOHP with the outer wall temperatures at the evaporator section of 60, 70 and 80°C, and ethanol as the working fluid. It was found that the times

to start-up for the heat transfer of the HOHP from the numerical model were about 500, 600 and 700 s for the temperatures at the evaporator section of 60, 70 and 80ºC, respectively. Moreover, this figure also shows the times required to reach the steady state heat transfer from the numerical model for the outer wall temperatures of 60, 70 and 80ºC, for which the times required were about 1900, 2100 and 2300 s, respectively. The temperature at the evaporator section of 60ºC gave a time to reach the steady state heat transfer that was less than the temperatures at the evaporator section of 70 and 80 ºC. The temperature at the evaporator section of 80ºC had a higher heat transfer that is more than the temperatures at the evaporator section of 70 and 60ºC. The temperature at the evaporator section of 80ºC had a greater heat at the HOHP than with the temperatures at the evaporator section of 70 and 60ºC. As seen from figure 4.5, the time required to reach the steady state heat transfer and the heat transfer of the HOHP depend on the outer wall temperatures at the evaporator section of the HOHP.

Figure 4.6 shows the heat transfer profiles from the numerical model under the transient condition of the HOHP with the outer wall temperatures at the evaporator section of 60, 70 and 80°C, and R11 as the working fluid. It was found that the times to start-up for the heat transfer of the HOHP from the numerical model were about 400, 500 and 600 s for the temperatures at the evaporator section of 60, 70 and 80ºC, respectively. Moreover, this figure also shows the times required to reach the steady state heat transfer from the numerical model for the outer wall temperatures of 60, 70 and 80ºC, for which the times required to reach the steady heat transfer were about 1700, 1900 and 2100 s, respectively. The temperature at the evaporator section of 60ºC gave a time to reach the steady state heat transfer that was less than the temperatures at the evaporator section of 70 and 80 ºC. The temperature at the evaporator section of 80ºC has a higher heat transfer than the temperatures at the evaporator section of 70 and 60ºC. The temperature at the evaporator section of 80ºC has a temperature for the HOHP that is more than the temperatures at the evaporator section of 70 and 60ºC. As seen from figure 4.6, the time required to reach the steady state heat transfer and the heat transfer of the HOHP depend on the outer wall temperatures at the evaporator section of the HOHP.
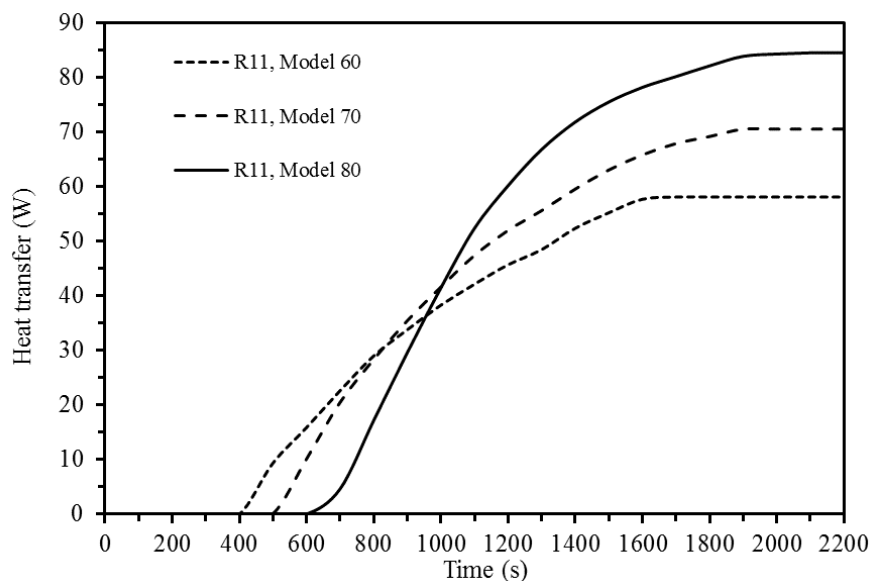
Figure 4.6 Heat transfer of HOHP from model at T_e = 60, 70 and 80ºC
with working fluid of R11

It can be concluded that the times required to reach the steady state heat transfer at the end of the runs from the numerical model of the HOHP used with the working fluid of R11 required a time that was less than the working fluids of ethanol and water. The HOHP used with the working fluid of R11 has a higher heat transfer than the working fluids of ethanol and water. Due to the working fluid of R11 having a lower boiling point than the working fluids of ethanol and water, it has a latent heat of vaporization that is more than those of ethanol and water. When the working fluid of R11 received the heat, it had faster evaporation and more convection than with ethanol and water. Therefore, the working fluid of R11 has a higher heat transfer that is more than the working fluids of ethanol and water.

4.1.3 Heat transfer of HOHP heat exchanger from model

Figure 4.7 shows the heat transfer profiles from the numerical model under the transient condition of the HOHP heat exchanger with the outer wall temperatures at the evaporator section of 60, 70 and 80°C and water as the working fluid. It was found that the times required from start-up to heat transfer for the temperatures at the evaporator section of 60, 70 and 80°C were about 700, 800 and 900 s, respectively.

Moreover, this figure shows that the times required to reach the steady state heat transfer from the numerical model with the temperatures at the evaporator section of 60, 70 and 80ºC were about 2100, 2300 and 2700 s, respectively. The temperature at the evaporator section of 80ºC had a higher heat transfer than the temperatures at the evaporator section of 70 and 60ºC. The temperature at the evaporator section of 60ºC gave a time to reach the steady state heat transfer that was less than the temperatures at the evaporator section of 70 and 80ºC. As seen from figure 4.7, the time required to reach the steady state heat transfer and the heat transfer of the HOHP heat exchanger depend on the temperatures input into the evaporator section of the HOHP heat exchanger.
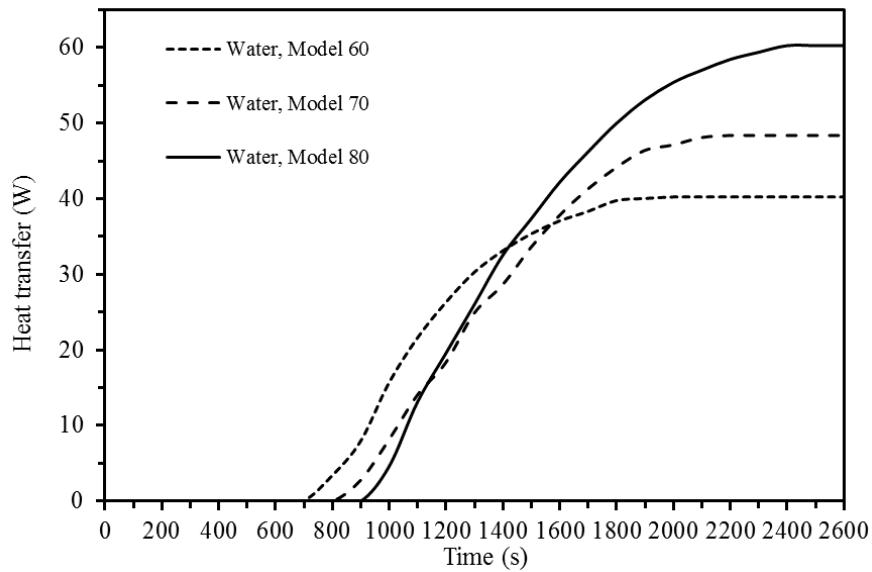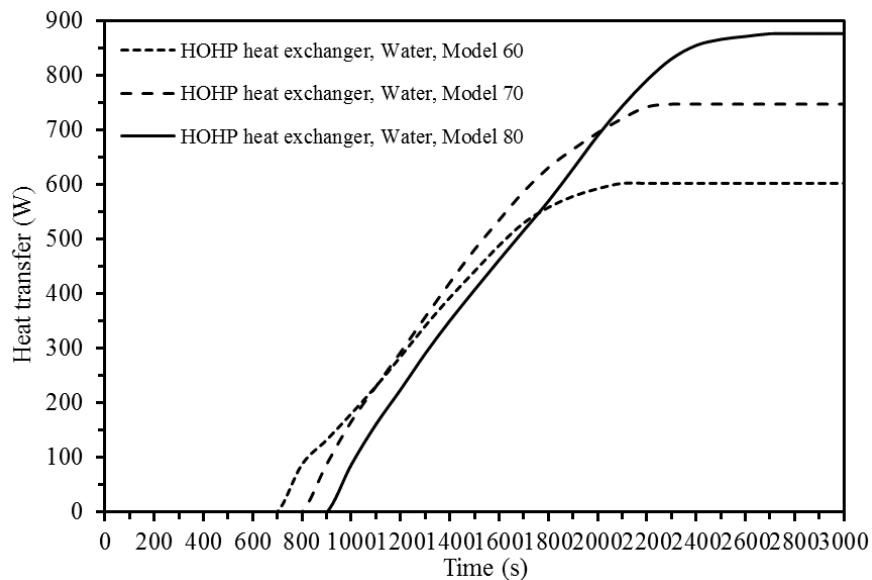

Figure 4.7 Heat transfer of HOHP heat exchanger from model
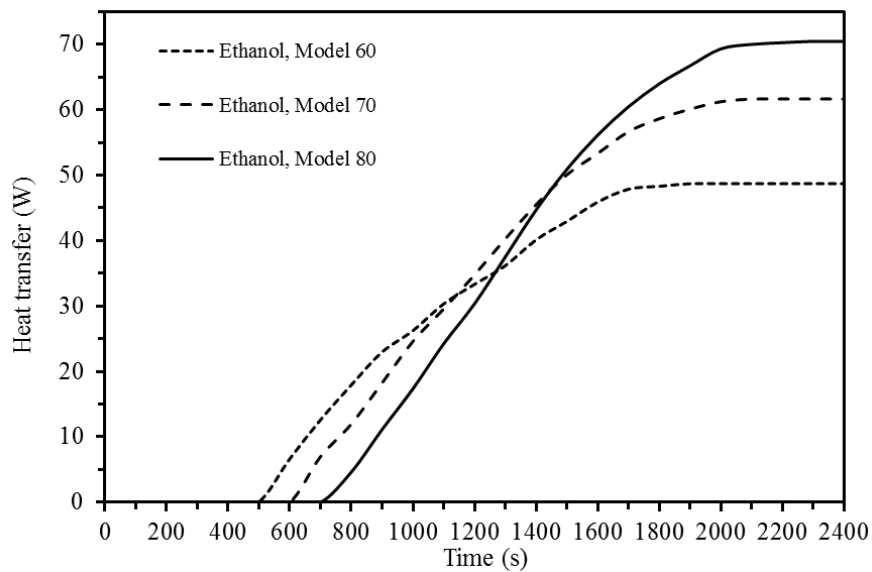at T_e = 60, 70 and 80ºC with working fluid of water

Figure 4.8 Heat transfer of HOHP heat exchanger from model

at T_e = 60, 70 and 80ºC with working fluid of ethanol

Figure 4.8 shows the heat transfer profiles from the numerical model under the transient condition of the HOHP heat exchanger with the temperatures at the evaporator section of 60, 70 and 80°C and ethanol as the working fluid. It was found that the times required from start-up to heat transfer for the temperatures at the evaporator section of 60, 70 and 80°C were about 500, 600 and 700 s, respectively. Moreover, this figure shows that the times required to reach the steady state heat transfer from the numerical model with the temperatures at the evaporator section of 60, 70 and 80ºC were about 1900, 2100 and 2600 s, respectively. The temperature at the evaporator section of 80ºC had a higher heat transfer than the temperatures at the evaporator section of 70 and 60ºC, respectively. The temperature at the evaporator section of 60ºC gave a time to reach the steady state heat transfer that was less than the temperatures at the evaporator section of 70 and 80ºC. As seen from figure 4.8, the time required to reach the steady state heat transfer and the heat transfer of the HOHP heat exchanger depend on the temperatures that are input to the evaporator section of the HOHP heat exchanger.
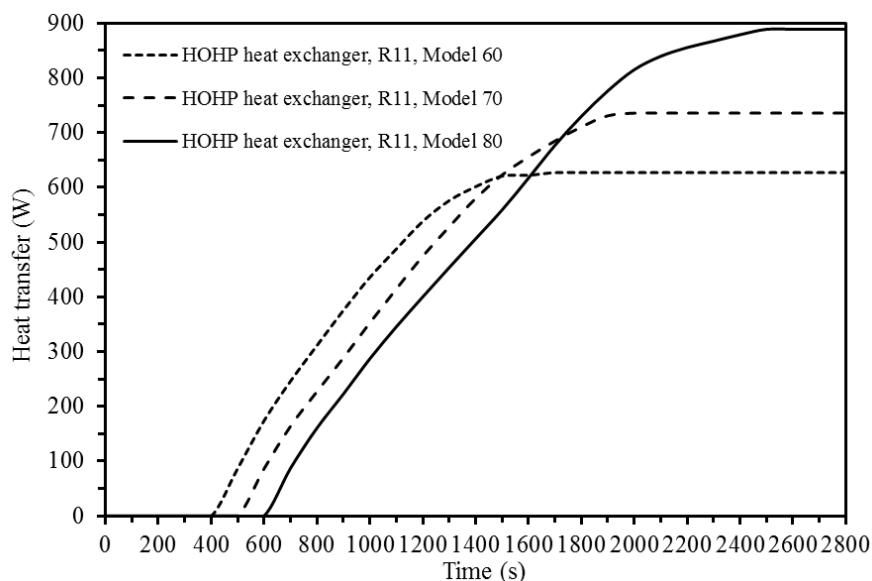
Figure 4.9 Heat transfer of HOHP heat exchanger from model
at $T_e = 60$, 70 and 80°C with working fluid of R11

Figure 4.9 shows the heat transfer profiles from the numerical model under
the transient condition of the HOHP heat exchanger with the temperatures at the
evaporator section of 60, 70 and 80°C and R11 as the working fluid. It was found that
the times required from start-up to heat transfer for the outer wall temperatures at the
evaporator section of 60, 70 and 80°C were about 400, 500 and 600 s, respectively.
Moreover, this figure shows that the times required to reach the steady state heat
transfer from the numerical model with the temperatures at the evaporator section of 60,
70 and 80°C were about 1700, 2000 and 2500 s, respectively. The temperature at the
evaporator section of 80°C has a higher heat transfer than the temperatures at the
evaporator section of 70 and 60°C. The temperature at the evaporator section of 60°C
gave a time to reach the steady state heat transfer that was less than the temperatures at
the evaporator section of 70 and 80°C. As seen from figure 4.9, the time required to
reach the steady state heat transfer and the heat transfer of the HOHP heat exchanger
depend on the temperatures that are input to the evaporator section of the HOHP heat
exchanger.

4.2 Results from experimental evaluation

4.2.1 Temperature at pipe wall of HOHP from experiment

Figure 4.10 shows the temperature profiles at the pipe wall of the HOHP at the evaporator, the adiabatic and the condenser sections from the experimental data with outer wall temperatures at the evaporator section of 60, 70 and 80°C, water as the working fluid and the inner diameter of 1.6 mm. The transient temperature profiles from the figure were plotted as functions of time. It was found that the transient temperature profiles in the evaporator section increased from the initial temperature at the outer pipe wall (25°C) to the temperatures that were input at the evaporator section (60, 70 and 80°C). Since the material of the pipe wall was copper, the thermal conduction was then induced from the outer wall of the pipe to the inner wall of the pipe. In the adiabatic section, heat was induced by thermal conduction from the evaporator section. The temperature of the adiabatic section increased until it reached a steady state, at which it was close to the working temperatures (the average value of the temperatures between the evaporator and the condenser sections). However, the transient temperature profiles in the condenser section decreased because the initial temperature of the outer pipe wall (25°C) was more than the temperature of the condenser section (20ºC). The times required to reach the steady state temperature at the end of the runs from the experimental data were about 996, 1256 and 1534 s for the temperatures at the evaporator section of 60, 70 and 80ºC, respectively. As seen from figure 4.10, the temperature at the evaporator section increased, and the time required to reach the steady state temperature was increased because the temperature was dependent on the time.

Figure 4.10 Temperature profiles at pipe wall of HOHP from experiment

at T_e = 60, 70 and 80°C with working fluid of water and D_i = 1.6 mm

Figure 4.11 Temperature profiles at pipe wall of HOHP from experiment

at T_e = 60, 70 and 80°C with working fluid of water and D_i = 1.8 mm

Figure 4.11 shows the temperature profiles at the pipe wall of the HOHP at the evaporator, the adiabatic and the condenser sections from the experimental data with outer wall temperatures at the evaporator section of 60, 70 and 80°C, water as the working fluid and the inner diameter of 1.8 mm. The transient temperature profiles from the figure were plotted as functions of time. It was found that the transient temperature profiles in the evaporator section increased from the initial temperature at the outer pipe wall (25°C) to the temperatures that were input at the evaporator section (60, 70 and 80°C). Since the material of the pipe wall was copper, the thermal conduction was then induced from the outer wall of the pipe to the inner wall of the pipe. In the adiabatic section, heat was induced by thermal conduction from the evaporator section. The temperature of the adiabatic section increased until it reached a steady state, at which it was close to the working temperatures (the average value of the temperatures between the evaporator and the condenser sections). However, the transient temperature profiles in the condenser section decreased because the initial temperature of the outer pipe wall (25°C) was more than the temperature of the condenser section (20ºC). The times required to reach the steady state temperature at the end of the runs from the experimental data were about 1196, 1274 and 1648 s for the temperatures at the evaporator section of 60, 70 and 80ºC, respectively. As seen from figure 4.11, the temperature at the evaporator section increased, and the time required to reach the steady state temperature was increased because the temperature was dependent on the time.

Figure 4.12 shows the temperature profiles at the pipe wall of the HOHP at the evaporator, the adiabatic and the condenser sections from the experimental data with the outer wall temperatures at the evaporator section of 60, 70 and 80°C, water as the working fluid and the inner diameter of 2.0 mm. The transient temperature profiles from the figure were plotted as functions of time. It was found that the transient temperature profiles in the evaporator section increased from the initial temperature at the outer pipe wall (25°C) to the temperatures that were input at the evaporator section (60, 70 and 80°C). Since the material of the pipe wall was copper, the thermal conduction was then induced from the outer wall of the pipe to the inner wall of the pipe. In the adiabatic section, heat was induced by thermal conduction from the evaporator section. The

temperature of the adiabatic section increased until it reached a steady state, at which it was close to the working temperature (the average value of the temperature between the evaporator and the condenser sections). However, the transient temperature profiles in the condenser section decreased because the initial temperature of the outer pipe wall (25°C) was more than the temperature of the condenser section (20°C). The times required to reach the steady state temperature at the end of the runs from the experimental data were about 1216, 1368 and 1698 s for the temperatures at the evaporator section of 60, 70 and 80°C, respectively. As seen from figure 4.12, the temperature at the evaporator section increased, and the time required to reach the steady state temperature was increased because the temperature was dependent on the time.

Figure 4.12 Temperature profiles at pipe wall of HOHP from experiment
at T_e = 60, 70 and 80°C with working fluid of water and D_i = 2.0 mm

Figure 4.13 Temperature profiles at pipe wall of HOHP from experiment
at T_e = 60, 70 and 80°C with working fluid of ethanol and D_i = 1.6 mm

Figure 4.13 shows the temperature profiles at the pipe wall of the HOHP at the evaporator, the adiabatic and the condenser sections from the experimental data with the outer wall temperatures at the evaporator section of 60, 70 and 80°C, ethanol as the working fluid and the inner diameter of 1.6 mm. The transient temperature profiles from the figure were plotted as functions of time. It was found that the transient temperature profiles in the evaporator section increased from the initial temperature at the outer pipe wall (25°C) to the temperatures that were input at the evaporator section (60, 70 and 80°C). Since the material of the pipe wall was copper, the thermal conduction was then induced from the outer wall of the pipe to the inner wall of the pipe. In the adiabatic section, heat was induced by thermal conduction from the evaporator section. The temperature of the adiabatic section increased until it reached a steady state, at which it was close to the working temperatures (the average value of the temperatures between the evaporator and the condenser sections). However, the transient temperature profiles in the condenser section decreased because the initial temperature of the outer pipe wall (25°C) was more than the temperature of the condenser section (20°C). The times required to reach the steady state temperature at the end of the runs from the

experimental data were about 940, 1316 and 1704 s for the temperatures at the evaporator section of 60, 70 and 80ºC, respectively. As seen from figure 4.13, the temperature at the evaporator section increased, and the time required to reach the steady state temperature was increased because the temperature was dependent on the time.
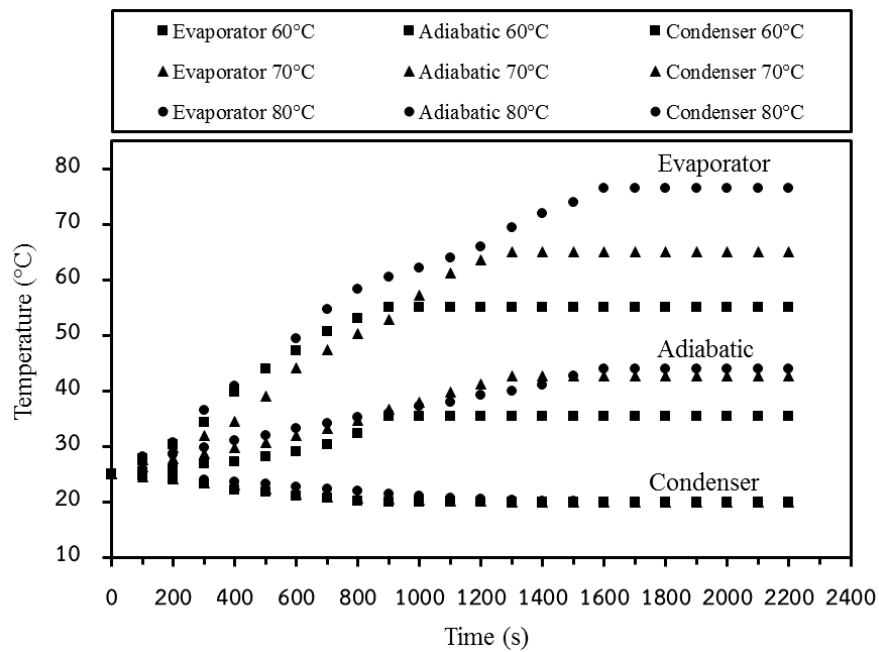
Figure 4.14 shows the temperature profiles at the pipe wall of the HOHP at the evaporator, the adiabatic and the condenser sections from the experimental data with the outer wall temperatures at the evaporator section of 60, 70 and 80°C, ethanol as the working fluid and the inner diameter of 1.8 mm. The transient temperature profiles from the figure were plotted as functions of time. It was found that the transient temperature profiles in the evaporator section increased from the initial temperature at the outer pipe wall (25°C) to the temperatures that were input at the evaporator section (60, 70 and 80°C). Since the material of the pipe wall was copper, the thermal conduction was then induced from the outer wall of the pipe to the inner wall of the pipe. In the adiabatic section, heat was induced by thermal conduction from the evaporator section. The temperature of the adiabatic section increased until it reached a steady state, at which it was close to the working temperatures (the average value of the temperatures between the evaporator and the condenser sections). However, the transient temperature profiles in the condenser section decreased because the initial temperature of the outer pipe wall (25°C) was more than the temperature of the condenser section (20ºC). The times required to reach the steady state temperature at the end of the runs from the experimental data were about 1032, 1360 and 1746 s for the temperatures at the evaporator section of 60, 70 and 80ºC, respectively. As seen from figure 4.14, the temperature at the evaporator section increased, and the time required to reach the steady state temperature was increased because the temperature was dependent on the time.
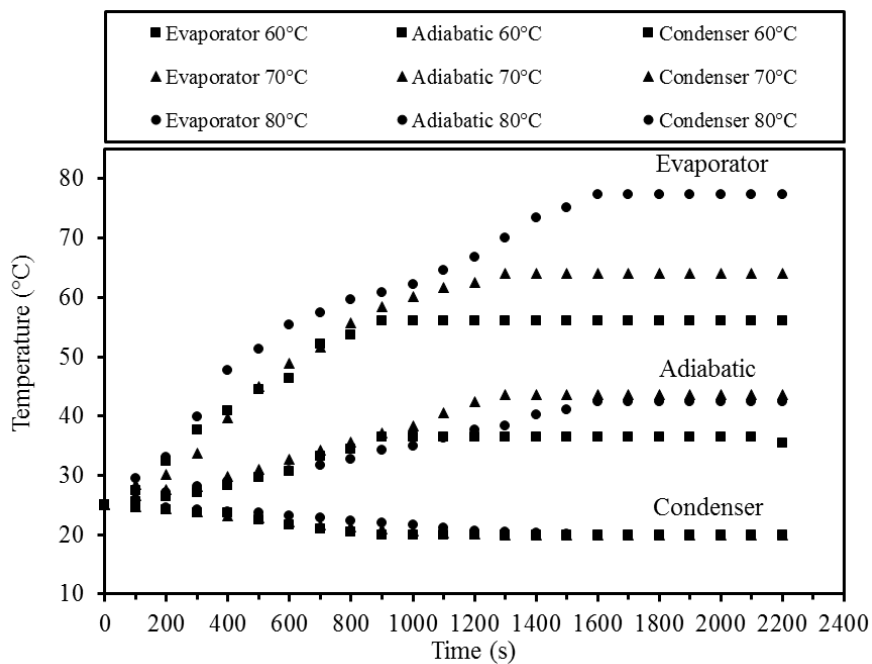
Figure 4.14 Temperature profiles at pipe wall of HOHP from experiment
at T_e = 60, 70 and 80°C with working fluid of ethanol and D_i = 1.8 mm

Figure 4.15 shows the temperature profiles at the pipe wall of the HOHP at
the evaporator, the adiabatic and the condenser sections from the experimental data with
the outer wall temperatures at the evaporator section of 60, 70 and 80°C, ethanol as the
working fluid and the inner diameter of 2.0 mm. The transient temperature profiles from
the figure were plotted as functions of time. It was found that the transient temperature
profiles in the evaporator section increased from the initial temperature at the outer pipe
wall (25°C) to the temperatures that were input at the evaporator section (60, 70 and
80°C). Since the material of the pipe wall was copper, the thermal conduction was then
induced from the outer wall of the pipe to the inner wall of the pipe. In the adiabatic
section, heat was induced by thermal conduction from the evaporator section. The
temperature of the adiabatic section increased until it reached a steady state, at which it
was close to the working temperatures (the average value of the temperatures between
the evaporator and the condenser sections). However, the transient temperature profiles
in the condenser section decreased because the initial temperature of the outer pipe wall
(25°C) was more than the temperature of the condenser section (20°C). The times

required to reach the steady state temperature at the end of the runs from the experimental data were about 1130 1430, and 1806 s for the temperatures at the evaporator section of 60, 70 and 80ºC, respectively. As seen from figure 4.15, the temperature at the evaporator section increased, and the time required to reach the steady state temperature was increased because the temperature was dependent on the time.
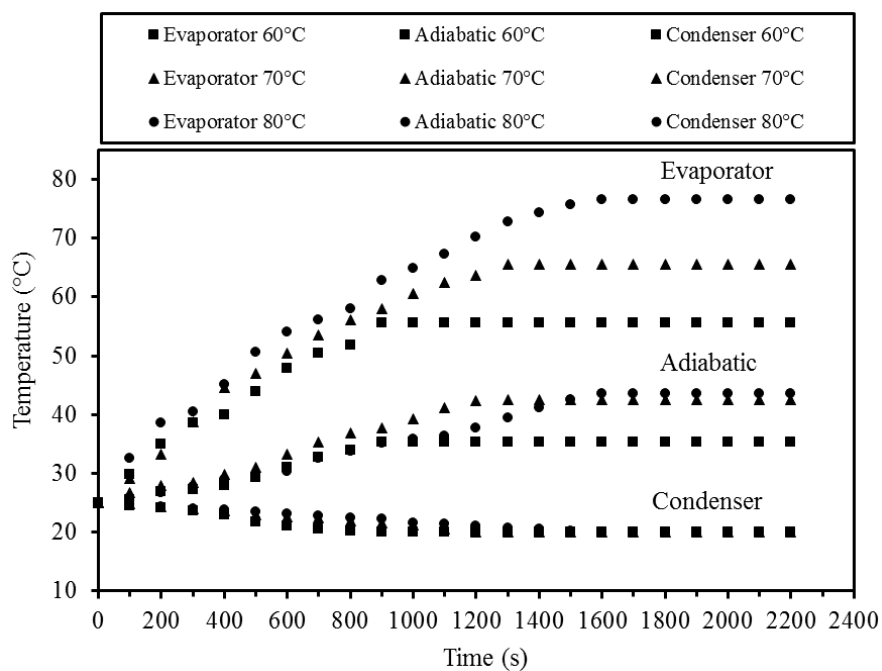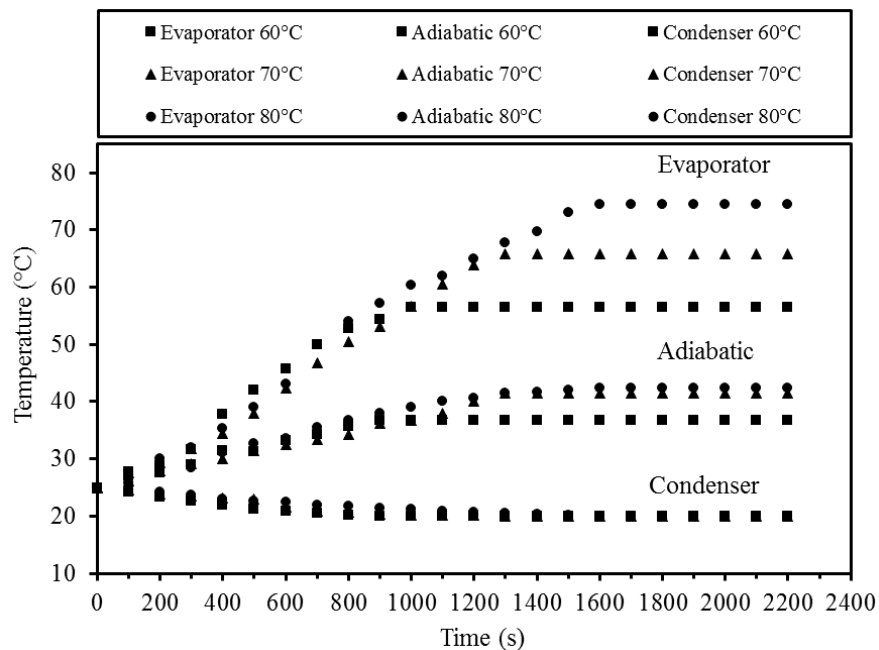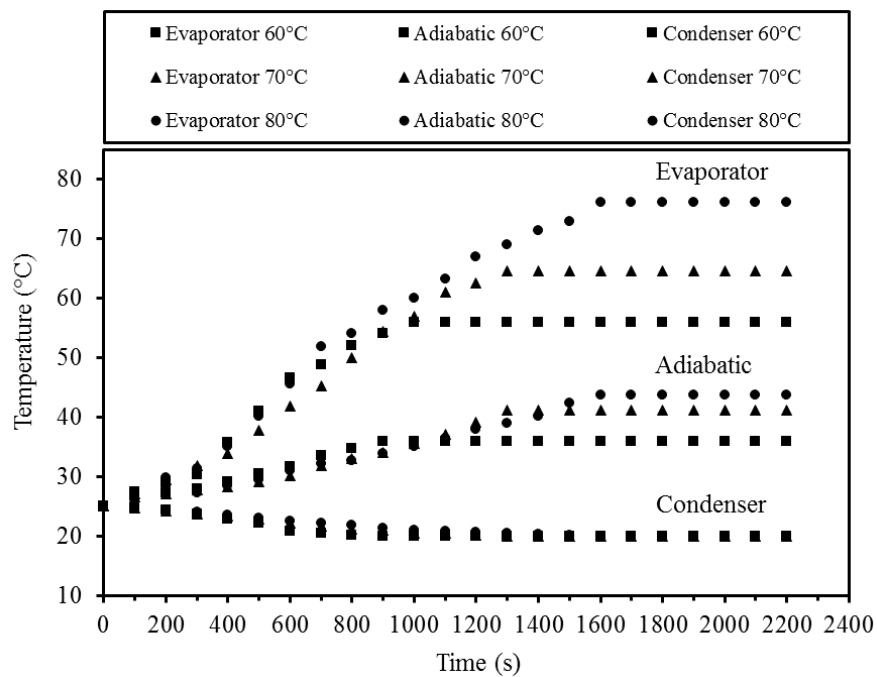

Figure 4.15 Temperature profiles at pipe wall of HOHP from experiment
at T_e = 60, 70 and 80ºC with working fluid of ethanol and D_i = 2.0 mm
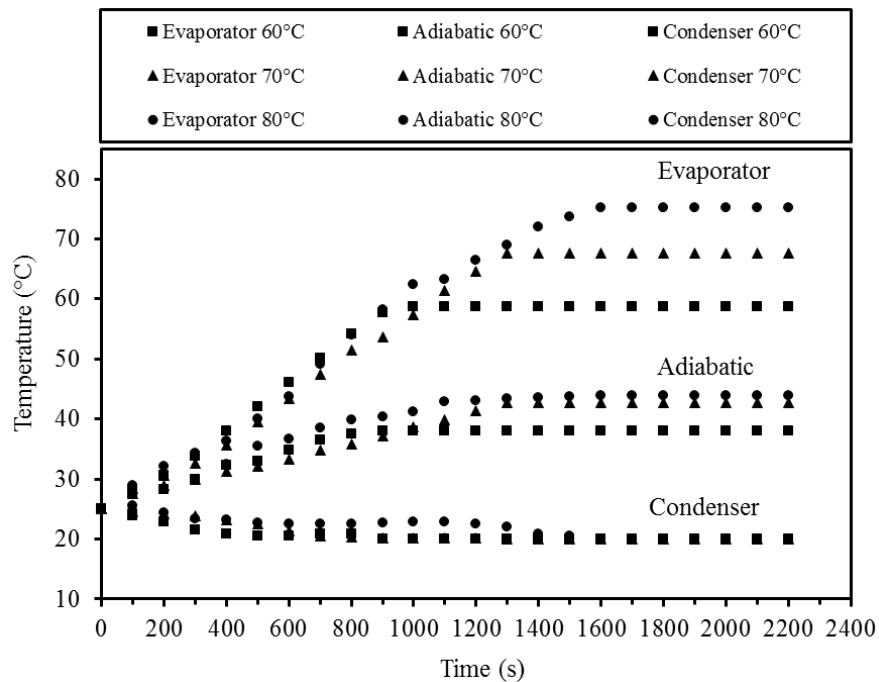
Figure 4.16 Temperature profiles at pipe wall of HOHP from experiment
at T_e = 60, 70 and 80°C with working fluid of R11 and D_i = 1.6 mm

Figure 4.16 shows the temperature profiles at the pipe wall of the HOHP at the evaporator, the adiabatic and the condenser sections from the experimental data with the outer wall temperatures at the evaporator section of 60, 70 and 80°C, R11 as the working fluid and the inner diameter of 1.6 mm. The transient temperature profiles from the figure were plotted as functions of time. It was found that the transient temperature profiles in the evaporator section increased from the initial temperature at the outer pipe wall (25°C) to the temperatures that were input at the evaporator section (60, 70 and 80°C). Since the material of the pipe wall was copper, the thermal conduction was then induced from the outer wall of the pipe to the inner wall of the pipe. In the adiabatic section, heat was induced by thermal conduction from the evaporator section. The temperature of the adiabatic section increased until it reached a steady state, at which it was close to the working temperatures (the average value of the temperatures between the evaporator and the condenser sections). However, the transient temperature profiles in the condenser section decreased because the initial temperature at the outer pipe wall (25°C) was more than the temperature of the condenser section (20°C). The times

required to reach the steady state temperature at the end of the runs from the experimental data were about 906, 1282 and 1556 s for the temperatures at the evaporator section of 60, 70 and 80ºC, respectively. As seen from figure 4.16, the temperature at the evaporator section increased, and the time required to reach the steady state temperature was increased because the temperature was dependent on the time.
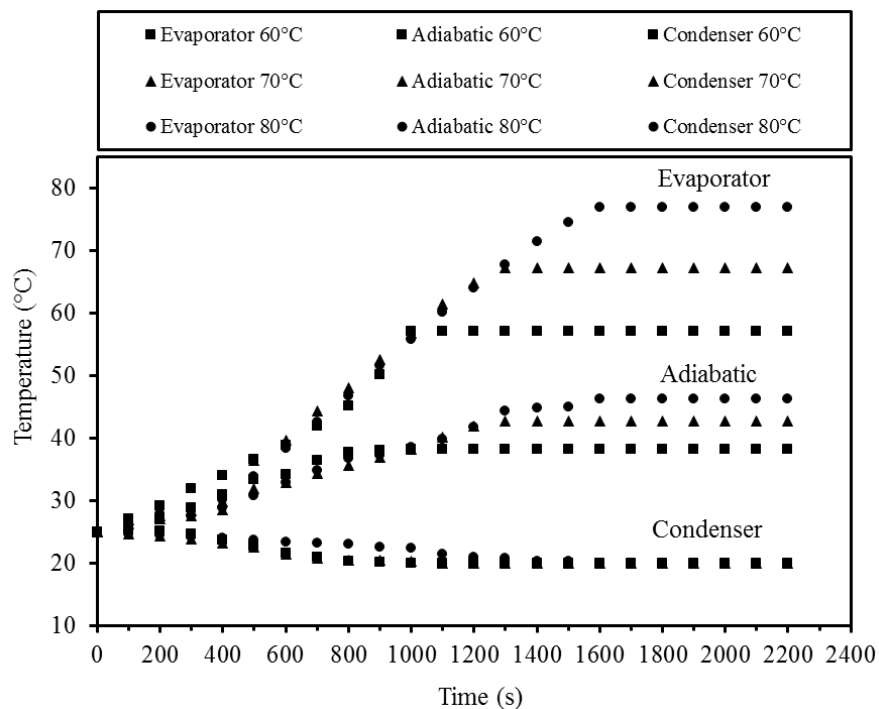
Figure 4.17 Temperature profiles at pipe wall of HOHP from experiment
at T_e = 60, 70 and 80ºC with working fluid of R11 and D_i = 1.8 mm

Figure 4.17 shows the temperature profiles at the pipe wall of the HOHP at the evaporator, the adiabatic and the condenser sections from the experimental data with the outer wall temperatures at the evaporator section of 60, 70 and 80°C, R11 as the working fluid and the inner diameter of 1.8 mm. The transient temperature profiles from the figure were plotted as functions of time. It was found that the transient temperature profiles in the evaporator section increased from the initial temperature at the outer pipe wall (25°C) to the temperatures that were input at the evaporator section (60, 70 and 80°C). Since the material of the pipe wall was copper, the thermal conduction was then

induced from the outer wall of the pipe to the inner wall of the pipe. In the adiabatic section, heat was induced by thermal conduction from the evaporator section. The temperature of the adiabatic section increased until it reached a steady state, at which it was close to the working temperatures (the average value of the temperatures between the evaporator and the condenser sections). However, the transient temperature profiles in the condenser section decreased because the initial temperature of the outer pipe wall (25°C) was more than the temperature of the condenser section (20°C). The times required to reach the steady state temperature at the end of the runs from the experimental data were about 922, 1294 and 1586 s for the temperatures at the evaporator section of 60, 70 and 80°C, respectively. As seen from figure 4.17, the temperature at the evaporator section increased, and the time required to reach the steady state temperature was increased because the temperature was dependent on the time.
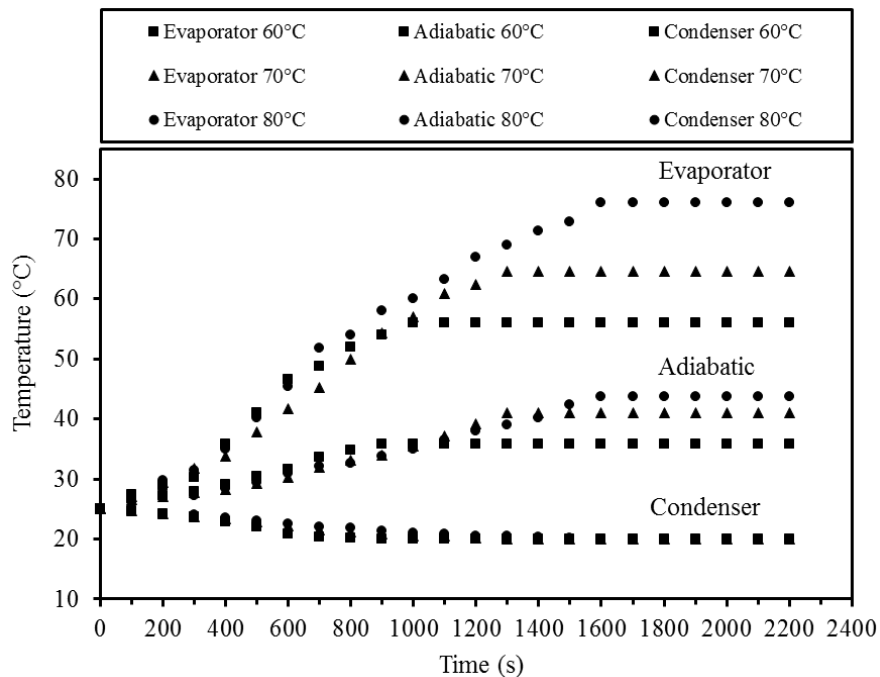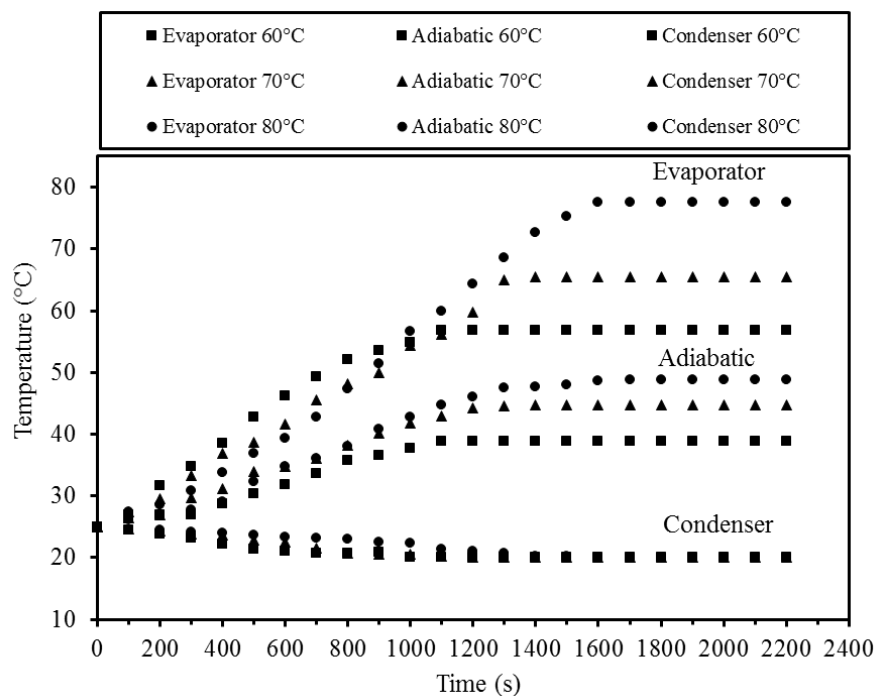

Figure 4.18 Temperature profiles at pipe wall of HOHP from experiment
at T_e = 60, 70 and 80°C with working fluid of R11 and D_i = 2.0 mm

Figure 4.18 shows the temperature profiles at the pipe wall of the HOHP at the evaporator, the adiabatic and the condenser sections from the experimental data with the outer wall temperatures at the evaporator section of 60, 70 and 80°C, R11 as the working fluid and the inner diameter of 2.0 mm. The transient temperature profiles from the figure were plotted as functions of time. It was found that the transient temperature profiles in the evaporator section increased from the initial temperature at the outer pipe wall (25°C) to the temperatures that were input at the evaporator section (60, 70 and 80°C). Since the material of the pipe wall was copper, the thermal conduction was then induced from the outer wall of the pipe to the inner wall of the pipe. In the adiabatic section, heat was induced by thermal conduction from the evaporator section. The temperature of the adiabatic section increased until it reached a steady state, at which it was close to the working temperatures (the average value of the temperatures between the evaporator and the condenser sections). However, the transient temperature profiles in the condenser section decreased because the initial temperature of the outer pipe wall (25°C) was more than the temperature of the condenser section (20°C). The times required to reach the steady state temperature at the end of the runs from the experimental data were about 1010, 1380 and 1618 s for the temperatures at the evaporator section of 60, 70 and 80°C, respectively. As seen from figure 4.18, the temperature at the evaporator section increased, and the time required to reach the steady state temperature was increased because the temperature was dependent on the time.

4.2.2 Heat transfer of HOHP from experiment

Figure 4.19 shows the heat transfer profiles from the experimental data under the transient condition of the HOHP with the temperatures at the evaporator section of 60, 70 and 80°C, water as the working fluid and the inner diameter of 1.6 mm. It was found that when the temperatures were applied to the evaporator section of the HOHP, the heat transfer did not occur at the start-up of the experiment. The heat transfer occurred at the times of 640, 752 and 880 s for the temperatures at the evaporator section of 60, 70 and 80°C, respectively. Due to the working fluid within the HOHP not receiving the heat from the outer wall of the evaporator section of the HOHP

to boil the working fluid within the HOHP. When the working fluid received enough heat, the working fluid will boil and there will be convection of the heat from the evaporator section to the condenser section of the HOHP. Moreover, this figure shows that the times required to reach the steady state heat transfer from the experimental data with the temperatures at the evaporator section of 60, 70 and 80ºC were about 1724, 1934 and 2132 s, respectively. As seen from figure 4.19, the time required to reach the steady state heat transfer depends on the temperatures that are input to the evaporator section of the HOHP. It should be mentioned that the heat recovered at the condenser section is always lower than the heat added to the evaporator section due to uncontrolled heat losses from the experimental setup.

Figure 4.19 Heat transfer of HOHP from experiment at T_e = 60, 70 and 80ºC with working fluid of water and D_i = 1.6 mm

Figure 4.20 shows the heat transfer profiles from the experimental data under the transient condition of the HOHP with the temperatures at the evaporator section of 60, 70 and 80°C, water as the working fluid and the inner diameter of 1.8 mm. It was found that when applying the temperatures to the evaporator section of the HOHP, the heat transfer did not occur at the start-up of the experiment. The heat

transfer occurs at the times of 610, 776 and 894 s for the temperatures at the evaporator section of 60, 70 and 80ºC, respectively. Due to the working fluid within the HOHP not receiving heat from the outer wall of the evaporator section of the HOHP to boil the working fluid within the HOHP. When the working fluid has received enough heat, the working fluid will boil and there will be convection of the heat from the evaporator section to the condenser section of the HOHP. Moreover, this figure shows that the times required to reach the steady state heat transfer from the experimental data with the temperatures at the evaporator section of 60, 70 and 80ºC were about 1800, 2082 and 2210 s, respectively. As seen from figure 4.20, the time required to reach the steady state heat transfer depends on the temperatures that are input to the evaporator section of the HOHP. It should be mentioned that the heat recovered at the condenser section is always lower than the heat added to the evaporator section due to uncontrolled heat losses from the experimental setup.

Figure 4.20 Heat transfer of HOHP from experiment at T_e = 60, 70 and 80ºC
with working fluid of water and D_i = 1.8 mm

Figure 4.21 Heat transfer of HOHP from experiment at T_e = 60, 70 and 80ºC
with working fluid of water and D_i = 2.0 mm

Figure 4.21 shows the heat transfer profiles from the experimental data under the transient condition of the HOHP with the temperatures at the evaporator section of 60, 70 and 80°C, water as the working fluid and the inner diameter of 2.0 mm. It was found that when applying the temperatures to the evaporator section of the HOHP, the heat transfer did not occur at the start-up of the experiment. The heat transfer occurred at the times of 644, 742 and 852 s for the temperatures at the evaporator section of 60, 70 and 80ºC, respectively. Due to the working fluid within the HOHP not receiving the heat from the outer wall of the evaporator section of the HOHP for the boiling of the working fluid within the HOHP. When the working fluid has received enough heat, the working fluid will boil and there is convection of the heat from the evaporator section to the condenser section of the HOHP. Moreover, this figure shows that the times required to reach the steady state heat transfer from the experimental data with the temperatures at the evaporator section of 60, 70 and 80ºC were about 1826, 2116 and 2290 s, respectively. As seen from figure 4.21, the time required to reach the steady state heat transfer depends on the temperatures that are input to the evaporator section of the HOHP. It should be mentioned that the heat

recovered at the condenser section is always lower than the heat added to the evaporator section due to uncontrolled heat losses from the experimental setup.

Figure 4.22 Heat transfer of HOHP from experiment at T_e = 60, 70 and 80°C
with working fluid of ethanol and D_i = 1.6 mm

Figure 4.22 shows the heat transfer profiles from the experimental data under the transient condition of the HOHP with the temperatures at the evaporator section of 60, 70 and 80°C, ethanol as the working fluid and the inner diameter of 1.6 mm. It was found that when applying the temperatures to the evaporator section of the HOHP, the heat transfer did not occur at the start-up of the experiment. The heat transfer occurred at the times of 502, 592 and 602 s for the temperatures at the evaporator section of 60, 70 and 80°C, respectively. Due to the working fluid within the HOHP not receiving the heat from the outer wall of the evaporator section of the HOHP to boil the working fluid within the HOHP. When the working fluid has received the enough heat, the working fluid will boil and there is convection of the heat from the evaporator section to the condenser section of the HOHP. Moreover, this figure shows that the times required to reach the steady state heat transfer from the experimental data with the temperatures at the evaporator section of 60, 70 and 80°C were about 1620,

1836 and 2002 s, respectively. As seen from figure 4.22, the time required to reach the steady state heat transfer depends on the temperatures that are input to the evaporator section of the HOHP. It should be mentioned that the heat recovered at the condenser section is always lower than the heat added to the evaporator section due to uncontrolled heat losses from the experimental setup.

Figure 4.23 Heat transfer of HOHP from experiment at T_e = 60, 70 and 80ºC
with working fluid of ethanol and D_i = 1.8 mm

Figure 4.23 shows the heat transfer profiles from the experimental data under the transient condition of the HOHP with the temperatures at the evaporator section of 60, 70 and 80°C, ethanol as the working fluid and the inner diameter of 1.8 mm. It was found that when applying the temperatures to the evaporator section of the HOHP, the heat transfer did not occur at the start-up of the experiment. The heat transfer occurred at the times of 504, 600 and 650 s for the temperatures at the evaporator section of 60, 70 and 80ºC, respectively. Due to the working fluid within the HOHP not receiving the heat from the outer wall of the evaporator section of the HOHP enough to boil the working fluid within the HOHP. When the working fluid has received enough heat, the working fluid will boil and there is convection of the heat

from the evaporator section to the condenser section of the HOHP. Moreover, this figure shows that the times required to reach the steady state heat transfer from the experimental data with the temperatures at the evaporator section of 60, 70 and 80ºC were about 1754, 1866 and 2092 s, respectively. As seen from figure 4.23, the time required to reach the steady state heat transfer depends on the temperatures that are input to the evaporator section of the HOHP. It should be mentioned that the heat recovered at the condenser section is always lower than the heat added to the evaporator section due to uncontrolled heat losses from the experimental setup.
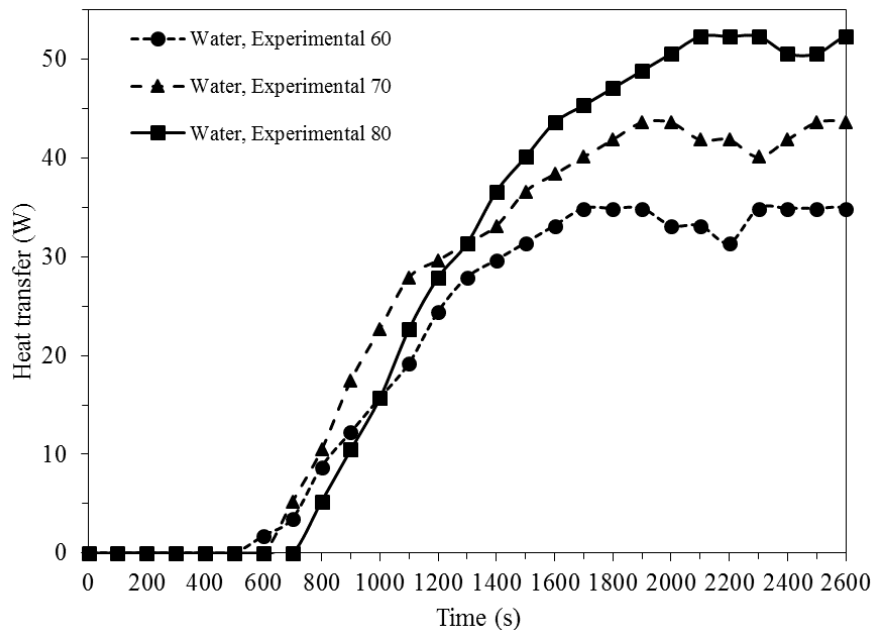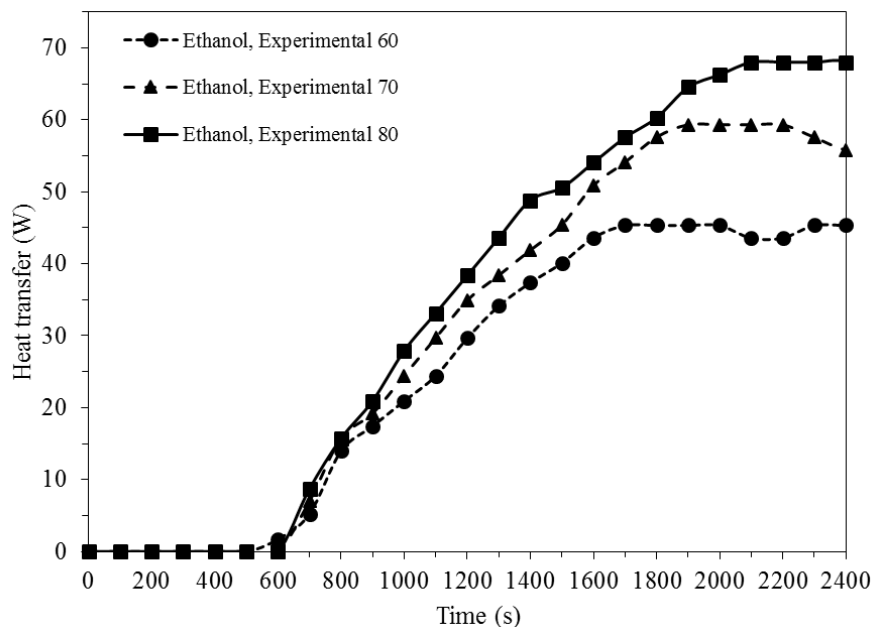

Figure 4.24 Heat transfer of HOHP from experiment at T_e = 60, 70 and 80ºC
with working fluid of ethanol and D_i = 2.0 mm

Figure 4.24 shows the heat transfer profiles from the experimental data under the transient condition of the HOHP with the temperatures at the evaporator section of 60, 70 and 80°C, ethanol as the working fluid and the inner diameter as 2.0 mm. It was found that when applying the temperatures to the evaporator section of the HOHP, the heat transfer did not occur at the start-up of the experiment. The heat transfer occurred at the times of 514, 554 and 630 s for the temperatures at the evaporator section of 60, 70 and 80ºC, respectively. Due to the working fluid within the

HOHP not receiving the heat from the outer wall of the evaporator section of the HOHP to boil the working fluid within the HOHP. When the working fluid has received enough heat, the working fluid will boil and there is convection of the heat from the evaporator section to the condenser section of the HOHP. Moreover, this figure shows that the times required to reach the steady state heat transfer from the experimental data with the temperatures of the evaporator section of 60, 70 and 80ºC were about 1786, 1880 and 2142 s, respectively. As seen from figure 4.24, the time required to reach the steady state heat transfer depends on the temperatures that are input to the evaporator section of the HOHP. It should be mentioned that the heat recovered at the condenser section is always lower than the heat added to the evaporator section due to uncontrolled heat losses from the experimental setup.
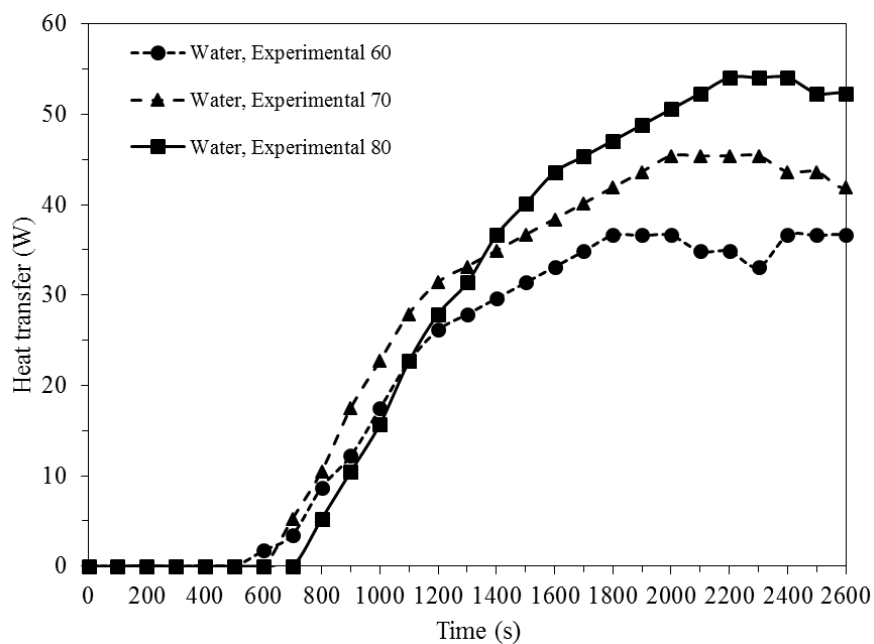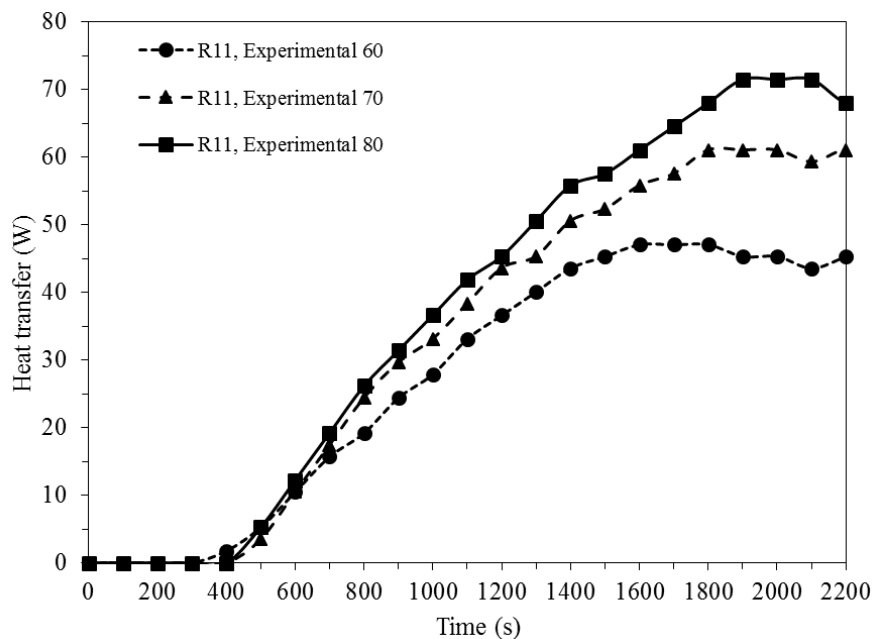

Figure 4.25 Heat transfer of HOHP from experiment at T_e = 60, 70 and 80ºC
with working fluid of R11 and D_i = 1.6 mm

Figure 4.25 shows the heat transfer profiles from the experimental data under the transient condition of the HOHP with the temperatures at the evaporator section of 60, 70 and 80°C, R11 as the working fluid and the inner diameter of 1.6 mm. It was found that when applying the temperatures to the evaporator section of the

HOHP, the heat transfer did not occur at the start-up of the experiment. The heat transfer occurred at the times of 388, 410 and 480 s for the temperatures at the evaporator section of 60, 70 and 80ºC, respectively. Due to the working fluid within the HOHP not received the heat from the outer wall of the evaporator section of the HOHP to boil the working fluid within the HOHP. When the working fluid has received enough heat, the working fluid will boil and there is convection of the heat from the evaporator section to the condenser section of the HOHP. Moreover, this figure shows that the times required to reach the steady state heat transfer from the experimental data with the temperatures at the evaporator section of 60, 70 and 80ºC were about 1584, 1760 and 1890 s, respectively. As seen from figure 4.25, the time required to reach the steady state heat transfer depends on the temperatures that are input to the evaporator section of the HOHP. It should be mentioned that the heat recovered at the condenser section is always lower than the heat added to the evaporator section due to uncontrolled heat losses from the experimental setup.
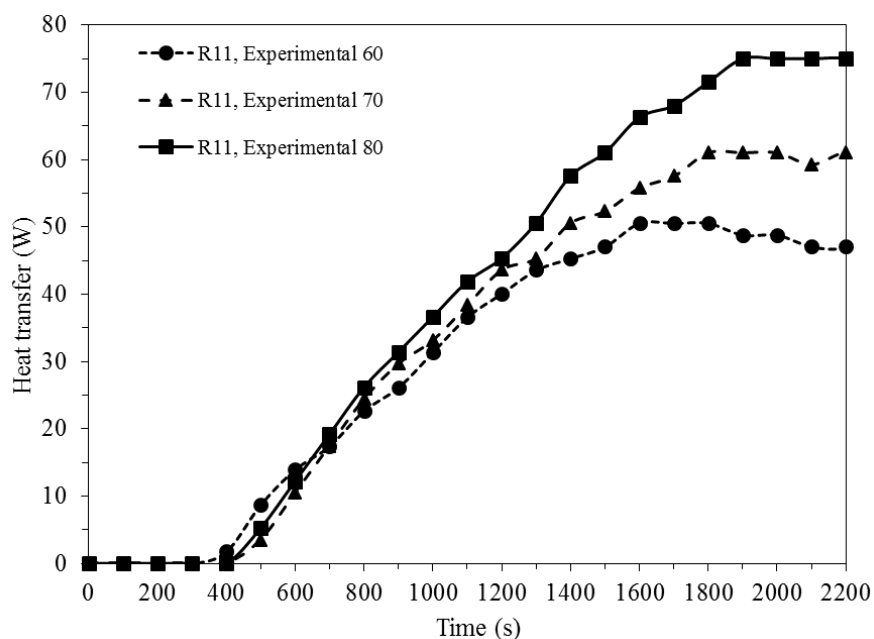
Figure 4.26 Heat transfer of HOHP from experiment at T_e = 60, 70 and 80ºC
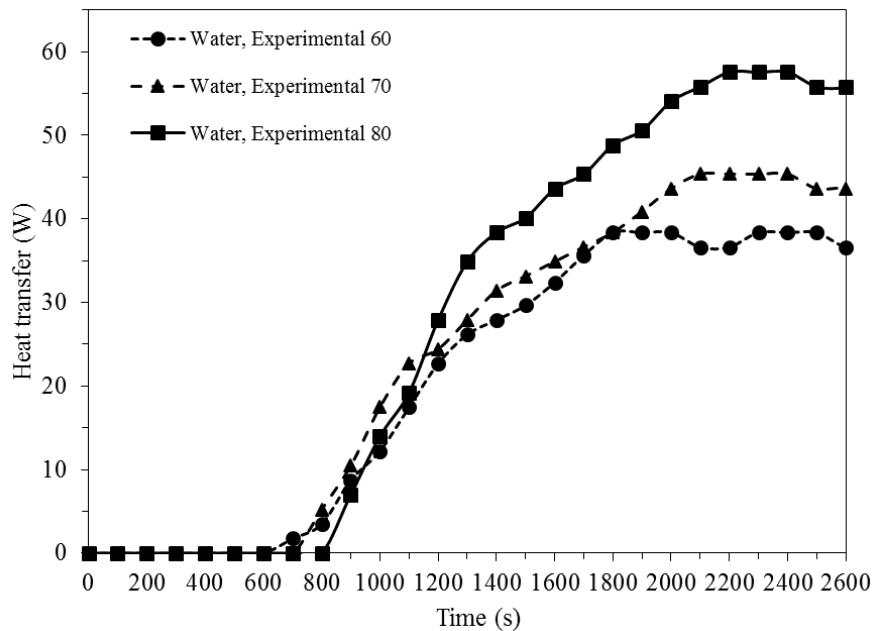
with working fluid of R11 and D_i = 1.8 mm

Figure 4.26 shows the heat transfer profiles from the experimental data under the transient condition of the HOHP with the temperatures at the evaporator section of 60, 70 and 80°C, R11 as the working fluid and the inner diameter of 1.8 mm. It was found that when applying the temperatures to the evaporator section of the HOHP, the heat transfer did not occur at the start-up of the experiment. The heat transfer occurred at the times of 384, 444 and 504 s for the temperatures at the evaporator section of 60, 70 and 80ºC, respectively. Due to the working fluid within the HOHP not receiving the heat from the outer wall of the evaporator section of the HOHP to boil the working fluid within the HOHP. When the working fluid has received enough heat, the working fluid will boil and there is convection of the heat from the evaporator section to the condenser section of the HOHP. Moreover, this figure shows that the times required to reach the steady state heat transfer from the experimental data with the temperatures at the evaporator section of 60, 70 and 80ºC were about 1612, 1790 and 1915 s, respectively. As seen from figure 4.26, the time required to reach the steady state heat transfer depends on the temperatures that are input to the evaporator section of the HOHP. It should be mentioned that the heat recovered at the condenser section is always lower than the heat added to the evaporator section due to uncontrolled heat losses from the experimental setup.
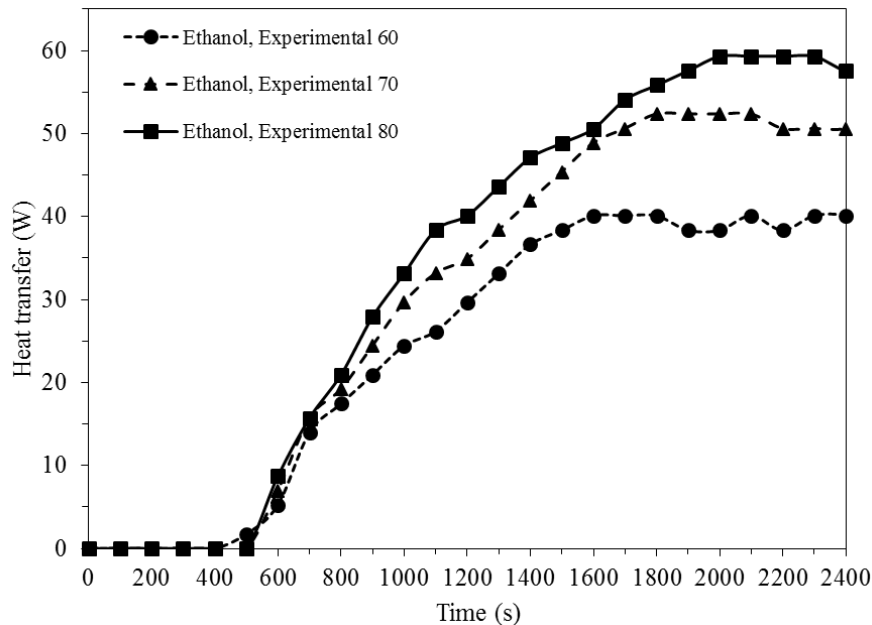
Figure 4.27 shows the heat transfer profiles from the experimental data under the transient condition of the HOHP with the temperatures at the evaporator section of 60, 70 and 80°C, R11 as the working fluid and the inner diameter of 2.0 mm. It was found that when applying the temperatures to the evaporator section of the HOHP, the heat transfer did not occur at the start-up of the experiment. The heat transfer occurred at the times of 396, 464 and 520 s for the temperatures at the evaporator section of 60, 70 and 80ºC, respectively. Due to the working fluid within the HOHP not receiving the heat from the outer wall of the evaporator section of the HOHP to boil the working fluid within the HOHP. When the working fluid has received enough heat, the working fluid will boil and there is convection of the heat from the evaporator section to the condenser section of the HOHP. Moreover, this figure shows that the times required to reach the steady state heat transfer from the experimental data with the temperatures at the evaporator section of 60, 70 and 80ºC were about 1634,

1818 and 1952 s, respectively. As seen from figure 4.27, the time required to reach the steady state heat transfer depends on the temperatures that are input to the evaporator section of the HOHP. It should be mentioned that the heat recovered at the condenser section is always lower than the heat added to the evaporator section due to uncontrolled heat losses from the experimental setup.
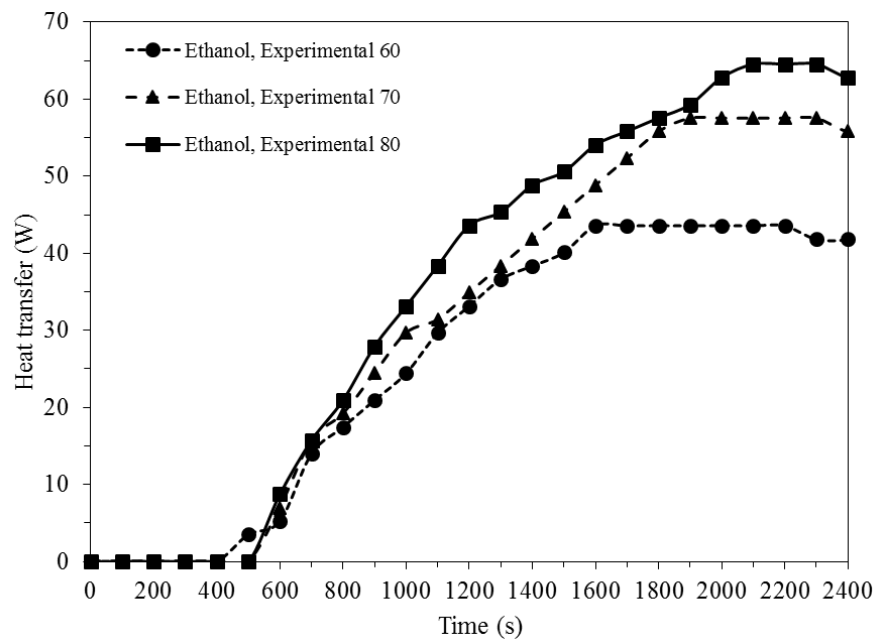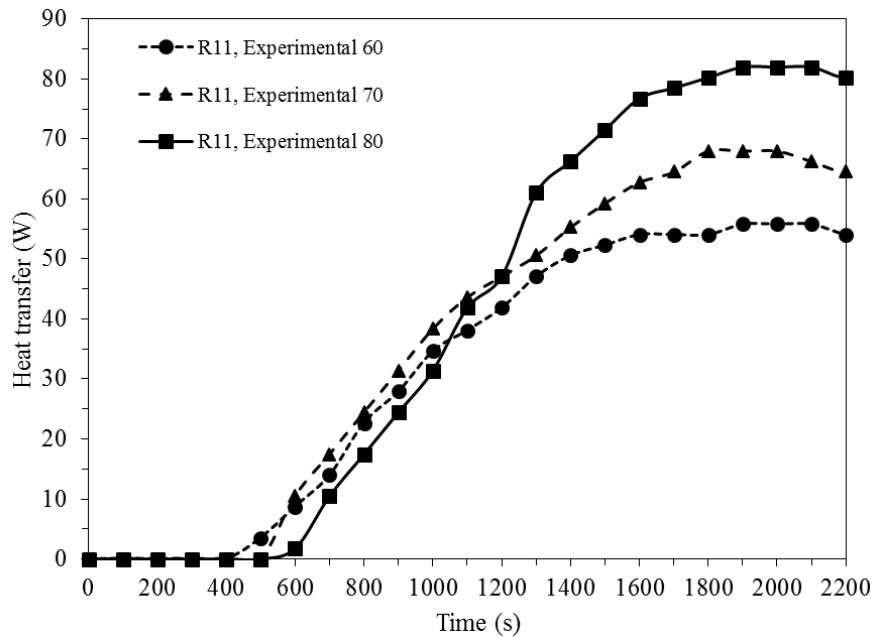

Figure 4.27 Heat transfer of HOHP from experiment at T_e = 60, 70 and 80ºC
with working fluid of R11 and D_i = 2.0 mm

4.2.3 Heat transfer of HOHP heat exchanger from experiment

Figure 4.28 shows the heat transfer profiles from the experimental data under the transient condition of the HOHP heat exchanger with the temperatures at the evaporator section of 60, 70 and 80°C, R11 as the working fluid and the inner diameter of 2.0 mm. It was found that the times to start-up for the heat transfer of the HOHP heat exchanger with the temperatures at the evaporator section of 60, 70 and 80°C were about 368, 456 and 544 s, respectively. Moreover, this figure shows that the times required to reach the steady state heat transfer of the HOHP heat exchanger for the temperatures at the evaporator section of 60, 70 and 80ºC were about 1634, 1912 and 2378 s, respectively. As seen from the figure, the times required to reach the steady

state heat transfer depend on the temperatures that are input to the evaporator section of the HOHP heat exchanger.
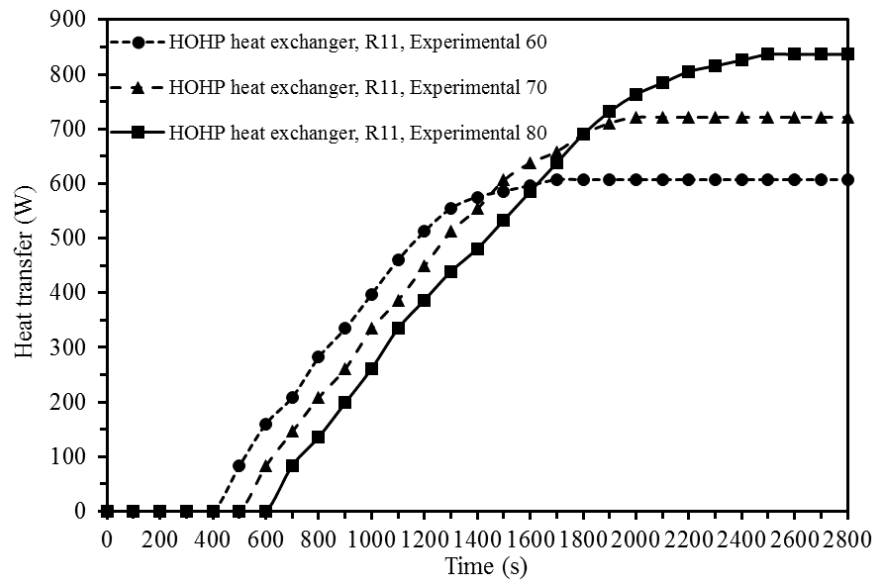
Figure 4.28 Heat transfer of HOHP heat exchanger from experiment at T_e = 60, 70 and 80ºC with working fluid of R11 and D_i = 2.0 mm

4.3 Comparison of results from model and experiment

4.3.1 Comparison of temperature at pipe wall of HOHP

The results of the temperatures for the pipe wall of the HOHP at the evaporator, the adiabatic and the condenser sections from the numerical model are compared with the experimental data, and are presented in figures 4.29, 4.30 and 4.31, respectively, for the outer wall temperatures at the evaporator section of 60, 70 and 80°C, working fluid of water and the inner diameter of 2.0 mm. The transient condition temperature profiles from the numerical model and the experimental data were plotted as functions of time. The temperatures from the experimental data were the average values for the evaporator, the adiabatic and the condenser sections. It was found that the transient temperature profiles in the evaporator section increased from the initial temperature of the pipe wall (25ºC) to the outer wall temperatures that were input to the evaporator section (60, 70 and 80°C). Since the pipe wall was copper, the thermal

conduction was then induced from the outer wall of the pipe to the inner wall of the pipe. In the adiabatic section, heat was induced by thermal conduction from the evaporator section, and the temperature of the adiabatic section increased until it reached a steady state temperature, at which it was close to the working temperatures (the average value of the temperatures between the evaporator and the condenser sections). However, the transient temperature profiles for the condenser section decreased because the initial temperature (25ºC) was more than the outer wall temperature of the condenser section (20ºC). The times required to reach the steady state temperature at the end of the runs from the numerical model were about 1300, 1600 and 2000 s for the outer wall temperatures at the evaporator section of 60, 70 and 80°C, respectively. As seen from the figures, when the temperatures at the evaporator section increased, the time required to reach the steady state temperature increased because the temperature was dependent on the time. The times required to reach the steady state temperature from the experiment were about 1216, 1368 and 1698 s for the outer wall temperatures at the evaporator section of 60, 70 and 80°C, respectively.

The solid lines correspond to the temperatures of the evaporator, the adiabatic, and the condenser sections from the numerical model predicting the response of the temperature with time, and the symbols correspond to the experimentally measured temperature average values. As seen from figures 4.29, 4.30 and 4.31, it was found that the comparisons between the results from the numerical model and the experimental data response curves are excellent for all three sections. The time required to reach the steady state temperature for the numerical model was not equal to the experiment because the numerical model was assumed to have no losses in the calculation, but the experiment had errors from some uncontrollable parameters. As seen from all figures, the time required to reach the steady state temperature between the numerical model and the experiment results was different, and the differences were 6.6%, 14.5% and 15.1% for the outer wall temperatures at the evaporator section of 60, 70 and 80°C, respectively. The time required to reach the steady state temperature is an important parameter for the start-up of the HOHP. The two values from the numerical model and the experimental data are in good agreement.

Figure 4.29 Compared temperature profiles at pipe wall of HOHP from model and experiment at $T_e = 60°C$ with working fluid of water

Figure 4.30 Compared temperature profiles at pipe wall of HOHP from model and experiment at $T_e = 70°C$ with working fluid of water

Figure 4.31 Compared temperature profiles at pipe wall of HOHP from model and experiment at $T_e = 80°C$ with working fluid of water

The results of the temperatures of the pipe wall of the HOHP at the evaporator, the adiabatic and the condenser sections from the numerical model are compared with the experimental data, and are presented in figures 4.32, 4.33 and 4.34, respectively, for the outer wall temperatures at the evaporator section of 60, 70 and 80°C, the working fluid as ethanol and the inner diameter of 2.0 mm. The transient condition temperature profiles from the numerical model and the experimental data were plotted as functions of time. The temperature from the experimental data was the average values for the evaporator, the adiabatic and the condenser sections. It was found that the transient temperature profiles in the evaporator section increased from the initial temperature of the pipe wall (25°C) to the outer wall temperatures that were input to the evaporator section (60, 70 and 80°C). Since the pipe wall was copper, the thermal conduction was then induced from the outer wall of the pipe to the inner wall of the pipe. In the adiabatic section, heat was induced by thermal conduction from the evaporator section, and the temperature of the adiabatic section increased until it reached a steady state temperature, at which it was close to the working temperatures (the average value of the temperatures between the evaporator and the condenser sections). However, the transient temperature profiles in the condenser section

decreased because the initial temperature (25ºC) was more than the outer wall temperature of the condenser section (20ºC). The times required to reach the steady state temperature at the end of the runs from the numerical model were about 1200, 1500 and 1900 s for the outer wall temperatures at the evaporator section of 60, 70 and 80°C, respectively. As seen from the figures, when the temperatures at the evaporator section increased, the time required to reach the steady state temperature was increased because the temperature was dependent on the time. The times required to reach the steady state temperature from the experiment were about 1130, 1430 and 1806 s for the outer wall temperatures at the evaporator section of 60, 70 and 80°C, respectively.

        The solid lines correspond to the temperatures of the evaporator, the adiabatic and the condenser sections from the numerical model predicting the response of the temperature with time and the symbols correspond to the experimentally measured temperature average values. As seen from figures 4.32, 4.33 and 4.34, it was found that the comparisons between the results from the numerical model and the experimental data response curves are excellent for all three sections. The time required to reach the steady state temperature for the numerical model was not equal to the experiment because the numerical model was assumed to have no losses in the calculation, but the experiment had errors from some uncontrollable parameters. As seen from all figures, the time required to reach the steady state temperature between the numerical model and the experiment results was different, and the differences were 5.8%, 4.7% and 4.9% for the outer wall temperatures at the evaporator section of 60, 70 and 80°C, respectively. The time required to reach the steady state temperature is an important parameter for the start-up of the HOHP. The two values from the numerical model and the experimental data are in good agreement.
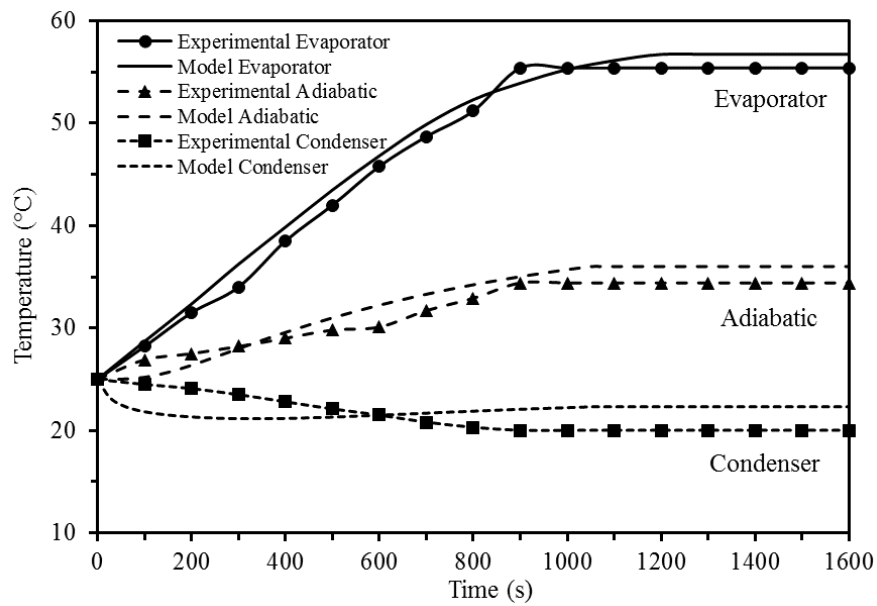
Figure 4.32 Compared temperature profiles at pipe wall of HOHP from model and
experiment at $T_e = 60°C$ with working fluid of ethanol
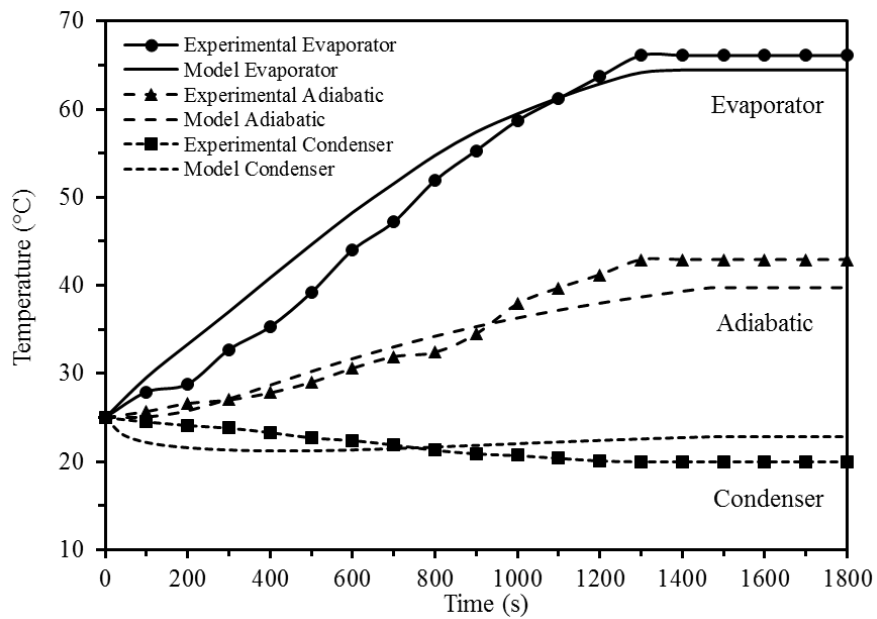
Figure 4.33 Compared temperature profiles at pipe wall of HOHP from model and
experiment at $T_e = 70°C$ with working fluid of ethanol
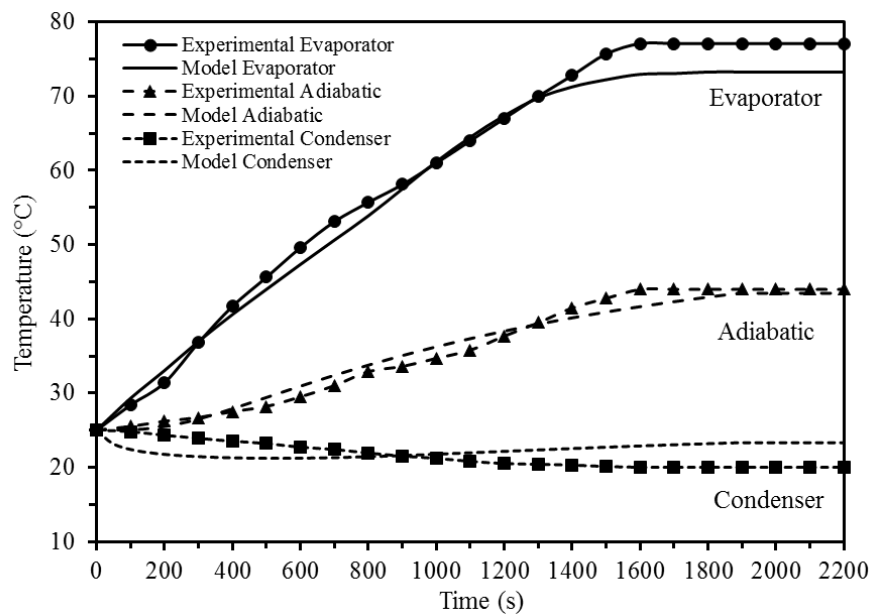
Figure 4.34 Compared temperature profiles at pipe wall of HOHP from model and experiment at $T_e = 80°C$ with working fluid of ethanol

The results of the temperatures for the pipe wall of the HOHP at the evaporator, the adiabatic and the condenser sections from the numerical model are compared with the experimental data and are presented in figures 4.35, 4.36 and 4.37, respectively, for the outer wall temperatures at the evaporator section of 60, 70 and 80°C, the working fluid as R11 and the inner diameter of 2.0 mm. The transient condition temperature profiles from the numerical model and the experimental data were plotted as functions of time. The temperature from the experimental data was the average values for the evaporator, the adiabatic and the condenser sections. It was found that the transient temperature profiles in the evaporator section increased from the initial temperature of the pipe wall (25°C) to the outer wall temperatures that were input to the evaporator section (60, 70 and 80°C). Since the pipe wall was copper, the thermal conduction was then induced from the outer wall of the pipe to the inner wall of the pipe. In the adiabatic section, heat was induced by thermal conduction from the evaporator section, and the temperature of the adiabatic section increased until it reached a steady state temperature, at which it was close to the working temperatures (the average value of the temperatures between the evaporator and the condenser sections). However, the transient temperature profiles in the condenser section

decreased because the initial temperature (25ºC) was more than the outer wall temperature of the condenser section (20ºC). The times required to reach the steady state temperature at the end of the runs from the numerical model were about 1100, 1400 and 1800 s for the outer wall temperatures at the evaporator section of 60, 70 and 80°C, respectively. As seen from the figures, when the temperatures of the evaporator section increased, the time required to reach the steady state temperature was increased because the temperature was dependent on the time. The times required to reach the steady state temperature from the experiment were about 1010, 1380 and 1618 s for the outer wall temperatures at the evaporator section of 60, 70 and 80°C, respectively.

The solid lines correspond to the temperatures of the evaporator, the adiabatic and the condenser sections from the numerical model predicting the response of the temperature with time and the symbols correspond to the experimentally measured temperature average values. As seen from figures 4.35, 4.36 and 4.37, it was found that the comparisons between the results from the numerical model and the experimental data response curves are excellent for all three sections. The time required to reach the steady state temperature for the numerical model was not equal to the experiment because the numerical model was assumed to have no losses in the calculation, but the experiment had errors from some uncontrollable parameters. As seen from all the figures, the time required to reach the steady state temperature between the numerical model and the experimental results was different, and the differences were 8.2%, 1.4% and 10.1% for the outer wall temperatures at the evaporator section of 60, 70 and 80°C, respectively. The time required to reach the steady state temperature is an important parameter for the start-up of the HOHP. The two values from the numerical model and the experimental data are in good agreement.
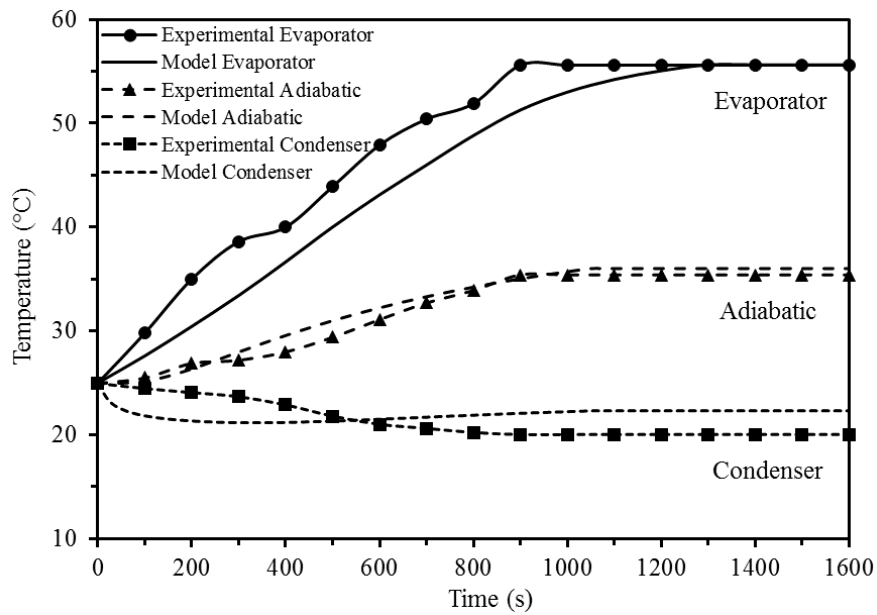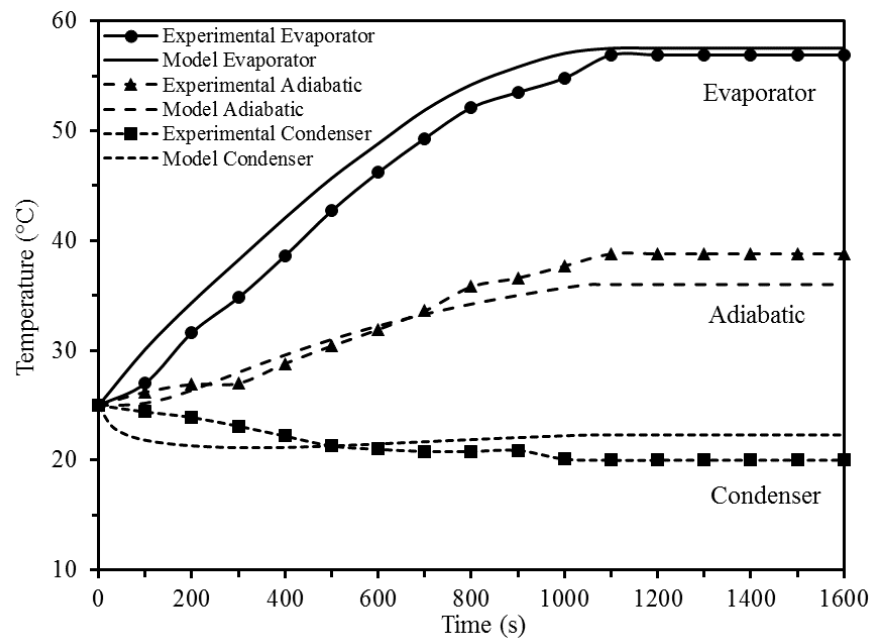
Figure 4.35 Compared temperature profiles at pipe wall of HOHP from model and
experiment at T_e = 60ºC with working fluid of R11
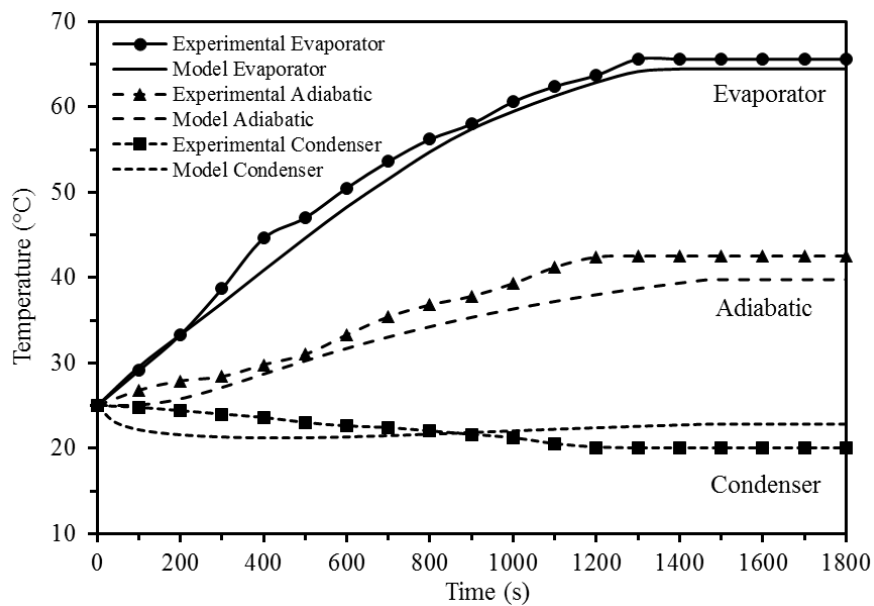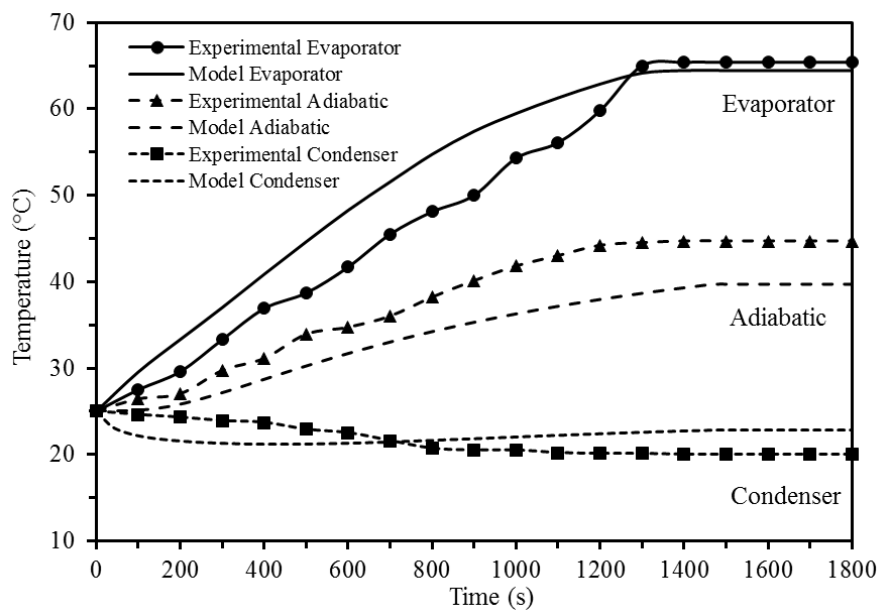

Figure 4.36 Compared temperature profiles at pipe wall of HOHP from model and
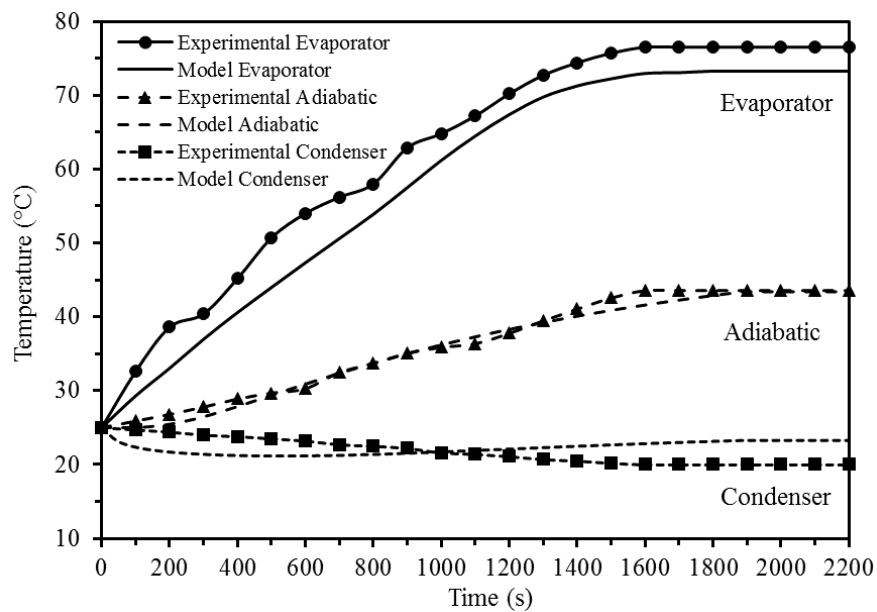experiment at T_e = 70ºC with working fluid of R11
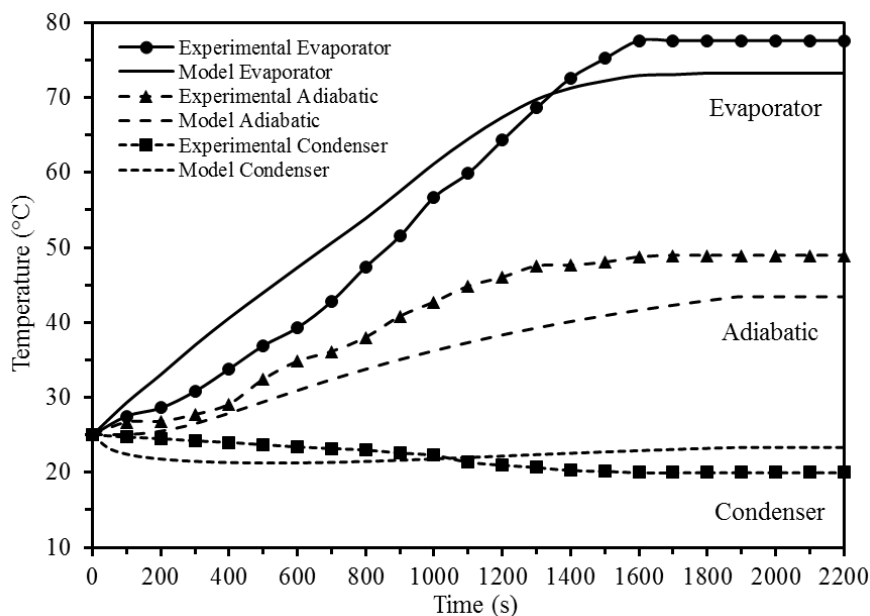
Figure 4.37 Compared temperature profiles at pipe wall of HOHP from model and

experiment at $T_e = 80°C$ with working fluid of R11

4.3.2 Comparison of heat transfer of HOHP

Figure 4.38 shows the comparisons of the heat transfer profiles from the numerical model and the experimental data under the transient condition of the HOHP with the temperatures at the evaporator section of 60, 70 and 80°C, the working fluid as water and the inner diameter of 2.0 mm. The figure identifies that the times to start-up for the heat transfer of the HOHP from the numerical model and the experimental data with the temperature at the evaporator section of 60°C were 700 and 644 s, respectively. The times to start-up for the heat transfer of the HOHP from the numerical model and the experimental data with the temperature at the evaporator section of 70°C were 800 and 742 s, respectively. The times to start-up for the heat transfer of the HOHP from the numerical model and the experimental data with the temperature at the evaporator section of 80°C were 900 and 852 s, respectively. Moreover, this figure shows that the times required to reach the steady state heat transfer from the numerical model and the experimental data with the temperature at the evaporator section of 60°C were 2000 and 1826 s, respectively. The times required to reach the steady state heat transfer from the numerical model and the experimental data with the temperature at the evaporator section of 70°C were 2200 and 2116 s, respectively. The times required to reach the

steady state heat transfer from the numerical model and the experimental data with the temperature at the evaporator section of 60ºC were 2400 and 2290 s, respectively. As seen from the figure, the time required to reach the steady state heat transfer depends on the temperatures that are input to the evaporator section of the HOHP. The heat transfer profiles between the numerical model and the experimental data were very similar, with the differences being 8.7%, 3.8% and 4.6% for the temperatures at the evaporator section of 60, 70 and 80ºC, respectively.
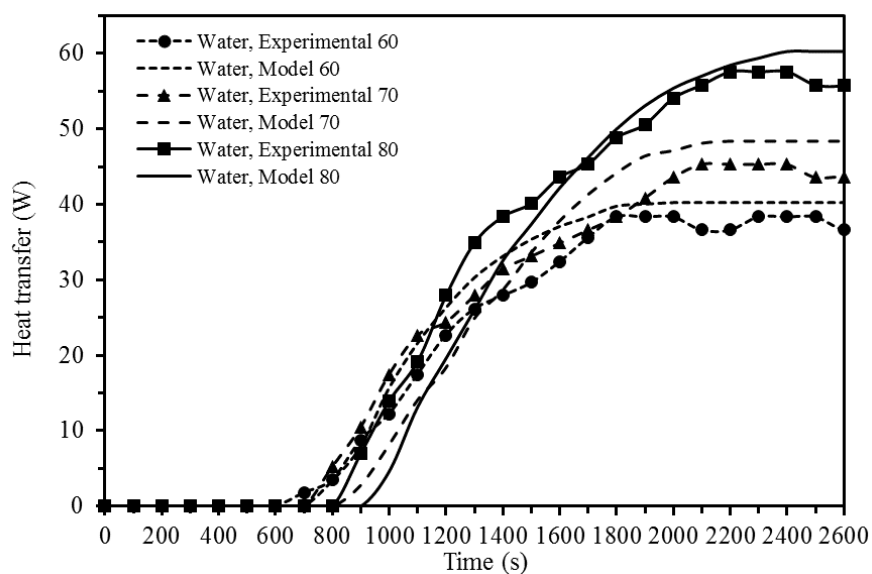
Figure 4.38 Compared heat transfer of HOHP from model and experiment
at T_e = 60, 70 and 80ºC with working fluid of water

Figure 4.39 shows the comparisons of the heat transfer profiles from the numerical model and the experimental data under the transient condition of the HOHP with the temperatures at the evaporator section of 60, 70 and 80ºC, the working fluid as ethanol and the inner diameter of 2.0 mm. The figure identifies that the times to start-up for the heat transfer of the HOHP from the numerical model and the experimental data with the temperature at the evaporator section of 60ºC were 500 and 514 s, respectively. The times to start-up for the heat transfer of the HOHP from the numerical model and the experimental data with the temperature at the evaporator section of 70ºC were 600 and 554 s, respectively. The times to start-up for the heat transfer of the

HOHP from the numerical model and the experimental data with the temperature at the evaporator section of 80ºC were 700 and 630 s, respectively. Moreover, this figure shows that the times required to reach the steady state heat transfer from the numerical model and the experimental data with the temperature at the evaporator section of 60ºC were 1900 and 1786 s, respectively. The times required to reach the steady state heat transfer from the numerical model and the experimental data with the temperature at the evaporator section of 70ºC were 2100 and 1880 s, respectively. The times required to reach the steady state heat transfer from the numerical model and the experimental data with the temperature at the evaporator section of 60ºC were 2300 and 2142 s, respectively. As seen from the figure, the time required to reach the steady state heat transfer depends on the temperatures that are input to the evaporator section of the HOHP. The heat transfer profiles between the numerical model and the experiment data were very similar, with the differences being 6.0%, 10.5% and 6.9% for the temperatures at the evaporator section of 60, 70 and 80ºC, respectively.
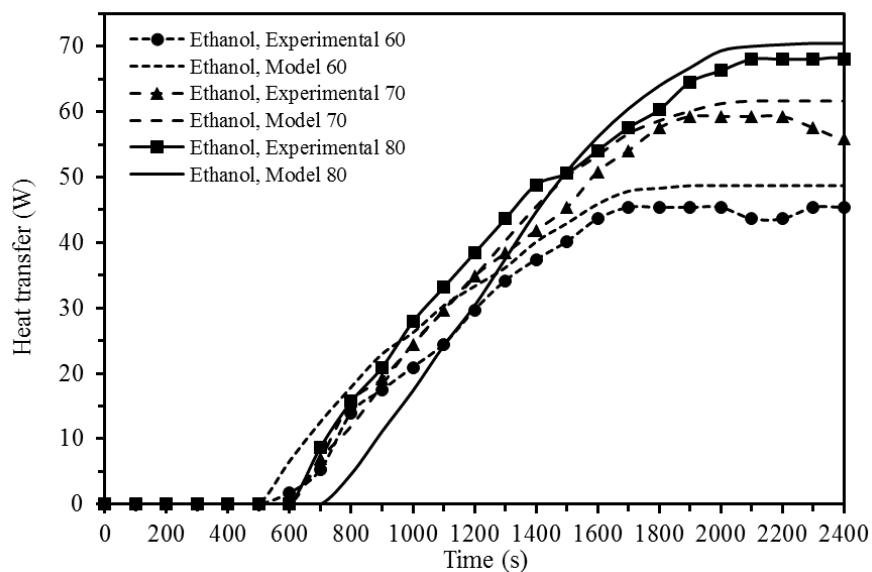
Figure 4.39 Compared heat transfer of HOHP from model and experiment
at T_e = 60, 70 and 80ºC with working fluid of ethanol
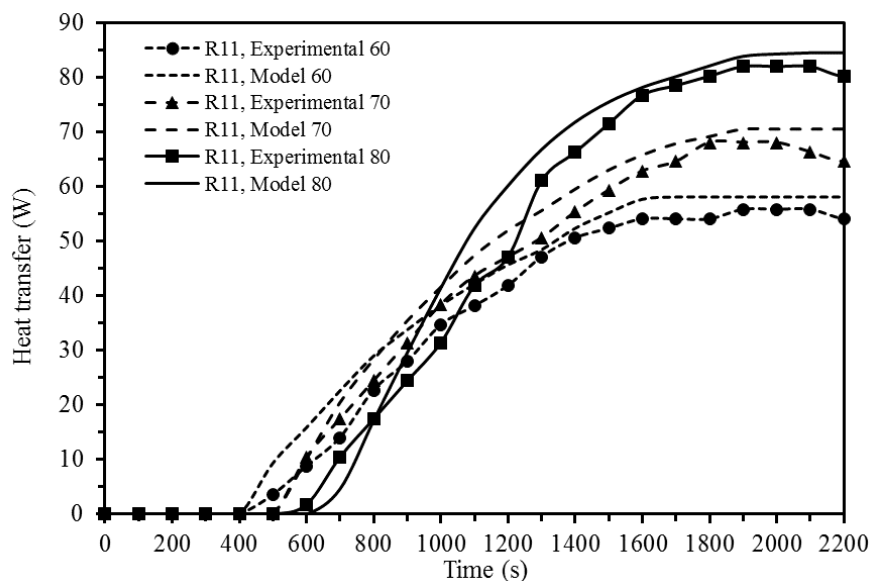
Figure 4.40 Compared heat transfer of HOHP from model and experimental

at T_e = 60, 70 and 80°C with working fluid of R11

Figure 4.40 shows the comparisons of the heat transfer profiles from the numerical model and the experimental data under the transient condition of the HOHP with the temperatures at the evaporator section of 60, 70 and 80°C, the working fluid as R11 and the inner diameter of 2.0 mm. The figure identifies that the times to start-up for the heat transfer of the HOHP from the numerical model and the experimental data with the temperature at the evaporator section of 60°C were 400 and 396 s, respectively. The times to start-up for the heat transfer of the HOHP from the numerical model and the experimental data with the temperature at the evaporator section of 70°C were 500 and 464 s, respectively. The times to start-up for the heat transfer of the HOHP from the numerical model and the experimental data with the temperature at the evaporator section of 80°C were 600 and 520 s, respectively. Moreover, this figure shows that the times required to reach the steady state heat transfer from the numerical model and the experimental data with the temperature at the evaporator section of 60°C were 1700 and 1634 s, respectively. The times required to reach the steady state heat transfer from the numerical model and the experimental data with the temperature at the evaporator section of 70°C were 1900 and 1818 s, respectively. The times required to reach the steady state heat transfer from the numerical model and the experimental data with the

temperature at the evaporator section of 60ºC were 2100 and 1952 s, respectively. As seen from the figure, the time required to reach the steady state heat transfer depends on the temperatures that are input into the evaporator section of the HOHP. The heat transfer profiles between the numerical model and the experiment data were very similar, with the differences being 3.9%, 4.3% and 7.0% for the temperatures at the evaporator section of 60, 70 and 80ºC, respectively.

4.3.3 Comparison of heat transfer of HOHP heat exchanger

Figure 4.41 shows the comparison of the heat transfer profiles from the numerical model and the experimental data under the transient condition of the HOHP heat exchanger with the temperatures at the evaporator section of 60, 70 and 80ºC, the working fluid as R11 and the inner diameter of 2.0 mm. The figure identified that the times to start-up for the heat transfer of the HOHP heat exchanger from the numerical model and the experimental data for the temperature at the evaporator section of 60ºC were 400 and 368 s, respectively; for the temperature at the evaporator section of 70ºC were 500 and 456 s, respectively; and for the temperature at the evaporator section of 80ºC were 600 and 544 s, respectively. Moreover, this figure shows that the times required to reach the steady state heat transfer from the numerical model and the experimental data for the temperature at the evaporator section of 60ºC were 1700 and 1634 s, respectively; for the temperature at the evaporator section of 70ºC were 2000 and 1912 s, respectively; and for the temperature at the evaporator section of 60ºC were 2500 and 2378 s, respectively. As seen from the figure, the time required to reach the steady state heat transfer depends on the temperatures that are input to the evaporator section of the HOHP heat exchanger. The heat transfer profiles between the numerical model and the experiment data were very similar, with the differences being 3.9%, 4.6% and 4.9% for the temperatures at the evaporator section of 60, 70 and 80ºC, respectively.
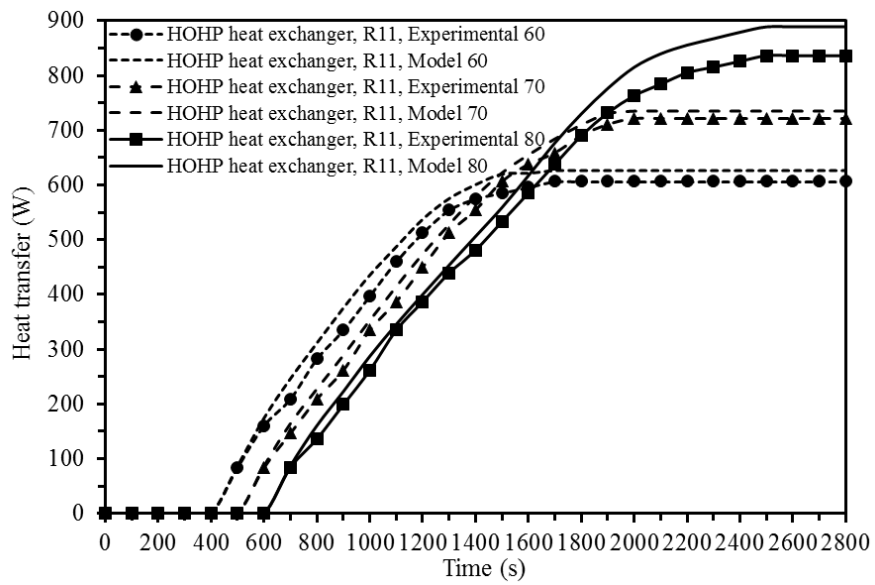
Figure 4.41 Compared heat transfer of HOHP heat exchanger from model and

experiment at T_e = 60, 70 and 80ºC with working fluid

of R11 and D_i = 2.0 mm

CHAPTER 5

CONCLUSIONS AND SUGGESTIONS

Following the objectives of this research to develop a mathematical model for the transient condition to prediction the heat transfer of the HOHP and to perform an experiment in which a HOHP under various conditions was studied, as well as to apply the HOHP results to the HOHP heat exchanger and design a HOHP heat exchanger from the simulation model, and to solve the equations and processes, the findings were presented in the results chapters. The summary of this thesis is presented in this chapter.

5.1 Conclusions

5.1.1 Conclusions from mathematical model

5.1.1.1   Temperature at pipe wall of HOHP from model

The temperature for the HOHP at the evaporator section of 60ºC gave the lowest time to reach a steady state temperature, follow by the temperatures at the evaporator section of 70 and 80ºC. The working fluid of R11 gave the lowest time to a steady state temperature, follow by the working fluids of ethanol and water.

5.1.1.2   Heat transfer of HOHP from model

The temperature at the evaporator section of 80ºC had the highest heat transfer for the HOHP, follow by the temperatures at the evaporator section of 70 and 60ºC. The working fluid of R11 had the highest heat transfer for the HOHP, follow by the working fluids of ethanol and water.

5.1.1.3   Heat transfer of HOHP heat exchanger from model

The temperature at the evaporator section of 80ºC had the highest heat transfer for the HOHP heat exchanger, follow by the temperatures at the evaporator section of 70 and 60ºC.

5.1.2 Conclusions from experiment

5.1.2.1   The working fluid has the major effect on the heat transfer of the HOHP. The working fluid of R11 was the best working fluid that had the highest heat transfer. The working fluid of R11 had the highest heat transfer when compared to the working fluids of ethanol and water.

5.1.2.2   The temperature at the evaporator section of 80ºC was the best temperature that gave the highest heat transfer. The temperature at the evaporator section of 80ºC had the highest heat transfer when compared to the temperatures at the evaporator section of 70 and 60ºC.

5.1.2.3   The inner diameter for the pipe of 2.0 mm was the best inner diameter that gave the highest heat transfer. The inner diameter for the pipe of 2.0 mm had the highest heat transfer when compared to the inner diameters for the pipe of 1.8 and 1.6 mm.

5.1.3 Conclusions from HOHP heat exchanger

5.1.3.1   The best temperature for the evaporator section from the numerical model and the experimental evaluation to give the highest heat transfer for the HOHP heat exchanger was the temperature at the evaporator section of 80ºC, follow by the temperatures at the evaporator section of 70 and 60ºC.

5.1.3.2   The results from the comparison of the heat transfer of the HOHP heat exchanger from the numerical model and the experimental data shows that the heat transfer from the numerical model had shorter times to the steady state heat transfer and had higher heat transfers than the results from the experimental evaluation, but the two values were in good agreement.

5.2 Suggestions

5.2.1 The simulation codes in this work can be used to predict the temperature and the heat transfer during the start-up operation of a HOHP in the future.

5.2.2 The numerical simulation in this study can be used to predict the temperature and the heat transfer from the working fluids, the temperatures at the evaporator section and the inner diameters of the pipe that are different from this study.

5.2.3 The numerical simulation of the HOHP heat exchanger in this study can be used to design heat exchangers in the future.

5.2.4 In future work, the HOHP can have many applications.

REFERENCES

REFERENCES

[1]   Rittidech S. Heat Pipe Technology. 3th Edition, Mahasarakham, Thailand; 2012.

[2]   Sakulchangsatjatai P. Operation Modeling of Closed-End and Closed-Loop Oscillating Heat Pipes. Chaingmai, Thailand; 2002.

[3]   Pipatpaiboon N, Rittidech S, Huchaiyaphum H, Dangton W. and Meena P. Effect of Working Temperature on Heat Transfer Characteristic of Helix Oscillating Heat Pipe (HOHP). International Conference Science 4th, Technology and Innovation for Sustainable Well-Being. 2012; 10-12 August, Thailand.

[4]   Germano M. On the effect of torsion on a helical pipe flow. Journal of Fluid Mechanics. 1982; 125:1-8.

[5]   Dechaamphai P. Numerical Method in Engineering. 4th Edition, Bangkok, Thailand; 2003.

[6]   Incropera FP, Dewitt DP, Bergman TL. and Lavine AS. Fundamentals of heat and mass transfer. 6th edition. Hoboken: John Wiley & Sons (Asia) Pte. Ltd.; 2007.

[7]   Akbaridoust F, Rakhsha M, Abbassi A. and Saffar-Avval M. Experimental and numerical investigation of nanofluid heat transfer in helically coiled tubes at constant wall temperature using dispersion model. International Journal of Heat and Mass Transfer. 2013; 58:480-491.

[8]   Boothaisong S, Ritidech S, Chompookham T, Thongmoon M, Ding Y. and Li Y. Three-dimensional transient mathematical model to predict the heat transfer of a heat pipe. Advances in Mechanical Engineering. 2015; 7(2).

[9]   Jayakumar JS, Mahajani SM, Mandal JC, Iyer KN. and Vijayan PK. CFD analysis of single-phase flows inside helically coiled tubes. Computers and Chemical Engineering. 2010; 34:430-446.

[10]   Litster S, Pharoah JG. and Djilali N. Convective mass transfer in helical pipes: effect of curvature and torsion. Heat and Mass Transfer. 2006; 42:387-397.

[11] Nobari MRH. and Malvandi A. Torsion and curvature effects on fluid flow in a helical annulus. International Journal of Non-Linear Mechanics. 2013; 57:90-101.

[12] Saffari H. and Moosavi R. Numerical study of the influence of geometrical characteristics of a vertical helical coil on a bubbly flow. Journal of Applied Mechanics and Technical Physics. 2014; 55(6):957-969.

[13] Sakulchangsatjatai P, Terdtoon P, Wongratanaphisan T, Kamonpet P. and Murakami M. Operation modeling of closed-end and closed-loop oscillating heat pipes at normal operating condition. Applied Thermal Engineering. 2004; 24:995-1008.

[14] Sriudom Y, Rittidech S. and Chompookham T. The helical oscillating heat pipe: flow pattern behavior study. Advances in Mechanical Engineering. 2015; 7(1).

[15] Chang-Nian Chen, Ji-Tian Han, Tien-Chien Jen, Li Shao. and Wen-wen Chen. Experimental study on critical heat flux characteristics of R134a flow boiling in horizontal helically-coiled tubes. International Journal of Thermal Science. 2011; 50:169-177.

[16] Colorado-Garrido D, Santoyo-Castelazo E, Hernandez J. A, Garcia-Valladares O, Siqueiros J. and Juarez-Romero D. Heat transfer of a helical double-pipe vertical evaporator: Theoretical analysis and experimental validation. Applied Energy. 2009; 86:1144-1153.

[17] Conte I. and Peng XF. Numerical and experimental investigations of heat transfer performance of rectangular coil heat exchangers. Applied Thermal Engineering. 2009; 29:1799-1808.

[18] Devanahalli GP, Timothy JR. and Vijaya Raghavan GS. Natural convection heat transfer from helical coiled tubes. International Journal of Thermal Sciences. 2004; 43:359-365.

[19] Huttl TJ. and Friedrich R. Influence of curvature and torsion on turbulent flow in helically coiled pipe. International Journal of Heat and Fluid Flow. 2000; 21:345-353.

[20]   Kumar V, Saini S, Sharma M. and Nigam K.D.P. Pressure drop and heat transfer study in tube-in-tube helical heat exchanger. Chemical Engineering Science. 2006; 61:4403-4416.

[21]   Liping C. and Andrey KV. Heat transfer in a laminar flow in a helical pipe filled with a fluid saturated porous medium. International Journal of Thermal Sciences. 2005; 44:787-798.

[22]   Neshat E, Hossainpour S. and Bahiraee F. Experimental and numerical study on unsteady natural convection heat transfer in helically coiled tube heat exchangers. Heat Mass Transfer. 2014; 50:877-885.

[23]   Nobari MRH, Shiniyan B. and Mirzaei M. Mixed convection in a vertical helical annular pipe. International Journal Heat and Mass Transfer. 2014; 73:468-482.

[24]   Shuang-Ying Wu, Su-Jun Chen, Lan Xiao. and You-Rong Li. Numerical investigation on developing laminar forced convective heat transfer and entropy generation in an annular helicoidal tube. Journal of Mechanical Science and Technology. 2011; 25:1439-1477.

[25]   Shuang-Ying Wu, Su-Jun Chen, You-Rong Li. and Long-Jian Li. Numerical investigation of turbulent flow, heat transfer and entropy generation in a helical coiled tube with larger curvature ratio. Heat and Mass Transfer. 2009; 45:569-578.

[26]   Wael I.A. Aly. Numerical study on turbulent heat transfer and pressure drop of nanofluid in coiled tube-in-tube heat exchangers. Energy Conversion and Management. 2014; 79:304-316.

[27]   Yang G, Dong ZF. and Ebadian MA. Laminar forced convection in a helicoidal pipe with finite pitch. International Journal of Heat and Mass Transfer. 1995; 38(5):853-862.

[28]   Dunn P. and Reay D. Heat Pipe. Pergamon International Library: n.p.; 1982.

APPENDIX

APPENDIX A

Example calculation

Example calculation

Example calculation heat transfer of HOHP from model

Consider the HOHP with the physical dimensions are lengths of the evaporator section $L_e = 50\ mm$, lengths of the adiabatic section $L_a = 50\ mm$, lengths of the condenser section $L_c = 50\ mm$, total lengths of pipe in the evaporator section $s_e = 850\ mm$, total lengths of the condenser section $s_c = 850\ mm$, outer diameters $D_o = 3.0\ mm$, inner diameters $D_i = 2.0\ mm$, diameters of coil $D_{coil} = 50\ mm$, pitch $p_s = 10\ mm$ and inclinations angle $\theta = 90°$. The temperatures of the evaporator section of 80ºC and the adiabatic section of 20ºC. The heat transfer of the HOHP can be calculated as following:

The equation in calculation the heat transfer of the HOHP as

$$Q_{out}^{new} = \pi D h_c (T_{v,i} - T_{w,i})$$

Where D is inner diameter of pipe (m).

h_c is convective heat transfer coefficient (J/kg).

$T_{v,i}$ is temperature of vapor (ºC).

$T_{w,i}$ is temperature of pipe wall (ºC).

Calculated the convective heat transfer coefficient of the cooling water at the condenser section h_c as

$$h_c = \frac{kNu}{D}$$

$$Nu = C \left[\frac{\rho v D}{\mu} \right]^n \Pr^{1/3}$$

The value of C depend on Re

The properties of cooling water at 20ºC are

$$k_c = 0.5984 \ W/m°C, \ Pr = 7.01, \ \rho_c = 998.2 \ kg/m^3,$$

$$\mu_c = 1002.1 \times 10^{-6} \ Pa.s.$$

From the model we obtained

$$T_w = 21.30°C \ and \ T_v = 23.24°C$$

Calculated Re as

$$Re = \frac{\rho v D}{\mu} = \frac{998.2 \times 0.3 \times 0.0020}{1002.1 \times 10^{-6}} = 597.66$$

The Re value used to open the C and n value from table in Table E4, and has the $C = 0.683$, $n = 0.466$.

Then Nu can be calculated as

$$Nu = C\left[\frac{\rho v D}{\mu}\right]^n Pr^{1/3} = 0.683[597.66]^{0.466} 7.01^{1/3}$$

$$Nu = 25.71$$

Therefore the h_c can be calculated as

$$h_c = \frac{kNu}{D} = \frac{0.5984 \times 25.71}{0.0020}$$

$$h_c = 6921.13 \ J/kg$$

Calculated the heat transfer of the HOHP from model

$$Q = \pi D h_c (T_v - T_w)$$

$$Q = \pi \times 0.0016 \times 6921.13 \times (23.24 - 21.30)$$

$$Q = 84.36 \ W$$

Example calculated heat transfer of HOHP from model

The heat transfer of the HOHP from the model equal 84.36 W, then we calculated the heat transfer of the HOHP heat exchanger from the model as following:

From scope of research of the heat exchanger to provide the HOHP heat exchanger can be exchanger heat of 1000W, then calculated the number of turn as

$$N = \frac{Q}{Q_{Theory}}$$

$$N = \frac{1000 \ W}{84.36 \ W}$$

$$N = 11.85 = 12 \ tube$$

The properties of hot water in the evaporator section (80°C).

$\rho_h = 971.8 \ kg/m^3$, $\mu_h = 0.000355$ Pa.s, $C_{p,h} = 4197 \ J/kg°C$,

$k_h = 0.67 \ W/m°C$, and $\Pr_h = 2.22$,

The properties of cooling water in the condenser section (20°C).

$\rho_c = 998 \ kg/m^3$, $\mu_c = 0.001002$ Pa.s, $C_{p,c} = 4182 \ J/kg°C$,

$k_c = 0.598 \ W/m°C$, and $\Pr_c = 7.01$,

Calculated the maximum heat transfer from the evaporator and the condenser sections as

$$Q_{\max} = C_{\min}(T_{hi} - T_{ci})$$

Calculated $C_{\min}$, when $T_{hi} = 74.27°C$ (from the model), $T_{ci} = 20°C$, $\dot{m}_h = 0.00417 \, kg/s$ and $\dot{m}_c = 0.00417 \, kg/s$.

$$C_c = \dot{m}_c C_{p,c}$$

$$C_c = 0.00417 \times 4182$$

$$C_c = 17.4 \ W/°C$$

$$C_h = \dot{m}_h C_{p,h}$$

$$C_c = 0.00417 \times 4185$$

$$C_c = 17.5 \ W/°C$$

Then we have the C_{min} as

$$C_{min} = C_c = 17.4 \ W/°C$$

Therefore we can calculated Q_{max} as

$$Q_{max} = C_{min}(T_{hi} - T_{ci})$$

$$Q_{max} = 17.4(74.27 - 20)$$

$$Q_{max} = 946.50 \ W$$

Calculated the overall heat transfer of HOHP heat exchanger as

$$U = \frac{1}{1/h_e} + \frac{1}{1/h_c}$$

Calculated h_e at the evaporator section as

$$h_e = Nu_{D,h} \frac{k_h}{D_o}$$

Calculated the velocity of hot water in the evaporator section as

$$v_h = \frac{\dot{m}_h}{\rho_h A_h}$$

$$v_h = \frac{0.00417}{971.8 \times \pi \times 0.005^2}$$

$$v_h = 0.055 \ m/s$$

From calculation the number of tube, we set the $S_T = S_L = 75\ mm$ and $S_D = 62.5\ mm$. Therefore we can calculated the maximum velocity as

$$v_{max,h} = \frac{S_T}{2(S_D - D_o)} v_h$$

$$v_{max,h} = \frac{0.075}{2(0.0625 - 0.003)} 0.055$$

$$v_{max,h} = 0.034\ m/s$$

Calculated the Reynold Number as

$$\mathrm{Re}_{D,max,h} = \frac{\rho_h V_{max,h} D_o}{\mu_h}$$

$$\mathrm{Re}_{D,max,h} = \frac{971.8 \times 0.034 \times 0.003}{0.000355}$$

$$\mathrm{Re}_{D,max,h} = 282.93$$

The staggered arrangement with the number of tube more than 10 tube, when S_T/D_o and $S_L/D_o = 2.5$ we can open $C_{1.h}$, $C_{2.h}$ and m_h from Table 2.1 and Table 2.2 and we have $C_{1.h} = 0.497$, $C_{2.h} = 0.92$ and $m_h = 0.558$.

The Nussult Number of the HOHP heat exchanger at the evaporator section can be calculated as

$$Nu_{D,h} = C_{1,h} C_{2,h}\, \mathrm{Re}_{D,max,h}^{m_h}$$

$$Nu_{D,h} = 0.497 \times 0.92 \times 282.93^{0.558}$$

$$Nu_{D,h} = 15.32$$

Therefore h_e can be calculated as

$$h_e = Nu_{D,h} \frac{k_h}{D_o}$$

$$h_e = 15.32 \frac{0.67}{0.003}$$

$$h_e = 3420.71 \ W/m^2{}^\circ C$$

Calculated h_c at the condenser section as

$$h_c = Nu_{D,c} \frac{k_c}{D_o}$$

Calculated the velocity of cooling water in the condenser section as

$$v_c = \frac{\dot{m}_c}{\rho_c A_c}$$

$$v_c = \frac{0.00417}{998 \times \pi \times 0.005^2}$$

$$v_c = 0.053 \ m/s$$

From calculation the number of tube, we set the $S_T = S_L = 75 \ mm$ and $S_D = 62.5 \ mm$. Therefore we can calculated the maximum velocity as

$$v_{max,c} = \frac{S_T}{2(S_D - D_o)} v_c$$

$$v_{max,h} = \frac{0.075}{2(0.0625 - 0.003)} 0.053$$

$$v_{max,c} = 0.034 \ m/s$$

Calculated the Reynold Number as

$$Re_{D,max,c} = \frac{\rho_c V_{max,c} D_o}{\mu_c}$$

$$Re_{D,max,c} = \frac{998 \times 0.034 \times 0.003}{0.001002}$$

$$Re_{D,max,c} = 100.24$$

The staggered arrangement with the number of tube more than 10 tube, when S_T/D_o and $S_L/D_o = 2.5$ we can open $C_{1.c}$, $C_{2.c}$ and m_c from Table 2.1 and Table 2.2 and we have $C_{1.c} = 0.497$, $C_{2,c} = 0.92$ and $m_c = 0.558$.

The Nussult Number of the HOHP heat exchanger at the condenser section can be calculated as

$$Nu_{D,c} = C_{1,c} C_{2,c} \, \mathrm{Re}_{D,\max,c}^{m_c}$$

$$Nu_{D,c} = 0.497 \times 0.92 \times 100.24^{0.558}$$

$$Nu_{D,c} = 12.12$$

The h_c can be calculated as

$$h_c = Nu_{D,c} \frac{k_c}{D_o}$$

$$h_c = 12.12 \frac{0.598}{0.003}$$

$$h_c = 2415.99 \ W/m^2 {}^\circ C$$

Therefore the can be calculated as

$$U = \frac{1}{1/h_e} + \frac{1}{1/h_c}$$

$$U = \frac{1}{\dfrac{1}{3420.71}} + \frac{1}{\dfrac{1}{2415.99}}$$

$$U = 1415.94 \ W/m^2 {}^\circ C$$

Calculated the area of pipe in heat transfer at the evaporator and the condenser sections can be calculated as

$$A = N\pi D_o (s_e + s_c)$$

$$A = 12 \times \pi \times 0.003 \times (0.85 + 0.85)$$

$$A = 0.19 \ m^2$$

Calculated the NTU as

$$NTU = \frac{UA}{C_{min}}$$

$$NTU = \frac{1415.94 \times 0.19}{17.4}$$

$$NTU = 15.39$$

The HOHP heat exchanger has staggered flow arrangement can be calculated C value as

$$C = \frac{C_{min}}{C_{max}}$$

$$C = \frac{17.4}{17.5}$$

$$C = 0.99$$

Calculated the effectiveness of the HOHP heat exchanger as

$$\varepsilon = \frac{1 - \exp[-NTU(1-C)]}{1 - C\exp[-NTU(1-C)]}$$

$$\varepsilon = \frac{1 - \exp[-15.39(1-0.99)]}{1 - 0.99\exp[-15.39(1-0.99)]}$$

$$\varepsilon = 0.94$$

Therefore the heat transfer of the HOHP heat exchanger can be calculated as

$$Q = \varepsilon Q_{max}$$

$$Q = 0.94 \times 946.50$$

$$Q = 889.0 \ W$$

Example calculated heat transfer of HOHP from experimental

Consider the HOHP with the physical dimensions as same with the model. The calculation of the heat transfer of the HOHP can be calculated as following:

The equation in calculation the heat transfer of the HOHP as

$$Q = \dot{m}c_p(T_{out} - T_{in})$$

Where Q is heat transfer of the HOHP (W).

$\dot{m}$ is mass flow rate of cooling water (kg/s).

c_p is specific heat of cooling water (J/kg°C).

T_{in} is inlet temperature of cooling water at the condenser (°C).

T_{out} is outlet temperature of cooling water at the condenser (°C).

The properties of cooling water at 20°C as

$C_{p,c} = 4183 \ J/kg°C$

In experimental of the HOHP we set the mass flow rate as

$\dot{m} = 0.00417 \ kg/s$

From the experimental we obtained

$T_{in} = 20.1°C$ and $T_{out} = 24.8°C$

Calculated the heat transfer of the HOHP from experimental as

$Q = \dot{m}c_p(T_{out} - T_{in})$

$Q = 0.00417 \times 4183 \times (24.8 - 20.1)$

$Q = 81.98 \ W$

Example calculation heat transfer of HOHP heat exchanger from experimental

Consider the HOHP heat exchanger with designed by best working fluid and best inner diameter, we have the physical dimension of the HOHP heat exchanger as length of the evaporator section $L_e = 50 \ mm$, length of the adiabatic section $L_a = 50 \ mm$, length of the condenser section $L_c = 50 \ mm$, total length of pipe in the evaporator section $s_e = 850 \ mm$, total length of the condenser section $s_c = 850 \ mm$, outer diameter $D_o = 3.0 \ mm$, inner diameter $D_i = 2.0 \ mm$, diameter of coil $D_{coil} = 50 \ mm$, pitch $p_s = 10 \ mm$ and inclination angle $\theta = 90°$. The temperature of the evaporator section of 80°C and the adiabatic section of 20°C. The calculation of the heat transfer of the HOHP can be calculated as following:

The equation in calculation the heat transfer of the HOHP heat exchanger as

$$Q = \dot{m}c_p(T_{out} - T_{in})$$

Where Q is heat transfer of the HOHP heat exchanger (W).

$\dot{m}$ is mass flow rate of cooling water (kg/s).

c_p is specific heat of cooling water (J/kg°C).

T_{in} is inlet temperature of cooling water at the condenser (°C).

T_{out} is outlet temperature of cooling water at the condenser (°C).

The properties of water at 20°C as

$C_{p,c} = 4183 \ J/kg°C$

In experimental of the HOHP heat exchanger we set the mass flow rate as

$\dot{m} = 0.025 \ kg/s$

From the experimental we obtained:

$$T_{in} = 19.8°C \text{ and } T_{out} = 27.8°C$$

Calculated the heat transfer of the HOHP heat exchanger from experimental as

$$Q = \dot{m}c_p(T_{out} - T_{in})$$

$$Q = 0.025 \times 4183 \times (27.8 - 19.8)$$

$$Q = 836.40 \ W$$

APPENDIX B

Data analysis

Table B.1   Results of temperatures from model and experimental of HOHP

with working fluid of water, $T_e = 60$ºC and $D_i = 2.0$ mm

Time	Model (°C)			Experimental (°C)		
(sec.)	Evaporator	Adiabatic	Condenser	Evaporator	Adiabatic	Condenser
0	25.00	25.00	25.00	25.0	25.0	25.0
100	27.61	25.20	21.85	29.8	25.5	24.5
200	30.45	26.37	21.34	35.0	26.9	24.1
300	33.42	28.00	21.18	38.6	27.2	23.7
400	36.66	29.59	21.20	40.0	28.0	22.9
500	40.01	31.02	21.33	43.9	29.4	21.8
600	43.12	32.26	21.51	47.9	31.1	21.0
700	45.99	33.33	21.71	50.4	32.7	20.6
800	48.83	34.26	21.90	51.9	33.9	20.2
900	51.29	35.05	22.08	55.6	35.4	20.0
1000	53.01	35.74	22.25	55.6	35.4	20.0
1100	54.22	36.05	22.32	55.6	35.4	20.0
1200	55.06	36.05	22.32	55.6	35.4	20.0
1300	55.63	36.05	22.32	55.6	35.4	20.0
1400	55.63	36.05	22.32	55.6	35.4	20.0
1500	55.63	36.05	22.32	55.6	35.4	20.0
1600	55.63	36.05	22.32	55.6	35.4	20.0

Table B.2   Results of temperatures from model and experimental of HOHP
with working fluid of water, $T_e = 70°C$ and $D_i = 2.0$ mm

Time	Model (°C)			Experimental (°C)		
(sec.)	Evaporator	Adiabatic	Condenser	Evaporator	Adiabatic	Condenser
0	25.00	25.00	25.00	25.0	25.0	25.0
100	29.56	25.09	22.11	29.1	26.8	24.8
200	33.32	25.90	21.53	33.3	27.9	24.4
300	37.01	27.36	21.28	38.7	28.4	24.0
400	40.87	29.00	21.20	44.6	29.8	23.6
500	44.63	30.61	21.24	47.0	31.0	23.0
600	48.28	32.10	21.36	50.5	33.3	22.6
700	51.56	33.46	21.53	53.6	35.4	22.4
800	54.75	34.68	21.72	56.2	36.8	22.0
900	57.41	35.77	21.92	58.0	37.8	21.6
1000	59.48	36.75	22.12	60.6	39.3	21.2
1100	61.29	37.62	22.32	62.4	41.2	20.5
1200	62.88	38.40	22.50	63.7	42.4	20.1
1300	64.16	39.10	22.67	65.6	42.5	20.0
1400	64.45	39.73	22.82	65.6	42.5	20.0
1500	64.45	39.73	22.82	65.6	42.5	20.0
1600	64.45	39.73	22.82	65.6	42.5	20.0
1700	64.45	39.73	22.82	65.6	42.5	20.0
1800	64.45	39.73	22.82	65.6	42.5	20.0

Table B.3   Results of temperatures from model and experimental of HOHP

with working fluid of water, $T_e = 80$ºC and $D_i = 2.0$ mm

Time	Model (°C)			Experimental (°C)		
(sec.)	Evaporator	Adiabatic	Condenser	Evaporator	Adiabatic	Condenser
0	25.00	25.00	25.00	25.0	25.0	25.0
100	29.31	25.02	22.52	32.6	25.9	24.7
200	33.05	25.67	21.66	38.6	26.8	24.4
300	36.98	26.68	21.43	40.4	27.8	24.0
400	40.60	27.94	21.29	45.2	28.9	23.8
500	43.99	29.31	21.23	50.7	29.7	23.5
600	47.34	31.35	21.26	54.0	30.3	23.2
700	50.62	32.65	21.34	56.2	32.5	22.7
800	53.90	33.88	21.46	58.0	33.7	22.5
900	57.51	35.03	21.60	62.9	35.1	22.2
1000	61.20	36.60	21.85	64.8	35.9	21.6
1100	64.49	37.57	22.02	67.2	36.4	21.4
1200	67.39	38.46	22.19	70.2	37.8	21.1
1300	69.76	39.29	22.36	72.7	39.5	20.7
1400	71.27	40.06	22.53	74.4	41.1	20.5
1500	72.23	41.11	22.76	75.7	42.6	20.2
1600	72.96	41.75	22.91	76.5	43.6	20.0
1700	73.06	42.35	23.05	76.5	43.6	20.0
1800	73.27	43.41	23.31	76.5	43.6	20.0
1900	73.27	43.41	23.31	76.5	43.6	20.0
2000	73.27	43.41	23.31	76.5	43.6	20.0
2100	73.27	43.41	23.31	76.5	43.6	20.0
2200	73.27	43.41	23.31	76.5	43.6	20.0

Table B.4   Results of temperatures from model and experimental of HOHP

with working fluid of ethanol, T_e = 60ºC and D_i = 2.0 mm

Time	Model (°C)			Experimental (°C)		
(sec.)	Evaporator	Adiabatic	Condenser	Evaporator	Adiabatic	Condenser
0	25.00	25.00	25.00	25.0	25.0	25.0
100	28.70	25.20	21.85	28.2	26.9	24.5
200	32.36	26.37	21.34	31.5	27.5	24.1
300	36.23	28.00	21.18	34.0	28.2	23.5
400	39.87	29.59	21.20	38.5	29.0	22.8
500	43.49	31.02	21.33	42.0	29.8	22.1
600	46.83	32.26	21.51	45.8	30.1	21.5
700	49.89	33.33	21.71	48.7	31.7	20.8
800	52.31	34.26	21.90	51.2	32.9	20.3
900	53.92	35.05	22.08	55.4	34.4	20.0
1000	55.26	35.74	22.25	55.4	34.4	20.0
1100	56.13	36.05	22.32	55.4	34.4	20.0
1200	56.73	36.05	22.32	55.4	34.4	20.0
1300	56.73	36.05	22.32	55.4	34.4	20.0
1400	56.73	36.05	22.32	55.4	34.4	20.0
1500	56.73	36.05	22.32	55.4	34.4	20.0
1600	56.73	36.05	22.32	55.4	34.4	20.0

Table B.5 Results of temperatures from model and experimental of HOHP

with working fluid of ethanol, $T_e = 70°C$ and $D_i = 2.0$ mm

Time	Model (°C)			Experimental (°C)		
(sec.)	Evaporator	Adiabatic	Condenser	Evaporator	Adiabatic	Condenser
0	25.00	25.00	25.00	25.0	25.0	25.0
100	29.56	25.09	22.11	27.9	25.7	24.5
200	33.32	25.90	21.53	28.8	26.6	24.1
300	37.01	27.36	21.28	32.7	27.0	23.8
400	40.87	29.00	21.20	35.3	27.8	23.3
500	44.63	30.61	21.24	39.2	29.0	22.7
600	48.28	32.10	21.36	44.0	30.6	22.4
700	51.56	33.46	21.53	47.2	31.9	21.9
800	54.75	34.68	21.72	51.9	32.4	21.3
900	57.41	35.77	21.92	55.3	34.5	20.9
1000	59.48	36.75	22.12	58.7	37.9	20.7
1100	61.29	37.62	22.32	61.2	39.7	20.4
1200	62.88	38.40	22.50	63.7	41.2	20.1
1300	64.16	39.10	22.67	66.1	42.9	20.0
1400	64.45	39.73	22.82	66.1	42.9	20.0
1500	64.45	39.73	22.82	66.1	42.9	20.0
1600	64.45	39.73	22.82	66.1	42.9	20.0
1700	64.45	39.73	22.82	66.1	42.9	20.0
1800	64.45	39.73	22.82	66.1	42.9	20.0

Table B.6   Results of temperatures from model and experimental of HOHP

with working fluid of ethanol, $T_e = 80$ºC and $D_i = 2.0$ mm

Time	Model (°C)			Experimental (°C)		
(sec.)	Evaporator	Adiabatic	Condenser	Evaporator	Adiabatic	Condenser
0	25.00	25.00	25.00	25.0	25.0	25.0
100	29.31	25.12	22.11	28.4	25.5	24.8
200	33.05	25.67	21.66	31.4	26.2	24.3
300	36.98	26.68	21.43	36.8	26.7	23.9
400	40.60	27.94	21.29	41.7	27.5	23.5
500	43.99	30.00	21.23	45.6	28.2	23.2
600	47.34	31.35	21.26	49.6	29.5	22.7
700	50.62	32.65	21.34	53.1	31.0	22.4
800	53.90	33.88	21.46	55.7	32.9	21.9
900	57.51	35.03	21.60	58.1	33.6	21.5
1000	61.20	36.60	21.85	61.0	34.7	21.2
1100	64.49	37.57	22.02	64.0	35.8	20.8
1200	67.39	38.46	22.19	67.0	37.7	20.5
1300	69.76	39.29	22.36	70.0	39.5	20.4
1400	71.27	40.78	22.69	72.8	41.5	20.3
1500	72.23	41.44	22.84	75.7	42.8	20.1
1600	72.96	42.35	23.05	77.1	44.0	20.0
1700	73.06	42.90	23.19	77.1	44.0	20.0
1800	73.27	43.41	23.31	77.1	44.0	20.0
1900	73.27	43.41	23.31	77.1	44.0	20.0
2000	73.27	43.41	23.31	77.1	44.0	20.0
2100	73.27	43.41	23.31	77.1	44.0	20.0
2200	73.27	43.41	23.31	77.1	44.0	20.0

Table B.7   Results of temperatures from model and experimental of HOHP

with working fluid of R11, $T_e = 60ºC$ and $D_i = 2.0$ mm

Time	Model (°C)			Experimental (°C)		
(sec.)	Evaporator	Adiabatic	Condenser	Evaporator	Adiabatic	Condenser
0	25.00	25.00	25.00	25.0	25.0	25.0
100	30.10	25.20	21.85	27.0	26.2	24.4
200	34.36	26.37	21.34	31.6	26.9	23.9
300	38.23	28.00	21.18	34.8	27.0	23.1
400	42.07	29.59	21.20	38.6	28.8	22.2
500	45.69	31.02	21.33	42.7	30.4	21.3
600	48.83	32.26	21.51	46.2	31.9	21.0
700	51.89	33.33	21.71	49.3	33.6	20.8
800	54.21	34.26	21.90	52.1	35.8	20.8
900	55.82	35.05	22.08	53.5	36.6	20.9
1000	57.06	35.74	22.25	54.8	37.7	20.1
1100	57.52	36.05	22.32	56.9	38.8	20.0
1200	57.52	36.05	22.32	56.9	38.8	20.0
1300	57.52	36.05	22.32	56.9	38.8	20.0
1400	57.52	36.05	22.32	56.9	38.8	20.0
1500	57.52	36.05	22.32	56.9	38.8	20.0
1600	57.52	36.05	22.32	56.9	38.8	20.0

Table B.8 Results of temperatures from model and experimental of HOHP

with working fluid of R11, $T_e = 70ºC$ and $D_i = 2.0$ mm

Time	Model (°C)			Experimental (°C)		
(sec.)	Evaporator	Adiabatic	Condenser	Evaporator	Adiabatic	Condenser
0	25.00	25.00	25.00	25.0	25.0	25.0
100	29.56	25.09	22.11	27.5	26.4	24.6
200	33.32	25.90	21.53	29.6	27.0	24.3
300	37.01	27.36	21.28	33.3	29.7	23.9
400	40.87	29.00	21.20	36.9	31.1	23.7
500	44.63	30.61	21.24	38.7	33.9	22.9
600	48.28	31.62	21.31	41.7	34.7	22.5
700	51.56	33.02	21.47	45.5	36.0	21.6
800	54.75	34.28	21.65	48.1	38.2	20.7
900	57.41	35.42	21.86	50.0	40.1	20.5
1000	59.48	36.11	21.99	54.3	41.8	20.5
1100	61.29	37.05	22.19	56.1	43.0	20.2
1200	62.88	37.89	22.38	59.8	44.2	20.1
1300	64.16	38.65	22.56	65.0	44.5	20.1
1400	64.45	39.73	22.82	65.4	44.7	20.0
1500	64.45	39.73	22.82	65.4	44.7	20.0
1600	64.45	39.73	22.82	65.4	44.7	20.0
1700	64.45	39.73	22.82	65.4	44.7	20.0
1800	64.45	39.73	22.82	65.4	44.7	20.0

Table B.9   Results of temperatures from model and experimental of HOHP

with working fluid of R11, T_e = 80ºC and D_i = 2.0 mm

Time	Model (°C)			Experimental (°C)		
(sec.)	Evaporator	Adiabatic	Condenser	Evaporator	Adiabatic	Condenser
0	25.00	25.00	25.00	25.0	25.0	25.0
100	29.31	25.02	22.52	27.5	26.7	24.7
200	33.05	25.33	21.85	28.6	26.8	24.5
300	36.98	26.13	21.53	30.8	27.7	24.2
400	40.60	27.29	21.35	33.8	29.1	24.0
500	43.99	29.31	21.23	36.9	32.4	23.7
600	47.34	30.68	21.24	39.3	34.8	23.4
700	50.62	33.27	21.40	42.8	36.1	23.2
800	53.90	34.46	21.53	47.4	38.0	23.0
900	57.51	35.57	21.68	51.5	40.8	22.6
1000	61.20	36.60	21.85	56.7	42.7	22.3
1100	64.49	38.02	22.10	59.9	44.8	21.4
1200	67.39	38.88	22.27	64.3	46.0	21.0
1300	69.76	39.68	22.44	68.6	47.5	20.7
1400	71.27	41.11	22.76	72.6	47.6	20.3
1500	72.23	41.75	22.91	75.2	48.0	20.2
1600	72.96	42.63	23.12	77.6	48.7	20.0
1700	73.06	43.16	23.25	77.6	48.9	20.0
1800	73.27	43.41	23.31	77.6	48.9	20.0
1900	73.27	43.41	23.31	77.6	48.9	20.0
2000	73.27	43.41	23.31	77.6	48.9	20.0
2100	73.27	43.41	23.31	77.6	48.9	20.0
2200	73.27	43.41	23.31	77.6	48.9	20.0

Table B.10   Results of heat transfer from model and experimental of HOHP

with working fluid of water, T_e = 60, 70 and 80ºC, and D_i = 2.0 mm

Time	Model			Experimental		
(sec.)	60ºC	70ºC	80ºC	60ºC	70ºC	80ºC
0	0.00	0.00	0.00	0.00	0.00	0.00
100	0.00	0.00	0.00	0.00	0.00	0.00
200	0.00	0.00	0.00	0.00	0.00	0.00
300	0.00	0.00	0.00	0.00	0.00	0.00
400	0.00	0.00	0.00	0.00	0.00	0.00
500	0.00	0.00	0.00	0.00	0.00	0.00
600	0.00	0.00	0.00	0.00	0.00	0.00
700	1.74	0.00	0.00	0.00	0.00	0.00
800	3.49	5.23	0.00	3.31	0.00	0.00
900	8.72	10.47	6.98	7.85	2.77	0.00
1000	12.21	17.44	13.95	15.59	8.12	4.62
1100	17.44	22.68	19.19	21.56	14.03	13.15
1200	22.68	24.42	27.91	26.26	18.31	19.59
1300	26.16	27.91	34.89	30.26	24.85	26.03
1400	27.91	31.40	38.37	33.11	28.59	32.55
1500	29.65	33.14	40.12	35.36	33.56	37.36
1600	32.40	34.89	43.61	37.08	37.76	42.19
1700	35.63	36.63	45.35	38.34	41.26	46.22
1800	38.37	38.37	48.84	39.78	44.11	49.99
1900	38.37	40.86	50.59	40.06	46.36	53.07
2000	38.37	43.61	54.07	40.26	47.08	55.39
2100	36.63	45.35	55.82	40.26	48.06	57.01
2200	36.63	45.35	57.56	40.26	48.34	58.44
2300	38.37	45.35	57.56	40.26	48.34	59.37
2400	38.37	43.61	55.82	40.26	48.34	60.25
2500	38.37	43.61	55.82	40.26	48.34	60.25
2600	38.37	45.35	57.56	40.26	48.34	60.25
2700	38.37	43.61	55.82	40.26	48.34	60.25
2800	36.63	43.61	55.82	40.26	48.34	60.25

Table B.11   Results of heat transfer from model and experimental of HOHP
with working fluid of ethanol, T_e = 60, 70 and 80ºC, and D_i = 2.0 mm

Time	Model			Experimental		
(sec.)	60ºC	70ºC	80ºC	60ºC	70ºC	80ºC
0	0.00	0.00	0.00	0.00	0.00	0.00
100	0.00	0.00	0.00	0.00	0.00	0.00
200	0.00	0.00	0.00	0.00	0.00	0.00
300	0.00	0.00	0.00	0.00	0.00	0.00
400	0.00	0.00	0.00	0.00	0.00	0.00
500	0.00	0.00	0.00	0.00	0.00	0.00
600	1.74	0.00	0.00	6.53	0.00	0.00
700	5.23	6.98	8.72	12.51	6.96	0.00
800	13.95	15.70	15.70	17.85	11.95	4.62
900	17.44	19.19	20.93	22.89	18.23	11.12
1000	20.93	24.42	27.91	26.16	24.59	17.35
1100	24.42	29.65	33.14	30.26	29.56	24.23
1200	29.65	34.89	38.37	33.26	34.76	30.33
1300	34.14	38.37	43.61	36.11	40.26	37.50
1400	37.37	41.86	48.84	40.06	45.51	44.69
1500	40.12	45.35	50.59	42.88	50.08	50.89
1600	43.61	50.84	54.07	45.84	53.34	56.13
1700	45.35	54.07	57.56	47.82	56.68	60.46
1800	45.35	57.56	60.31	48.26	58.66	63.97
1900	45.35	59.31	64.54	48.66	60.13	66.73
2000	45.35	59.31	66.28	48.66	61.27	69.32
2100	43.61	59.31	68.03	48.66	61.68	70.00
2200	43.61	59.31	68.03	48.66	61.68	70.27
2300	45.35	57.56	68.03	48.66	61.68	70.46
2400	45.35	55.82	68.03	48.66	61.68	70.46
2500	45.35	55.82	64.54	48.66	61.68	70.46
2600	43.61	59.31	66.28	48.66	61.68	70.46
2700	43.61	59.31	66.28	48.66	61.68	70.46
2800	43.61	59.31	66.28	48.66	61.68	70.46

Table B.12   Results of heat transfer from model and experimental of HOHP

with working fluid of R11, T_e = 60, 70 and 80ºC, and D_i = 2.0 mm

Time	Model			Experimental		
(sec.)	60ºC	70ºC	80ºC	60ºC	70ºC	80ºC
0	0.00	0.00	0.00	0.00	0.00	0.00
100	0.00	0.00	0.00	0.00	0.00	0.00
200	0.00	0.00	0.00	0.00	0.00	0.00
300	0.00	0.00	0.00	0.00	0.00	0.00
400	0.00	0.00	0.00	0.00	0.00	0.00
500	3.49	0.00	0.00	9.31	0.00	0.00
600	8.72	10.47	1.74	15.85	9.96	0.00
700	13.95	17.44	10.47	22.59	20.35	4.62
800	22.68	24.42	17.44	28.96	28.23	17.15
900	27.91	31.40	24.42	33.76	35.33	29.59
1000	34.63	38.37	31.40	38.26	41.50	41.43
1100	38.12	43.61	41.86	42.11	47.29	52.35
1200	41.86	47.10	47.10	45.66	51.89	60.16
1300	47.10	50.59	61.05	48.44	55.53	66.79
1400	50.59	55.31	66.28	52.34	59.46	71.82
1500	52.33	59.31	71.52	55.18	62.97	75.49
1600	54.07	62.80	76.75	57.66	65.73	78.17
1700	54.07	64.54	78.49	58.08	67.82	80.14
1800	54.07	68.03	80.24	58.08	69.11	82.11
1900	55.82	68.03	81.98	58.08	70.46	83.85
2000	55.82	68.03	81.98	58.08	70.46	84.27
2100	55.82	66.28	81.98	58.08	70.46	84.49
2200	54.07	64.54	80.24	58.08	70.46	84.49
2300	54.07	66.28	81.98	58.08	70.46	84.49
2400	54.07	64.54	78.49	58.08	70.46	84.49
2500	55.82	62.80	80.24	58.08	70.46	84.49
2600	55.82	64.54	76.75	58.08	70.46	84.49
2700	38.37	43.61	55.82	40.26	48.34	60.25
2800	36.63	43.61	55.82	40.26	48.34	60.25

Table B.13 Results of heat transfer from model and experimental
of HOHP heat exchanger with working fluid of R11, T_e = 60, 70
and 80ºC and D_i = 2.0 mm

Time	Model			Experimental		
(sec.)	60ºC	70ºC	80ºC	60ºC	70ºC	80ºC
0	0	0	0	0	0	0
100	0	0	0	0	0	0
200	0	0	0	0	0	0
300	0	0	0	0	0	0
400	0	0	0	0	0	0
500	86.61	0	0	83.64	0	0
600	174.05	86.56	0	160.28	83.64	0
700	246.18	164.13	86.92	209.10	146.37	83.64
800	311.12	227.37	160.30	282.29	209.10	135.92
900	375.18	288.93	222.66	334.56	261.38	198.65
1000	435.28	352.81	287.01	397.29	334.56	261.38
1100	487.09	414.57	345.40	460.02	386.84	334.56
1200	537.41	474.34	400.00	512.30	449.57	386.84
1300	575.30	528.01	453.65	554.12	512.30	439.11
1400	600.73	579.73	506.14	575.03	554.12	480.93
1500	620.17	622.55	558.89	585.48	606.39	533.21
1600	621.75	655.53	617.21	595.94	637.76	585.48
1700	626.56	684.62	676.93	606.39	658.67	637.76
1800	626.56	710.36	730.00	606.39	690.03	690.03
1900	626.56	730.72	776.63	606.39	710.94	731.85
2000	626.56	735.61	815.26	606.39	721.40	763.22
2100	626.56	735.61	839.81	606.39	721.40	784.13
2200	626.56	735.61	855.60	606.39	721.40	805.04
2300	626.56	735.61	867.45	606.39	721.40	815.49
2400	626.56	735.61	879.22	606.39	721.40	825.95
2500	626.56	735.61	889.05	606.39	721.40	836.40
2600	626.56	735.61	889.05	606.39	721.40	836.40
2700	626.56	735.61	889.05	606.39	721.40	836.40
2800	626.56	735.61	889.05	606.39	721.40	836.40
2900	626.56	735.61	889.05	606.39	721.40	836.40
3000	626.56	735.61	889.05	606.39	721.40	836.40

Appendix C

Simulation source code

Simulation source code

```
clear all
clc
close all

fprintf('Program Calculate of a Helical Oscillating Heat Pipe\n')

%% Input data %%

T_e=60; T_c=20; T_iv=35; T_iw=25;
p_s=0.01; zeta=90; D_coil=0.05; D_o=0.0026; D_i=0.0016;
L_e=0.05; L_a=0.05; L_c=0.05;s_e=0.850; s_c=0.850;
m_e=0.00417; m_c=0.00417;
S_T=0.02; S_L=0.02; Q_want=1000;
C1=0.4; C2=0.8; mm=0.5; %h = 456;
ns = 12; tmax = 10;

%% Calculate Working Temperature %%
T_work = (T_e+T_c)/2;
T_work_v = (T_e+T_iv)/2;

% Properties of pipe wall (T_work)
Ro_w=8933; Cp_w=385; k_w=401; %%%%%% load properties of copper

% Properties of working fluid at working temperature (water)
Ro_work=992.2; Mew_work=653.2*10^(-6); Cp_work=4182; k_work=0.6305;
h_fg = 2405900;
```

Mahasarakham University

% Properties of water at evaporator section % (T_e=60)

Ro_e=983.2; Mew_e=466.5*10^(-6); Cp_e=4183; k_e=0.6543;

% Properties of water at condenser section % (T_c=20)

Ro_c=998.2; Mew_c=1002.1*10^(-6); Cp_c=4183; k_c=0.5984;

%% Calculation grid

s = s_e+L_a+s_c;

ds = s/ns

dt = 0.01

s0 = 0; t0 = 0;

sx = s0:ds:s;

n = length(sx);

tx = t0:dt:tmax;

tst = length(tx);

%% Constant in calculation of HOHP

r_a = D_coil/2;

% Loop for V_in

if D_i == 0.0016

   V_in = 0.3;

elseif D_i == 0.0018

   V_in = 0.4;

else

   V_in = 0.5;

end

```
A_v = (pi*D_i^2)/4;
m_v = Ro_work*V_in*A_v;
Curv = r_a^2/(r_a^2+p_s^2);
Tor = p_s^2/(r_a^2+p_s^2);
hs = 1+Curv*(D_i/2)*sin(zeta-Tor*(s/(D_o/2)));
Re_work = (Ro_work*V_in*D_i)/Mew_work;
Pr_work = (Cp_work*Mew_work)/k_work;


%% Constant in calculation of equation
alpha_w = (k_w*dt)/(Ro_w*Cp_w*ds^2);
alpha_v1 = dt/(2*hs*ds);
alpha_v2 = ((dt*Curv)/hs)*(sin(zeta-Tor*s)+cos(zeta-Tor*s));
alpha_v3 = dt/(hs^2*ds^2);
alpha_v4 = (dt)/(2*hs*ds);
alpha_v5 = dt/(Re_work*Pr_work*hs^2*ds^2);


%% Initial condition of temperature and velocity at wall and vapor
 for i = 1:tst,
   for j = 1,
     Tw(i,j) = 60;
     Wv(i,j) = 0.3;
     Tv(i,j) = 60;
   end
   for j = 2:n-1
     Tw(i,j) = 25;
     Wv(i,j) = 0.3;
     Tv(i,j) = 25;
   end
   for j = n,
     Tw(i,j) = 20;
     Wv(i,j) = 0.3;
```

```
    Tv(i,j) = 20;
  end
 end

%% Check error of data
err = 1e-9;
chk_err_Tw = 1;
chk_err_Wv = 1;
chk_err_Tv = 1;
Twn = Tw;
Wvn = Wv;
Tvn = Tv;
k = 1;

%% Loop in calculation

while max(max(chk_err_Tw) > err)
   for t = 2:tst,
      for i = 2:n-1,
         Twn(t,i) = (alpha_w*Tw(t-1,i-1) + 2*(1-alpha_w)*Tw(t-1,i) +
                     alpha_w*Tw(t-1,i+1)+alpha_w*Tw(t,i-1) +
                     alpha_w*Tw(t,i+1))/(2*(1+alpha_w));
         Wvn(t,i) = ((alpha_v1+alpha_v3)*Wv(t-1,i-1) +
                     (2-alpha_v2-2*alpha_v3)*Wv(t-1,i) –
                     (alpha_v1-alpha_v3)*Wv(t-1,i+1) +
                     (alpha_v1+alpha_v3)*Wv(t,i-1) –
                     (alpha_v1-alpha_v3)*Wv(t,i+1))/(2+alpha_v2+2*alpha_v3);
         Tvn(t,i) = ((alpha_v4*(Wvn(t,i)-Wvn(t-1,i))+alpha_v5)*Tv(t-1,i-1) +
                     2*(1-alpha_v5)*Tv(t-1,i) –
                     (alpha_v4*(Wvn(t,i)-Wvn(t-1,i))-alpha_v5)*Tv(t-1,i+1) +
                     (alpha_v4*(Wvn(t,i)-Wvn(t-1,i))+alpha_v5)*Tv(t,i-1) –
```

```
                              (alpha_v4*(Wvn(t,i)-Wvn(t-1,i))-alpha_v5)*Tv(t,i+1))/
                              (2*(1+alpha_v5));
            end
        end
    chk_err_Tw = (abs(Twn - Tw)./Twn)*100;
    Tw = Twn;
    Wv = Wvn;
    Tv = Tvn;
    k = k+1
    end


    %% Plot Tw Wv and Tv by s Compare dt = 0.01 %%
     figure(1)
     plot(sx,Tw(t,:)','-b','LineWidth',1,'MarkerEdgeColor','k','MarkerFaceColor','y',
                        'MarkerSize',6);
     xlabel('s'); ylabel('Temperature(C)');
     title('Temperature of Wall')


     figure(2)
     plot(sx,Wv(t,:)','-b','LineWidth',1,'MarkerEdgeColor','k','MarkerFaceColor','y',
                        'MarkerSize',6);
     xlabel('s'); ylabel('Velocity(m/s)');
     title('Velocity of Vapor')


     figure(3)
     plot(sx,Tv(t,:)','-b','LineWidth',1,'MarkerEdgeColor','k','MarkerFace(
                        'MarkerSize',6);
     xlabel('s'); ylabel('Temperature(C)');
     title('Temperature of Vapor')
```

Appendix D
Experimental Set
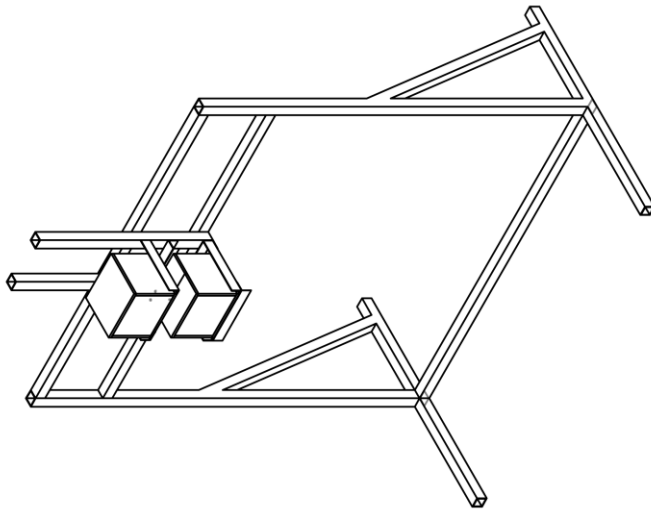
SIZE: A4	Faculty of Engineering Mahasarakham University Thailand		
Scale : 1:15	Title: Experimental set of HOHP		DWG. NO. DATE:
DESIGN BY: NARIN SIRIWAN	CHECKED: Prof. Dr. SAMPAN RITTIDECH		

Mahasarakham University
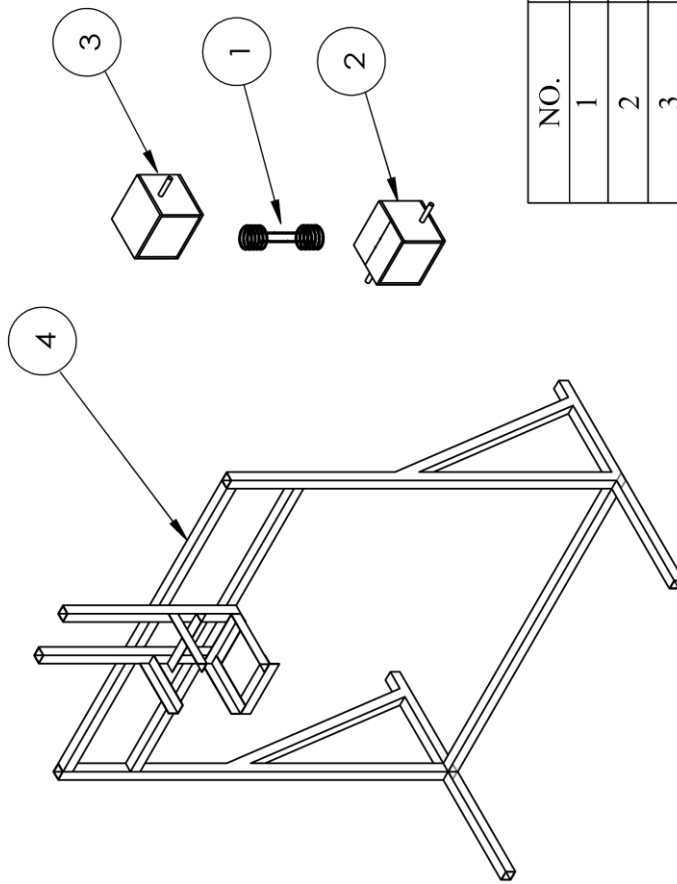
NO.	PART
1	Helical Oscillating Heat Pipe
2	Hot Water Box
3	Cool Water Box
4	Experimental Platform

Faculty of Engineering
Mahasarakham University Thailand

SIZE: A4	Title: Assembly of Helical Oscillating Heat Pipe	DWG. NO.
Scale : 1:15		DATE:

CHECKED: Prof. Dr. SAMPAN RITTIDECH
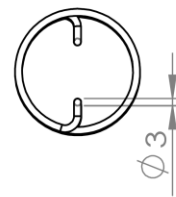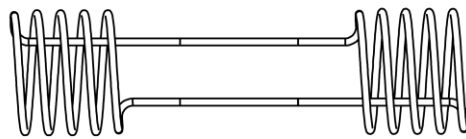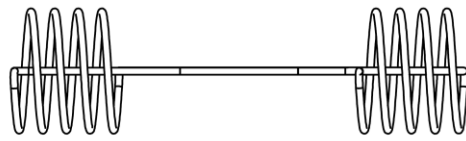
DESIGN BY: NARIN SIRIWAN

SIZE:
A4

Scale :
1:3

Title:
Helical Oscillating Heat Pipe

Faculty of Engineering
Mahasarakham University Thailand

DWG. NO.
DATE:

DESIGN BY:
NARIN SIRIWAN

CHECKED:
Prof. Dr. SAMPAN RITTIDECH

$\emptyset\,3$

Mahasarakham University

100
120
60
60
Ø 10

25
50
25

22.44
60
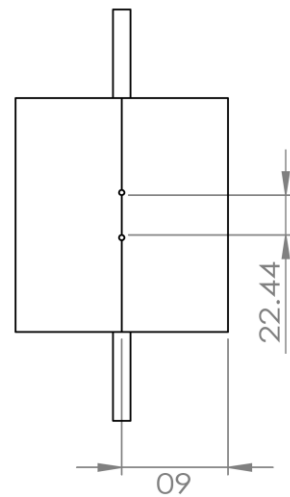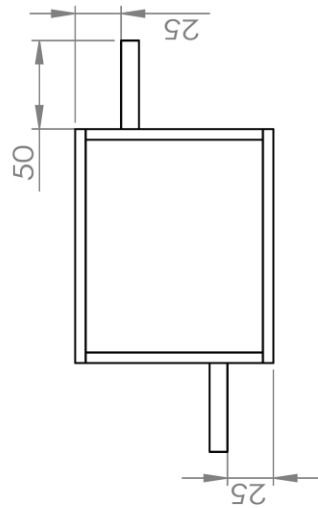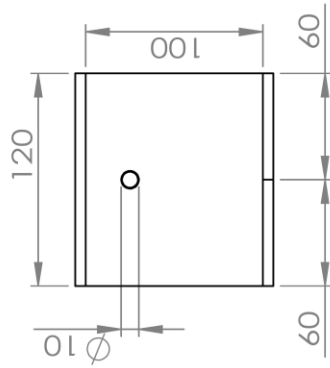
SIZE:
A4

Scale :
1:4

Title:
Hot Water Box
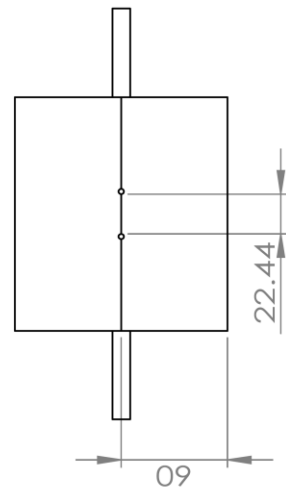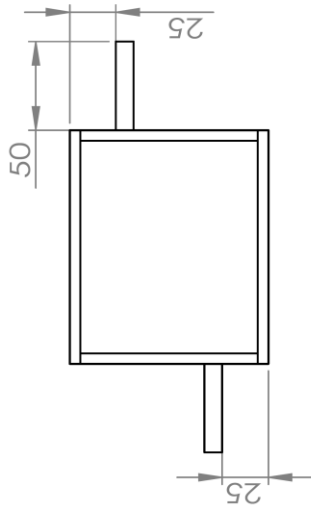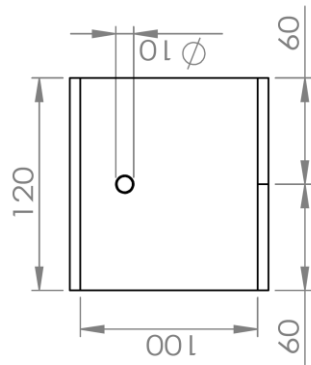
Faculty of Engineering
Mahasarakham University Thailand

DWG. NO.
DATE:

CHECKED:
Prof. Dr. SAMPAN RITTIDECH

DESIGN BY:
NARIN SIRIWAN

SIZE: A4	Faculty of Engineering Mahasarakham University Thailand		DWG. NO.
			DATE:
Scale : 1:4	Title: Cool Water Box	CHECKED:	
DESIGN BY: NARIN SIRIWAN		Prof. Dr. SAMPAN RITTIDECH	

SIZE: A4	Faculty of Engineering Mahasarakham University Thailand		DWG. NO.
			DATE:
Scale : 1:20	Title: Experimental Platform		
	CHECKED:		
DESIGN BY: NARIN SIRIWAN	Prof. Dr. SAMPAN RITTIDECH		
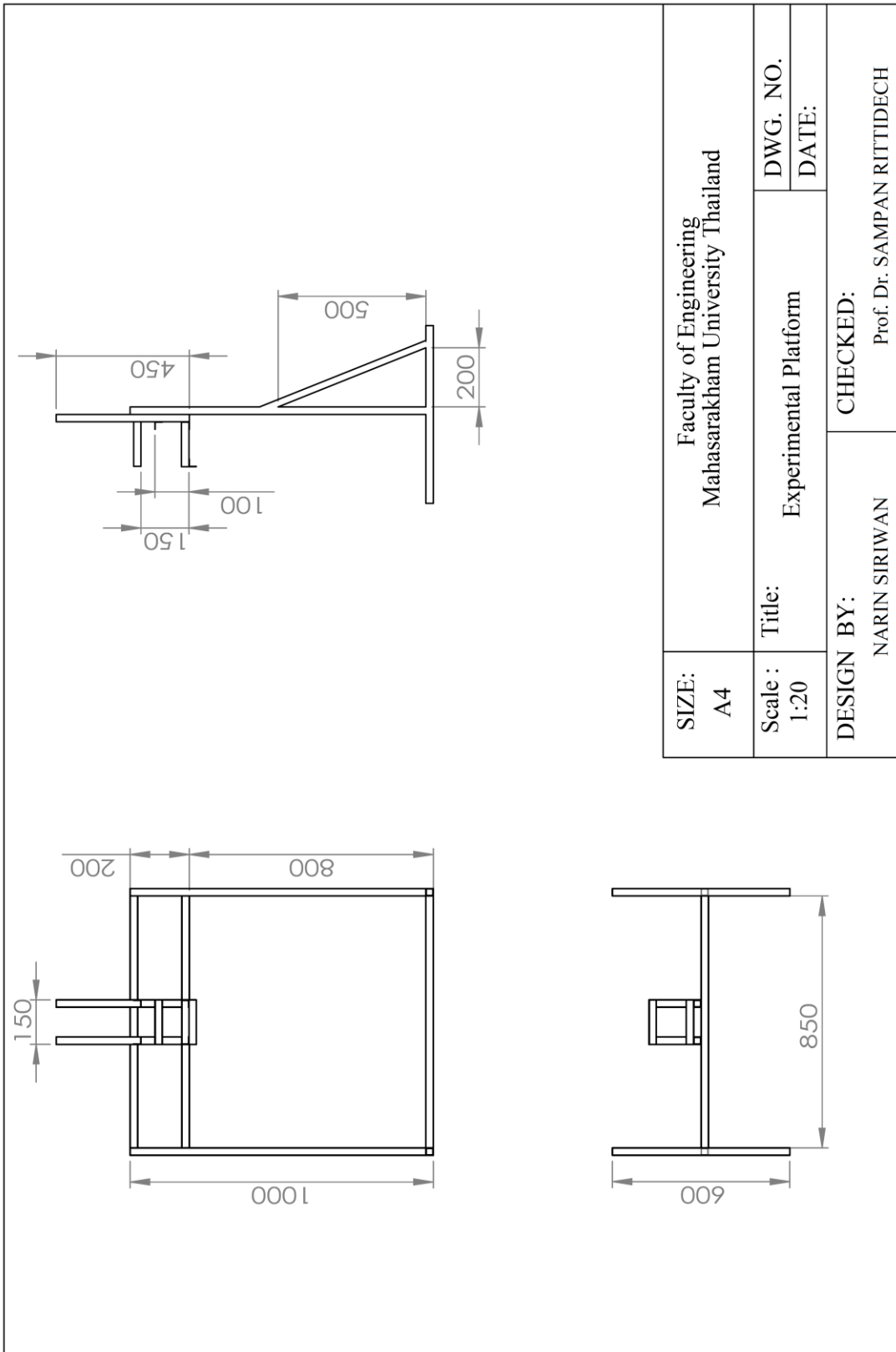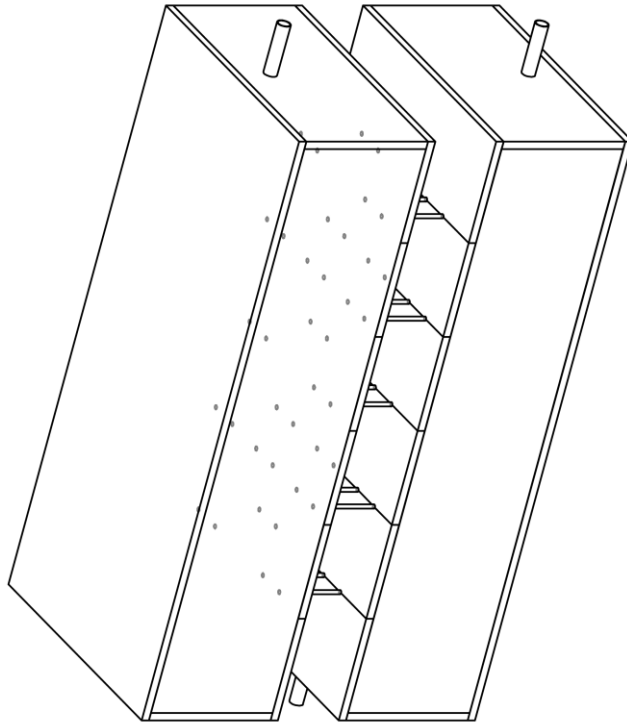
SIZE: A4		
Scale : 1:5	Title: HOHP Heat Exchanger	
DESIGN BY: NARIN SIRIWAN	CHECKED: Prof. Dr. SAMPAN RITTIDECH	
Faculty of Engineering Mahasarakham University Thailand	DWG. NO.	
	DATE:	

146

Mahasarakham University

Faculty of Engineering
Mahasarakham University Thailand
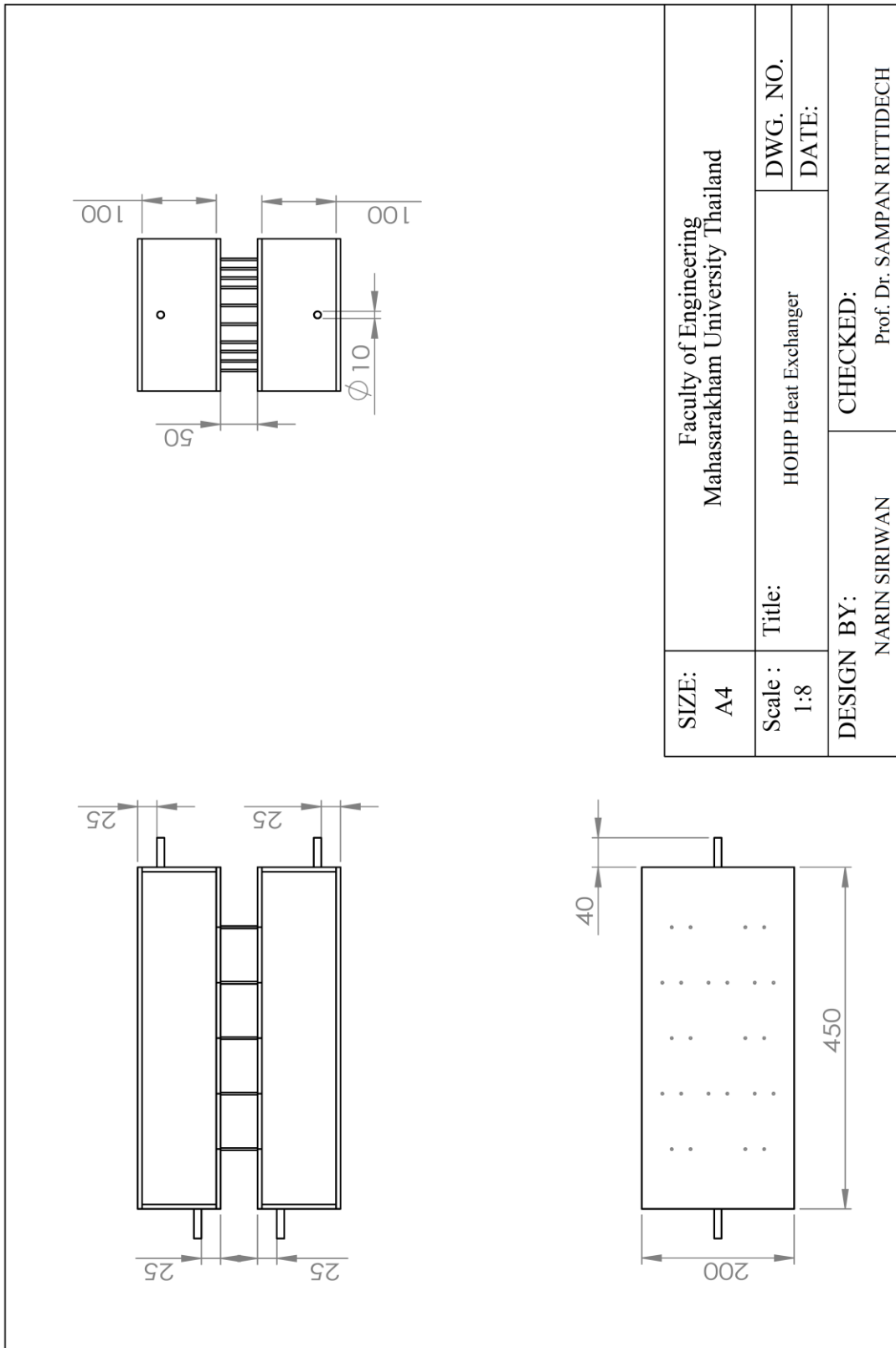
DWG. NO.
DATE:

Title: HOHP Heat Exchanger

CHECKED:
Prof. Dr. SAMPAN RITTIDECH

SIZE:
A4

Scale :
1:8

DESIGN BY:
NARIN SIRIWAN

APPENDIX E

Properties of working fluids

Table E.1 Properties of water

Temp (°C)	Pressure (Mpa)	Density (kg/m³) Liquid	Volume (m³/kg) Vapor	Enthalpy (kJ/kg)		Entropy (kJ/(kg.K))		Specific Heat Cp (kJ/ (kg.K))		Surface Tension (mN/m)
				Liquid	Vapor	Liquid	Vapor	Liquid	Vapor	
0.01	0.00061	999.8	205.98	0.0	2500.5	0.0000	9.1541	4.229	1.868	75.65
5.00	0.00087	999.9	147.02	21.0	2509.7	0.0763	9.0236	4.200	1.871	74.95
10.00	0.00123	999.7	106.32	42.0	2518.9	0.1510	8.8986	4.188	1.874	74.22
15.00	0.00171	999.1	77.900	62.9	2528.0	0.2242	8.7792	4.184	1.878	73.49
20.00	0.00234	998.2	57.777	83.8	2537.2	0.2962	8.6651	4.183	1.882	72.74
25.00	0.00317	997.0	43.356	104.8	2546.3	0.3670	8.5558	4.183	1.887	71.98
30.00	0.00425	995.6	32.896	125.7	2555.3	0.4365	8.4513	4.183	1.892	71.20
35.00	0.00563	994.0	25.221	146.6	2564.4	0.5050	8.3511	4.183	1.898	70.41
40.00	0.00738	992.2	19.528	167.5	2573.4	0.5723	8.2550	4.182	1.905	69.60
45.00	0.00959	990.2	15.263	188.4	2582.3	0.6385	8.1629	4.182	1.912	68.78
50.00	0.01234	988.0	12.037	209.3	2591.2	0.7037	8.0745	4.182	1.919	67.95
55.00	0.01575	985.6	9.5730	230.2	2600.0	0.7680	7.9896	4.182	1.928	67.10
60.00	0.01993	983.2	7.6746	251.2	2608.8	0.8312	7.9080	4.183	1.937	66.24
65.00	0.02502	980.5	6.1996	272.1	2617.5	0.8935	7.8295	4.184	1.947	65.37
70.00	0.03118	977.8	5.0447	293.0	2626.1	0.9549	7.7540	4.187	1.958	64.49
75.00	0.03856	974.8	4.1333	314.0	2634.6	1.0155	7.6813	4.190	1.970	63.59
80.00	0.04737	971.8	3.4088	334.9	2643.1	1.0753	7.6112	4.194	1.983	62.68
85.00	0.05781	968.6	2.8289	355.9	2651.4	1.1343	7.5436	4.199	1.996	61.76
90.00	0.07012	965.3	2.3617	376.9	2659.6	1.1925	7.4784	4.204	2.011	60.82
95.00	0.08453	961.9	1.9828	398.0	2667.7	1.2501	7.4154	4.210	2.027	59.88
100.00	0.10132	958.4	1.6736	419.1	2675.7	1.3069	7.3545	4.217	2.044	58.92
105.00	0.12079	954.8	1.4200	440.2	2683.6	1.3630	7.2956	4.224	2.062	57.95
110.00	0.14324	951.0	1.2106	461.3	2691.3	1.4186	7.2386	4.232	2.082	56.97
115.00	0.16902	947.1	1.0370	482.5	2698.8	1.4735	7.1833	4.240	2.103	55.98
120.00	0.19848	943.2	0.89222	503.8	2706.2	1.5278	7.1297	4.249	2.126	54.97
125.00	0.23201	939.1	0.77089	525.1	2713.4	1.5815	7.0777	4.258	2.150	53.96
130.00	0.27002	934.9	0.66872	546.4	2720.4	1.6346	7.0272	4.268	2.176	52.94
135.00	0.31293	930.6	0.58234	567.8	2727.2	1.6873	6.9780	4.278	2.203	51.91
140.00	0.36119	926.2	0.50898	589.2	2733.8	1.7394	6.9302	4.288	2.233	50.86

ASHRAE HANDBOOK, 1993

Properties of water (continuous)

Temp (°C)	Pressure (Mpa)	Density (kg/m³) Liquid	Volume (m³/kg) Vapor	Enthalpy (kJ/kg)		Entropy (kJ/(kg.K))		Specific Heat Cp (kJ/ (kg.K))		Surface Tension (mN/m)
				Liquid	Vapor	Liquid	Vapor	Liquid	Vapor	
165.00	0.70029	902.6	0.27270	697.4	2763.3	1.9927	6.7078	4.353	2.415	45.51
170.00	0.79147	897.5	0.24283	719.3	2768.5	2.0421	6.6662	4.369	2.460	44.41
175.00	0.89180	892.3	0.21679	741.2	2773.3	2.0910	6.6254	4.386	2.507	43.31
180.00	1.0019	887.1	0.19406	763.2	2777.8	2.139	6.5853	4.403	2.558	42.20
185.00	1.1225	881.7	0.17406	785.4	2782.0	2.1879	6.5459	4.423	2.612	41.08
190.00	1.2542	876.1	0.15650	807.6	2785.8	2.2358	6.5071	4.443	2.670	39.95
195.00	1.3976	870.5	0.14102	829.9	2789.4	2.2834	6.4689	4.465	2.731	38.82
200.00	1.5536	864.7	0.12732	852.4	2792.5	2.3308	6.4312	4.489	2.797	37.68
205.00	1.7229	858.9	0.11517	875.0	2795.3	2.3778	6.3940	4.515	2.867	36.54
210.00	1.9062	852.8	0.10438	897.7	2797.7	2.4246	6.2572	4.542	2.943	35.39
215.00	2.1042	846.6	0.09475	920.5	2799.7	2.4712	6.3208	4.572	3.023	34.24
220.00	2.3178	840.3	0.08615	943.5	2801.3	2.5175	6.2847	4.604	3.109	33.08
225.00	2.5749	833.9	0.07846	966.7	2802.4	2.5637	6.2488	4.638	3.201	31.91
230.00	2.7951	827.2	0.07155	990.0	2803.1	2.6097	6.2131	4.675	3.300	30.75
235.00	3.0604	820.5	0.06534	1013.5	2803.3	2.6556	6.1777	4.715	3.405	29.58
240.00	3.3447	813.5	0.05974	1037.2	2803.0	2.7013	6.1423	4.759	3.519	28.40
245.00	3.6488	806.4	0.05469	1061.2	2802.1	2.7470	6.1070	4.806	3.641	27.23
250.00	3.9736	799.1	0.05011	1085.3	2800.7	2.7926	6.0717	4.857	3.772	26.05
255.00	4.3202	791.5	0.04395	1109.7	2798.8	2.8382	6.0363	4.912	3.914	24.88
260.00	4.6894	783.8	0.04219	1134.4	2796.2	2.8838	6.0009	4.973	4.069	23.70
265.00	5.0823	775.9	0.03876	1159.3	2793.0	2.9294	5.9652	5.039	4.236	22.52
270.00	5.4999	767.7	0.03564	1184.6	2789.1	2.9751	5.9293	5.111	4.418	21.35
275.00	5.9431	759.2	0.03278	1210.1	2784.5	3.0209	5.8931	5.191	4.617	20.17
280.00	6.4132	750.5	0.03016	1236.1	2779.2	3.0669	5.8565	5.279	4.835	19.00
285.00	6.9111	741.5	0.02777	1262.4	2773.0	3.1131	5.8195	5.377	5.077	17.84
290.00	7.4380	732.2	0.02556	1289.1	2765.9	3.1595	5.7818	5.485	5.345	16.68
295.00	7.9952	722.5	0.02354	1316.3	2757.8	3.2062	5.7434	5.607	5.644	15.52
300.00	8.5838	712.4	0.02167	1344.1	2748.7	3.2534	5.7042	5.746	5.981	14.37

ASHRAE HANDBOOK, 1993

Table E.2 Properties of ethanol

Temp (^{O}C)	Press P_V x10^5 (Pa)	Latent h_{fg} (kJ/kg)	ρ_l x10^3 (kg/m^3) Liquid	ρ_V (kg/m^3) Vapor	μ_l x10^{-3} (N.s/m^2) Liquid	μ_V x10^{-5} (N.s/m^2) Vapor	K_l (W/m.K) Liquid	K_v (W/m.K) Vapor	σ x10^{-3} (N/m) Liquid	$C_{P,l}$ (kJ/kg.K) Liguid	$C_{P,V}$ (kJ/kg.K) Vapor
0	0.012	1048.4	0.901	0.036	1.7990	0.774	0.183	0.0117	24.4	0.541	1.34
20	0.058	1030.0	0.800	0.085	1.1980	0.835	0.179	0.0139	22.8	0.574	1.40
40	0.180	1011.9	0.789	0.316	0.8190	0.900	0.175	0.160	21.0	0.615	1.48
60	0.472	988.9	0.770	0.748	0.5880	0.959	0.171	0.0179	19.2	0.665	1.54
80	1.086	960.0	0.757	1.430	0.4320	1.030	0.169	0.0199	17.3	0.723	1.61
100	2.260	927.0	0.730	3.410	0.3180	1.092	0.167	0.0219	15.5	0.789	1.68
120	4.290	885.5	0.710	6.010	0.2430	1.157	0.165	0.0238	13.4	0.863	1.75
140	7.530	834.0	0.680	10.670	0.1900	1.219	0.163	0.0256	11.2	0.945	
160	12.756	772.9	0.650	17.450	0.1500	1.293	0.161	0.0272	9.0		
180	19.600	698.8	0.610	27.650	0.1200	1.369	0.159	0.0288	6.7		
200	29.400	598.3	0.564	44.480	0.0950	1.464	0.157	0.0395	4.3		
220	42.800	468.5	0.510	74.350	0.0725	1.618	0.155	0.0321	2.2		
240	60.200	280.5	0.415	135.500	0.0488	1.948	0.153		0.1		

Dunn P. and Reay D.A., 1982

Table E.3 Properties of R11

Temp (ºC)	Pressure (MPa)	Density (kg/m³) Liquid	Volume (m³/kg) Vapor	Enthalpy (kJ/kg)		Entropy (kJ/(kg.K))		Specific Heat Cp (kJ/ (kg.k))		Surface Tension x10⁻³ (N/m)
				Liquid	Vapor	Liquid	Vapor	Liquid	Vapor	
0	0.0402	1534.1	0.40328	200.00	389.77	1.0000	1.6947	0.859	0.576	21.04
2	0.04377	1529.6	0.37264	201.72	390.80	1.0063	1.6935	0.861	0.578	20.77
4	0.04759	1525.0	0.34479	203.44	391.83	1.0125	1.6922	0.862	0.581	20.51
6	0.05167	1520.5	0.31943	205.17	392.86	1.0187	1.6911	0.864	0.584	20.25
8	0.05603	1515.9	0.29630	206.90	393.89	1.0249	1.6900	0.865	0.586	19.98
10	0.06068	1511.3	0.27518	208.64	394.92	1.0310	1.6889	0.867	0.589	19.72
12	0.06562	1506.7	0.25587	210.38	395.95	1.0371	1.6879	0.869	0.592	19.46
14	0.07088	1502.1	0.23819	212.12	396.99	1.0432	1.6970	0.871	0.595	19.20
16	0.07647	1497.4	0.22198	213.86	398.02	1.0492	1.6861	0.872	0.597	18.93
18	0.08240	1492.8	0.20710	215.61	399.05	1.0552	1.6853	0.874	0.600	18.67
20	0.08868	1488.1	0.19342	217.36	400.08	1.0612	1.6845	0.876	0.603	18.42
22	0.09534	1483.4	0.18083	219.12	401.10	1.0672	1.6838	0.878	0.606	18.16
24	0.10238	1478.6	0.16922	220.88	402.13	1.0731	1.6831	0.880	0.608	17.90
26	0.10982	1473.9	0.15852	222.64	403.16	1.0790	1.6824	0.882	0.611	17.64
28	0.11767	1496.1	0.14864	224.41	404.18	1.0849	1.6818	0.884	0.614	17.39
30	0.12596	1464.3	0.13950	226.19	405.28	1.0907	1.6813	0.886	0.617	17.13
32	0.13470	1459.3	0.13104	227.96	406.23	1.0965	1.6807	0.888	0.620	16.87
34	0.14389	1454.7	0.12320	229.74	407.25	1.1023	1.6803	0.890	0.622	16.62
36	0.15357	1449.8	0.11593	231.53	408.27	1.1081	1.6798	0.892	0.625	16.37
38	0.16374	1444.9	0.10918	233.32	409.28	1.1139	1.6794	0.894	0.628	16.11
40	0.17743	1440.0	0.10290	235.11	410.30	1.1196	1.6790	0.896	0.631	15.86
42	0.18564	1435.0	0.09706	236.91	411.31	1.1253	1.6787	0.899	0.634	15.61
44	0.19740	1430.0	0.09162	238.71	412.31	1.1310	1.6784	0.901	0.637	15.36
46	0.20973	1425.0	0.08656	240.52	413.32	1.1366	1.6781	0.903	0.640	-
48	0.22263	1420.0	0.08183	242.33	414.32	1.1423	1.6778	0.906	0.643	-
50	0.23614	1414.9	0.07741	244.15	415.32	1.1479	1.6776	0.908	0.646	-
55	0.27264	1402.1	0.06758	248.72	417.80	1.1618	1.6771	0.914	0.654	-
60	0.31329	1389.1	0.05924	253.32	420.25	1.1756	1.6767	0.921	0.662	-
65	0.35837	1375.9	0.05212	257.95	422.68	1.1893	1.6765	0.928	0.670	-
70	0.40818	1362.4	0.04601	262.62	425.08	1.2030	1.6764	0.935	0.679	-
75	0.46303	1348.7	0.04075	267.33	427.44	1.2165	1.6763	0.943	0.688	-
80	0.52323	1334.7	0.03620	272.08	429.76	1.2299	1.6764	0.951	0.698	-

Table E.4 Constant values in calculation convective heat transfer coefficient

Re$_D$	C	n
0.4 to 4	0.989	0.330
4 to 40	0.911	0.385
40 to 4,000	0.683	0.466
4,000 to 40,000	0.193	0.618
40,000 to 400,000	0.0266	0.805

Biography

Biography

Name	Mr. Narin Siriwan.
Date of birth	October 17, 1988.
Place of birth	Roi-Et, Thailand.
Address	11 M 10, Phoyai Sub-District, Phanomprai District, Roi-Et Province, Thailand, 45140.

Institution attended

20011	Bachelor of Mechanical Engineering (Energy), B.Eng. Mahasarakham University, Thailand.
2013	Master of Mechanical Engineering, M.Eng. Mahasarakham University, Thailand.
2016	Doctor of Philosophy (Ph.D.) (Mechanical Engineering) Mahasarakham University, Thailand.

Collaborative internship 2016

School of Chemical Engineering, University of Birmingham, Birmingham, United Kingdom.

Scholarship

Royal Golden Jubilee Ph.D. Program
(RGJ-Grant No. PHD/0014/2556).

Contact address

11/10, Phoyai Sub-District, Phanomprai District,
Roi-Et Province, Thailand, 45140.